Curso 2005/06
CIENCIAS Y TECNOLOGÍAS/5
I.S.B.N.: 84-7756-685-2

ALEJANDRO MANUEL GARCÍA GIL

Estudio óptico-UV de estrellas de tipo medio y tardío

Directores
RAMÓN J. GARCÍA LÓPEZ
CARLOS ALLENDE PRIETO

SERVICIO DE PUBLICACIONES
UNIVERSIDAD DE LA LAGUNA

SOPORTES AUDIOVISUALES E INFORMÁTICOS
Serie Tesis Doctorales

a los divulgadores científicos, que encendieron la llama de mi curiosidad por el Universo

Agradecimientos

Debo agradecer su ayuda en la realización de la tesis sobre todo a mis directores de tesis. A Ramón J. García López quien, a pesar de haber estado parte del tiempo metido en obligaciones ajenas, ha sabido encontrar tiempo cuando lo necesitaba para ayudarme en la elaboración y corrección de la tesis y otros asuntos relacionados, dándome ideas, consejos y ánimos para continuar el trabajo. Y a Carlos Allende Prieto con quien, a pesar de la distancia, he mantenido un contacto fluido a través del correo electrónico y durante los períodos en los que le he visitado en Austin, enseñándome el uso de los programas utilizados, entre otras muchas cosas, útiles para la elaboración de la tesis, además de enseñarme a desenvolverme en un mundo diferente como es Texas.

También agradezco al programa de formación de personal investigador del Instituto de Astrofísica de Canarias (y a su director, el Profesor Francisco Sánchez) la beca y posterior contrato que me concedieron y la formación proporcionada por algunos cursos de doctorado, bastante útil para mejorar mis conocimientos de Astrofísica, que fueron escasos durante la carrera. Además, estoy en deuda con la Universidad de La Laguna y con los profesores a cuyas clases he asistido como oyente: Basilio Ruiz Cobo, Inés Rodríguez Hidalgo y Charo Villamariz. Gracias también al proyecto 'Evolución Química del Grupo Local' (PNAYA 2001-0436), sin el cual no habría podido asistir a congresos ni pasar algunos períodos de formación en Austin. De gran utilidad fueron también los comentarios de los miembros del tribunal (Basilio Ruiz Cobo y Artemio Herrero) acerca de la memoria del DEA y de mi revisora interna de la tesis, Charo Villamariz, por su meticulosidad en la revisión.

Por otro lado, agradezco la confianza depositada en mí por los profesores de la UAM Carlos Eiroa y M. Ángeles Díaz Beltrán, que escribieron las cartas de recomendación que me permitieron hacer el doctorado en el IAC.

Agradezco también al Departamento de Astronomía de la Universidad de Texas en Austin lo agradable que han hecho mis estancias allí, tanto dentro de

la Universidad, con la ayuda del grupo de espectroscopía estelar (especialmente David Yong y David Lambert), como fuera de ella, tanto las charlas distendidas en 'The Crown and the Ancor' como los divertidos partidos de volley-ball que organizaba Michael Endl.

La ayuda del grupo que trabaja en estrellas calientes, fundamentalmente Sergio y Miguel, ha sido decisiva en el modelado de atmósferas estelares y la síntesis espectral. También agradezco a Ivan Hubeny su colaboración para la realización del artículo sobre el estudio del espectro UV cercano de Vega, así como a Ralph Bohlin por su revisión del mismo. Por otro lado, debo agradecer a Nuno Santos, a Garik Israelian, a Michel Mayor, a Rafael Rebolo y a los demás autores, la oportunidad que me han dado para colaborar con ellos en la elaboración del artículo sobre la comparación de abundancias en estrellas con y sin planetas. Para el estudio de Vega usando modelos con rotación rápida han sido decisivas las conversaciones mantenidas con Fernando Pérez Hernández.

Tampoco me olvido de mis compañeros del 'Corralón', que me han ayudado a resolver dudas sobre la tesis u otros asuntos relacionados con el doctorado, ni de mis amigos del IAC (algunos también compañeros de despacho), con los que he pasado buenos momentos en la cafetería, en la cancha o fuera del IAC y han hecho más agradable mi estancia en Tenerife. Asimismo han sido importantes mis amigos que no pertenecen al IAC, que me han mostrado su interés por el transcurrir de la tesis.

Por último, pero no por ello menos importante, agradezco a mi familia, especialmente a mis padres y hermanos, el apoyo que me han dado para continuar con la tesis y el interés que han mostrado por su marcha, a pesar de no saber muy bien de lo que trataba.

Alejandro Manuel García Gil

Sumario

En esta tesis presentamos un análisis cuantitativo de los espectros ultravioleta (UV) cercano, óptico e infrarrojo (IR) cercano de las estrellas Vega y Proción, con el propósito de determinar sus propiedades físicas así como sus abundancias químicas superficiales.

Hemos comparado diferentes espectros observados con espectros sintéticos considerando en detalle las opacidades metálicas para escoger entre ellos. Este aspecto es especialmente importante en el ultravioleta, ya que hay una controversia sobre cuál es la mejor escala de flujo: la del Telescopio Espacial Hubble (HST) o la de INES, calibrada directamente a partir del satélite *International Ultraviolet Explorer* (IUE). La comparación de los flujos sintéticos del UV cercano, del visible y del IR cercano con los observados favorece la escala de flujo del HST sobre la escala de INES. También hemos obtenido nuevos espectros de resolución intermedia de Proción con STIS a bordo del HST y espectros de alta resolución de Vega desde el Observatorio McDonald.

Hemos derivado la temperatura efectiva y la metalicidad a partir de modelos de atmósfera en equilibrio termodinámico local (ETL), fijando la gravedad superficial, comparando flujos sintéticos con el observado en regiones donde la opacidad del continuo de elementos distintos al hidrógeno no es importante, lo que suele ser válido en la región visible.

Utilizando los parámetros previamente derivados, hemos identificado los principales contribuyentes a la opacidad del continuo en Vega y Proción. Las abundancias químicas de estos principales contribuyentes han sido investigadas comparando flujos sintéticos con el observado en el ultravioleta en regiones donde la opacidad del continuo producido por estos elementos es importante. También hemos derivado abundancias químicas a partir de líneas espectrales del visible y comparado los resultados con los obtenidos usando la región ultravioleta.

Finalmente hemos llevado a cabo un estudio del espectro de Vega usando

modelos estelares con rotación rápida, comparando los flujos sintéticos con e observado. De esta manera hemos obtenido nuevos parámetros físicos (veloci dad de rotación, inclinación del eje de rotación, la temperuatura y la graveda polar y ecuatorial, la metalicidad y la microturbulencia) y abundancias química fotosféricas. La alta velocidad de rotación y la baja inclinación obtenidas so consistentes con otros trabajos que tienen en cuenta la rotación, mientras qu la microturbulencia y la velocidad ecuatorial proyectada obtenidas compara bien con los resultados donde el efecto de la rotación rápida sobre la superfici estelar y sobre el flujo emitido no fue considerado. Se han obtenido diferente valores de la gravedad, la temperatura efectiva y algunas abundancias al tene en cuenta el efecto de la velocidad de rotación en detalle.

Códigos UNESCO: 2101.10, 2101.11, 2101.12, 2103.03

Contenidos

Agradecimientos v

Sumario vii

Contenidos ix

Resumen xi

Agradecimientos en inglés xxxix

Resumen en inglés xli

1 Introducción **1**
1.1 Opacidad de las líneas y del continuo 1
1.2 Espectro estelar UV 2
1.3 Dificultades para reproducir el espectro solar y estelar UV 5
1.4 Vega y Proción como casos de estudio 5
1.5 Vega como una estrella con rotación rápida 7

2 Datos atómicos y herramientas para estudiar espectros **9**
2.1 Modelos de atmósfera 9
2.2 Síntesis espectral 11
2.3 Datos atómicos y listas de líneas 12
2.4 Procedimiento de minimización 13

3 Espectros observados **17**
3.1 Espectros observados de Vega 17
3.1.1 Espectros UV 17

3.1.2 Espectros visibles e IR cercanos 21
3.2 Espectros observados de Proción 22
3.2.1 Espectros UV cercanos 22
3.2.2 Espectros visibles 22
3.2.3 Espectros IR cercanos 24
4 El estudio del espectro de Vega usando modelos de atmósfera clásicos 29
4.1 Principales contribuyentes a la opacidad en Vega 30
4.2 Estimación de los parámetros de Vega usando las regiones visible e IR y UV cercana 32
4.3 Estimación de las abundancias de Si y C a partir del continuo UV . . 40
4.4 Estimación de las abundancias a partir de las líneas espectrales de la región visible 44

5 El estudio de Proción usando modelos de atmósfera clásicos . . 51
5.1 Principales contribuyentes a la opacidad de Proción 52
5.2 Estimación de la temperatura efectiva y el diámetro angular 52
5.3 Estimación de las abundancias químicas a partir del continuo UV . 57
5.4 Estimación de las abundancias químicas a partir de las líneas espectrales 59
6 El estudio del espectro de Vega usando modelos estelares con rotación rápida 63
6.1 Modelos estelares con rotación rápida 64
6.2 Cálculos preliminares de los parámetros estelares 68
6.3 Cálculos de los parámetros del modelo 71
6.4 Cálculos de abundancias y nuevos valores de i y T_{polar} 73
6.5 Comparación del resultado con el de los modelos clásicos 76

7 Conclusiones y trabajo futuro 83
7.1 Conclusiones 83
7.2 Trabajo futuro 85
8 Apéndice: atlas UV cercano de Proción 87
Bibliografía 103

Resumen

Cap. 1: Introducción

- La opacidad de las líneas y del continuo:

  La radiación electromagnética que recibimos de las estrellas adquiere su particular patrón espectral como consecuencia de diferentes fuentes de opacidad de las líneas (producidas por transiciones ligado-ligado) y del continuo (producidas por transiciones ligado-libre y libre-libre). En esta tesis no discutimos las líneas de emisión, por ser poco relevantes en las estrellas estudiadas, que son de tipo espectral medio y tardío.

  Hace mucho tiempo que se descubrieron las primeras líneas espectrales en el Sol (Wollaston 1802) y poco después Joseph Fraunhofer (1817, 1821, 1823) las descubrió en otros cuerpos celestes. Hoy en día disponemos de espectros estelares de alta resolución con alta relación señal a ruido (S/R), lo que nos permite determinar con precisión la velocidad radial y la velocidad de rotación proyectada de las estrellas. Otras mediciones tales como las abundancias químicas se pueden obtener a partir de la anchura equivalente (AE) de las líneas espectrales, pero hace falta además conocer las condiciones físicas de la atmósfera, para lo que se cuenta con modelos de atmósfera construidos usando primeros principios y simplificaciones.

  El estudio del flujo del continuo nos permite determinar los parámetros estelares de los que dependen estos modelos (temperatura efectiva, gravedad superficial y metalicidad) comparando los flujos calculados usando los modelos con el flujo observado de las estrellas. También es posible detectar compañeros estelares o discos a partir del continuo, o calcular abundancias químicas de elementos con una absorción del continuo importante, lo que no se había explorado en profundidad anteriormente y es uno de los objetivos de esta tesis.

- El espectro estelar UV:

  La mayor parte de los estudios astronómicos llevados a cabo desde la invención del telescopio solamente han tenido en cuenta la radiación visible, debido a que la mayoría de la radiación que nos llega en otras regiones del espectro es absorbida por la atmósfera. Hasta los años 70 no se lanzó el primer satélite que estudiaba el ultravioleta (UV) cercano: el IUE y poco tiempo después se construyeron los primeros modelos de atmósfera que contenían suficientes líneas para intentar reproducir el UV.

  A pesar de las dificultades, es esencial entender la formación del espectro UV de las estrellas para determinar abundancias de elementos químicos que sólo producen rasgos medibles en esta región espectral, tales como los elementos ligeros boro y berilio (producidos por astillado en el medio interestelar y quizá en parte en la nucleosíntesis primordial) y el germanio, producido por captura de neutrones. Aparte del germanio, hay otros elementos cuyas transiciones atómicas más fuertes se encuentran en el UV, como el osmio y la plata. Un entendimiento adecuado de la región UV en las estrellas es también crucial para interpretar la luz integrada de galaxias y otros sistemas estelares. El campo de radiación UV tiene un efecto importante en la construcción de modelos de atmósfera a través del balance de energía. Por tanto, un error de las opacidades UV implica propiedades físicas (como composición química y parámetros atmosféricos para estrellas o edades para galaxias) derivadas erróneamente.

- Dificultades al tratar de reproducir el espectro UV observado:

  Se ha propuesto una fuente de opacidad UV perdida para intentar explicar un fallo al ajustar el espectro UV solar. Se ha sugerido que la absorción metálica de las líneas (e.g. Holweger 1970; Vernazza, Avrett & Loeser 1976) o del continuo (Bell, Paltoglou & Tripicco 1994; Bell, Balachandran & Bautista 2001) podrían proporcionar esa opacidad extra. Sin embargo, estudios recientes del espectro UV de otras estrellas sugieren que hay un acuerdo razonable entre los modelos teóricos (Kurucz 1992) y las observaciones (e.g. Fitzpatrick & Massa 1999, Allende Prieto & Lambert 2000, Peterson et al. 2001). El análisis del espectro solar de Bell, Balachandran & Bautista (2001) concluye que, incluso con los cálculos más recientes de las opacidades de las líneas y del continuo, los modelos de atmósfera clásicos predicen demasiado flujo UV. Sin embargo, Allende Prieto et al. (2003) encuentran que el modelado en equilibrio termodinámico local (ETL) puede reproducir con precisión el flujo solar observado a longitudes de onda mayores de ~ 2600 Å, y las incertidumbres en los datos atómicos

de las líneas son suficientes para explicar las diferencias entre los flujos observados y sintéticos. Las observaciones de alta calidad de estrellas con parámetros atmosféricos diferentes a los del Sol son necesarias para resolver la controversia.

- Vega y Proción como casos de estudio:

  Una de las estrellas que estudiamos es Vega (α Lyr, HD 172167, A0 V). Esta estrella no es fácil de modelar, porque tiene un disco de polvo y gas (Walgate 1983; Wilner et al. 2002) que produce un exceso de flujo IR; es un rotor rápido con un polo apuntando casi hacia nosotros (Gulliver et al. 1994); y es posiblemente variable (Vasil'Yev et al. 1989). Además, tiene un patrón de abundancias peculiar, similar al de las estrellas λ Boo (Ilijić et al. 1998). A pesar de estas dificultades, Vega es una de las pocas estrellas enanas con medidas espectrofotométricas UV precisas y medidas independientes de su diámetro angular. También se han obtenido espectros visibles de alta resolución y alta relación señal a ruido (S/R) desde tierra. Además, se espera que el disco no contribuya apreciablemente al espectro visible ni UV de la estrella, y se ha encontrado que la influencia de la rotación rápida sólo es importante para la forma de las líneas espectrales, siendo el efecto sobre el continuo limitado a la región espectral de la vecindad del salto de Balmer (Gulliver et al. 1994).

  La otra estrella a estudiar es Proción A (α CMi, HD61421, F5 IV-V). Es más fría que Vega, así que tiene más líneas espectrales y opacidad en el UV y es más difícil de modelar. Además, tiene una enana blanca compañera. Sin embargo, Proción A es una de las pocas estrellas enanas que se puede usar para testear cálculos detallados de irradiancia UV: se dispone tanto de espectrofotometría UV precisa como de medidas independientes del diámetro angular. Por otra parte, se ha podido determinar con precisión su masa a partir de sus parámetros orbitales. Además hay espectros visibles de Proción en baja y alta resolución con alta S/R tomados desde tierra.

- Vega como una estrella que rota rápidamente:

  David Gray (1988) fue el primero que sugirió que Vega era un rotor rápido con uno de sus polos apuntando casi hacia nosotros para explicar el exceso en luminosidad de Vega en la banda V con respecto a otras estrellas de su mismo tipo espectral (0.7 magnitudes), que ya había notado Petrie (1964) a partir de la calibración absoluta de flujo de las anchuras equivalentes de Hγ. Gray sugirió que una velocidad algo mayor de 300 km s^{-1} (alta, pero no inusual en estrellas tipo A temprano) podría explicar el exceso de

flujo, lo que implica que la inclinación del eje de rotación de Vega sería de 4 grados o menos. Esta hipótesis es reforzada por el hecho de que el diámetro angular de esta estrella es mayor que el esperado para una estrella sin rotación (Hanbury Brown et al. 1967).

Además, los perfiles de sus líneas débiles vistos en alta resolución con alta S/R tienen su fondo claramente plano, mientras que las líneas profundas tienen perfiles ensanchados normales (Gulliver et al. 1991). Gulliver et al. (1994) estudiaron en detalle el efecto de la rotación rápida sobre el espectro de Vega. Ajustando el espectro sintético al observado entre 1200 y 10500 Å con baja dispersión, fijando la velocidad de rotación proyectada a partir del valor obtenido de las líneas ($v_{\rm equat} \cdot \sin\, i = 21.8$ km s^{-1}), obtuvieron la inclinación del eje de rotación, la temperatura efectiva y la gravedad superficial ecuatorial y polar. La calidad del ajuste para el modelo con rotación rápida es tan bueno como usando el modelo de Kurucz preferido en Castelli & Kurucz (1994) excepto en la region 2850-3700 Å, donde el modelo del rotor rápido mejora el ajuste. Gulliver et al. (1994) también ajustaron dos líneas con perfiles planos en el fondo, con una calidad del ajuste mucho mejor que usando modelos sin rotación. Estos valores son compatibles con los obtenidos ajustando el continuo si usamos estimaciones realistas de los errores, según los autores.

Finalmente, imágenes recientes en alta resolución en el IR medio y lejano del disco de polvo de Vega desde el satélite *Spitzer* (Su et al. 2005) muestran un disco circular, suave y mayor de lo que se pensaba, apoyando la hipótesis de Vega como un rotor rápido con un polo casi apuntando hacia la Tierra.

Cap. 2: Datos atómicos y herramientas para estudiar espectros

- Modelos de atmósfera:

  Hemos basado nuestros análisis espectroscópicos en los modelos de atmósfera desarrollados por Kurucz (1979, 1993) y Castelli & Kurucz (2003). Éstos forman una malla definida por tres parámetros: la temperatura efectiva (T_{eff}), la gravedad superficial (g) y la metalicidad. Contienen las aproximaciones de atmósfera homogénea y plano-paralela y equi/-li/-brio termodinámico local (ETL) y tienen en cuenta el "line-blanketing". También consideran la convección mediante la teoría de la longitud de mezcla.

  Se incluyen las opacidades de 58 millones de líneas atómicas y moléculas diatómicas. Las funciones de distribución de las opacidades de las líneas se usan como entrada para el programa que calcula los modelos de atmósfera, llamado ATLAS9, que se distribuye con el CD-ROM número 13. Para cada profundidad, se muestran la temperatura, la presión, y las densidades de electrones y de partículas.

  La metalicidad M/H de un modelo de atmósfera implica que todos los elementos con Z>2 están acoplados con el hierro (Fe) en proporciones solares. Se supone normalmente que [M/H] = [Fe/H], con el significado habitual del corchete en Astrofísica. Sin embargo, la abundancia de Fe en el Sol usada en los modelos de Kurucz (1993) fue adoptada de Anders & Grevesse (1989): $\log \epsilon_{\mathrm{Fe,Kurucz}} = 7.67 \pm 0.03$ y es diferente al valor meteorítico, que es la abundancia fotosférica solar que usamos en las síntesis: $\log \epsilon_{\mathrm{Fe,meteorítica}} = 7.51 \pm 0.01$, así que obtenemos: [M/H] = [Fe/H] − 0.16, donde [Fe/H] ya (y en adelante) no es la metalicidad escrita en los modelos de atmósfera, sino la abundancia de Fe comparada con la solar usada en las síntesis espectrales para ser compatible con la abundancia de Fe usada en los modelos de atmósfera.

  Se supone una microturbulencia de 2 km s^{-1} en los modelos. Además, hay errores sistemáticos en los modelos más fríos porque las opacidades de las líneas moleculares no se incluyen, excepto algunas diatómicas. En algunos casos, hemos calculado flujos usando nuevos modelos de atmósfera (Castelli & Kurucz 2003) calculados sin "overshooting" (ODFNEW; Castelli, Gratton & Kurucz 1997) para comprobar su efecto sobre los colores. Hay otra malla de modelos de atmósfera (NextGen; Hauschildt, Allard & Baron 1999) para 3000 K $\leq T_{eff} \leq$ 10000 K que usa distintas

ecuaciones de estado y distinto tratamiento de las opacidades moleculares. Una comparación entre estos modelos y los de Kurucz (Bertone et al. 2004) concluye que los parámetros atmosféricos obtenidos al ajustar espectros sintéticos a observados son en general más similares al usar modelos de Kurucz que al usar NextGen. Otra malla importante es la de OSMARCS (Gustafsson et al. 1975; Bell et al. 1976), con modelos de atmósfera estáticos y con simetría esférica en ETL para estrellas frías y para estrellas pobres en metales. Finalmente, se han desarrollado modelos de atmófera 3D dependientes del tiempo, inhomogéneos, en ETL (Asplund et al. 2000), que no contienen parámetros libres ajustables. Los modelos de atmósfera más apropiados para nuestro trabajo son los de Kurucz, como explicamos en la tesis comparándolos con los demás modelos.

- Síntesis espectral:

  Los cálculos de los flujos sintéticos se hicieron con el programa SYNPLOT, un programa para IDL de los códigos SYNSPEC (Hubeny & Lanz 2000, que calcula el espectro emitido por una atmósfera estelar) y ROTINS (que calcula el ensanchamiento rotacional e instrumental). El programa SYNSPEC supone que introducimos el modelo de atmósfera; o es calculado por TLUSTY (Hubeny & Lanz 2003), usado en este trabajo para calcular poblaciones de los niveles sin suponer ETL, o tomado de la literatura, como la malla de modelos de atmósfera de Kurucz (Kurucz 1992). El programa lee una lista de líneas general y selecciona líneas que contribuyen a la opacidad total, basándose en los parámetros físicos del modelo de atmósfera. SYNSPEC resuelve después la ecuación de transporte radiativo, para cada longitud de onda, en una región y con una resolución en longitud de onda específica.

  Para la opacidad del continuo se consideraron las siguientes fuentes: fotoionización y opacidad libre-libre de los iones que más contribuyen a la opacidad y la dispersión por electrones. Aunque las fuentes de opacidad al calcular un modelo de atmósfera y al calcular el espectro detallado deberían ser idénticas, los modelos de atmósfera en no-ETL fueron calculados con menos fuentes de opacidad, ya que la estructura atmosférica está influida sobre todo por las fuentes de opacidad más fuertes, mientras que el espectro emergente debe calcularse en detalle.

  El resultado consiste en el flujo emitido medido en la superficie de la estrella (más concretamente, el primer momento de la intensidad específica, H_ν) entre las longitudes de onda especificadas y la identificación de las líneas cuando se indica. El flujo astrofísico es $F = 4H$, y el flujo físico (el

que usamos) es $F = 4\pi H$.

- Datos atómicos y listas de líneas:

  Para interpretar adecuadamente las observaciones necesitamos opacidades realistas. Las secciones eficaces de fotoionización se toman de TOPBASE (Cunto et al. 1993, del Opacity Project) para las especies más importantes. Estos datos son precisos, aunque la posición exacta de la resonancia predicha es incierta, por lo que se suavizan las secciones eficaces a la resolución adecuada (ver Bautista, Romano & Pradhan 1998, y Allende Prieto et al. 2003), mejorando la estimación de la opacidad total. Para algunas especies no incluidas en la nueva librería de TOPBASE, se han usado modelos atómicos MODION (ver `http://tlusty.gsfc.nasa.gov/`), que contienen estructuras desde muy simples hasta bastante completas de algunos iones, de donde hemos tomado: H I, He I, C II, N I, O II y Si I.

  La opacidad de las líneas es también importante y hay que considerar millones de ellas para modelar con precisión la forma del espectro UV de las estrellas de tipo tardío. Comparamos diferentes fuentes para los datos de las líneas atómicas, y usamos una lista basada en datos compilados por Kurucz y distribuida con SYNPLOT, ya que proporciona los mejores resultados, excepto en algunas líneas particulares, en las que hemos usado parámetros de ensanchamiento Stark actualizados extraídos de VALD (*Vienna Atomic Line Database*, Kupka et al. 1999). Las constantes de ensanchamiento por colisiones con H neutro (un contribuyente importante a la anchura de las líneas) están también en VALD con secciones eficaces muy precisas (ver, por ejemplo, Barklem, Piskunov & O'Mara 2000).

  Además de las secciones de fotoionización, se necesitan los ritmos radiativos al hacer cálculos en no-ETL. Las probabilidades de transición radiativa fueron adoptadas de la base de datos NIST[1], y complementadas con los cálculos del Opacity Project. Los ritmos colisionales necesarios se calcularon basándose en fórmulas generales debidas a van Regemorter (1962), Mihalas (1972) y Auer & Mihalas (1973), complementadas con datos de laboratorio cuando estaban disponibles (Nahar & Pradhan 1997; Nahar 1999). La mayoría de los datos necesarios ya habían sido compilados previamente.

- Método de minimización:

  Hemos usado la rutina Amoeba de IDL para la minimización de χ^2. Este método lleva a cabo una minimización multidimensional de una función

[1] `http://physics.nist.gov/cgi-bin/AtData/main_asd`

Func(x), donde x es un vector de n dimensiones, usando el algoritmo de Nelder-Mead *downhill simplex* (Nelder & Mead 1965), que no requiere evaluaciones de derivadas, sino tan sólo de la función. Se han realizado estudios sobre su convergencia y se ha descubierto que, para algunas funciones convexas, el método converge a un punto que no es el mínimo (McKinnon 1998), pero en general se comporta adecuadamente para nuestro estudio.

El método utiliza una figura geométrica llamada *simplex*, en N dimensiones, con N+1 puntos (o vértices) y todos sus segmentos, caras, etc. de interconexión. Evalúa la función a minimizar en cada punto y obtiene un nuevo *simplex*, buscando nuevos puntos donde la función sea menor. El resultado es un vector de n dimensiones en el que la función es mínima con una incertidumbre que introducimos en el programa.

Cap. 3: Espectros observados

- Espectros observados de Vega:

  - Espectros UV:

    Como el Telescopio Espacial Hubble (HST) no ha tomado espectros que cubran una región grande del UV cercano, hemos usado en este trabajo espectros tomados por el IUE. Hemos considerado tres espectros promedios de calibraciones de Vega en baja resolución y gran apertura observados por el satélite IUE:

    - calibración de Bohlin (Bohlin 1996): obtenida de la página Web de CALSPEC. Se utilizan ocho estrellas estándar (entre ellas, cuatro enanas blancas de H puro, DAs) para calibrar los espectros de FOS, que estaba a bordo del HST. Se determina un factor corrector de los flujos de IUE para cada longitud de onda para pasarlos a la escala de flujo de FOS-HST.
    - calibración de M&F (Massa & Fitzpatrick 2000, en adelante M&F): tiene en cuenta errores sistemáticos de los espectros de NEWSIPS con el tiempo de observación y la temperatura de la cámara amplificadora para pasar los datos a la escala del HST.
    - INES: no es una calibración de datos de IUE procesados con NEWSIPS (véase Garhart et al. 1997), sino un nuevo procesado de los datos crudos. Los flujos relativos fueron calibrados usando una enana DA, G191B2B, fácil de modelar por tener un espectro casi libre de rasgos. La escala absoluta de flujo es la del satélite UV OAO-2 (González-Riestra, Cassatella & Wamsteker 2001).

    Las tres versiones anteriores tienen una resolución espectral de ~ 6 Å. Hemos combinado varios espectros de IUE de los servidores de INES[2] y de MAST[3], para producir las versiones de INES y M&F, respectivamente, usando los espectros individuales de la tabla 3.1. El espectro de Bohlin se obtuvo directamente de la página Web de STScI, proporcionada por R. Bohlin[4].

    Observamos que los flujos de Bohlin y de M&F (en la misma escala de flujo) son ~ 10 % mayores que los flujos de INES para Vega, mayor que la diferencia global de González-Riestra, Cassatella &

[2] http://ines.vilspa.esa.es/ines/
[3] http://archive.stsci.edu/iue/
[4] ftp://ftp.stsci.edu/cdbs/cdbs2/calspec/

Wamsteker (2001) para la estrella de referencia G191B2B aunque consistente dentro de las barras de error. Sin embargo, en este artículo se habla de una reducción casi lineal de la diferencia de flujos de $\sim$ 7 % en 1500 Å a $\sim$ 6 % en 3000 Å, mientras que en Vega encontramos mayor variación. También obtenemos que el flujo de M&F es mayor que el de Bohlin a $\sim$ 1800 y $\sim$ 2000 Å, siendo la mayor incertidumbre del flujo de IUE a $\sim$ 2000 Å por ser el borde de las cámaras de longitud de onda corta y larga la posible causa de la diferencia a esta longitud de onda.

También hemos comparado los flujos de Bohlin e INES para las ocho estrellas estándar en las que se basan los flujos de Bohlin. Obtenemos de nuevo un flujo mayor de INES para todas las longitudes de onda para todas las estrellas, excepto para el espectro SWP de BD +75 325. La diferencia media de flujos para las otras siete estrellas es $(F_{Bohlin}-F_{INES})/F_{INES} = 0.066\pm0.013$, consistente con las diferencias globales de González-Riestra, Cassatella & Wamsteker (2001), aunque en el caso anterior hay mayor variación en la diferencia de flujos respecto a la longitud de onda.

Por último, hemos comparado flujos sintéticos con espectros de alta resolución de IUE (véase la tabla 3.1) calibrados por INES (los únicos disponibles), con una cobertura espectral grande y una resolución de $\sim$ 0.2 Å.

– Espectros visibles e IR cercanos:

Para el estudio del espectro de Vega usando modelos de atmósfera clásicos, consideramos el espectro de baja dispersión compilado por Hayes (1985) combinando seis fuentes diferentes de medidas tomadas desde tierra. Este espectro tiene una incertidumbre de flujo de 1-2% en el visible y cubre de 3300 a 10500 Å con una resolución de 50 Å.

Para estudiar el espectro de Vega usando modelos de rotación rápida, hemos usado el espectro tomado recientemente con el espectrógrafo STIS del HST. El flujo absoluto se midió con gran precisión desde el UV cercano hasta el IR cercano en la escala de flujo de HST (Bohlin & Gilliland 2004). Es un espectro de baja dispersión (R $\sim$ 500) con una relación señal a ruido muy alta (S/R $\sim$ 1000).

Hemos usado dos espectros de alta dispersión distintos, tomados por nuestro grupo en el Observatorio McDonald (Mount Locke, Texas), usando el espectrógrafo echelle de dispersión cruzada *2dcoudé* (Tull et al. 1995) acoplado al Telescopio Harlan J. Smith de 2.7m. El primer espectro tiene un poder resolutivo ($R \equiv \frac{\lambda}{\delta\lambda}$) de $\sim 5 \times 10^4$,

cubriendo toda la región visible, extendiéndose hasta el IR cercano. El segundo espectro tiene R $\sim$ 173 000, cubriendo de $\sim$ 4400 a $\sim$ 7600 Å con algunos pequeños huecos.

Una cuidadosa reducción de datos fue aplicada a ambos espectros, usando IRAF [5], que consistía en corrección de "overscan" ("bias") y sustracción de luz dispersada, "flatfielding", extracción de espectros en una dimensión, calibración en longitud de onda y normalización del continuo.

- Espectros observados de Proción:

  – Espectro UV cercano:

  Hemos usado datos espectroscópicos adquiridos por nuestro grupo con STIS, que han sido calibrados en flujo con mucha precisión (Bohlin, Dickinson & Calzetti 2001). Se usaron las rendijas G230MB (con seis inclinaciones que proporcionaban una cobertura de $\sim$2200 a $\sim$3050 Å) y G430M (con cuatro inclinaciones que cubrían el espectro desde 3022 hasta poco más de 4000 Å) para realizar observaciones con resolución intermedia de Proción.

  Usando los espectros proporcionados por HST, creamos un sistema de coordenadas de longitud de onda con la misma resolución que el espectro observado y corregido el efecto de las diferentes velocidades radiales para cada observación. Luego interpolamos los espectros a este sistema de coordenadas, promediando los espectros cuando había solapamiento.

  – Espectros visibles:

  Hemos encontrado los siguientes catálogos espectrofotométricos que contuvieran datos de Proción:

  - el Catálogo Espectrofotométrico de Pulkovo de Estrellas Brillantes (Alekseeva et al. 1996, en adelante "espectro de Pulkovo"), con una cobertura de 320 a 1080 nm, una resolución de 5 nm y una precisión no inferior a 1.5-2.0 %,

  - el Catálogo Espectrofotométrico de Sternberg (Glushneva et al. 1984, en adelante "espectro de Sternberg"), que cubre la región de 3225 a 7625 Å con un paso de 50 Å. La precisión media de los datos

[5] IRAF is distributed by the National Optical Astronomy Observatories, which are operated by the Association of Universities for Research in Astronomy, Inc., under cooperative agreement with the National Science Foundation

del catálogo es del 3.2 %,

- el Catálogo Espectrofotométrico de Estrellas de Burnashev (Burnashev 1985), que contiene espectros en la región espectral 320-817 nm en pasos de 2.5 nm.

Hemos comparado los diferentes espectros visibles de Proción entre 3500 y 4050 Å (incluyendo el espectro de HST para discriminar entre ellos). La diferencia en flujo absoluto entre algunos de estos espectros visibles es grande, así que tratamos de escoger uno comparando los flujos con el del HST en la región de solapamiento. El mejor ajuste se obtiene para los flujos de Burnashev y Glushneva, así que hemos usado la media de ambos como espectro visible observado.

Aunque el atlas fotométrico de Griffin & Griffin (1979) cubre una amplia región espectral (de 3140 a 7470 Å), hemos usado el espectro visible de Allende Prieto et al. (2002) como espectro de alta resolución de Proción para derivar abundancias a partir de las líneas espectrales, ya que tiene mejor S/R y está disponible en la red. Este espectro fue obtenido con el telescopio Harlan J. Smith de 2.7 m. del Observatorio McDonald el 30 y 31 de enero de 1999. Tiene un poder resolutivo de R $\sim 2 \times 10^5$ y cubre la región de 4559 a 5780 Å. Se juntaron diferentes exposiciones para alcanzar una S/R en el rango 550-2000.

– Espectro IR cercano:

  Para el espectro rojo e IR cercano (longitudes de onda > 6600 Å), se ha usado el Catálogo Espectrofotométrico de Moscú (Glushneva et al. 1991). Cubre la región de 5975 a 10825 Å, con un paso de 50 Å. Este espectro ajusta muy bien al espectro visible observado en casi toda la zona de solapamiento.

Cap. 4: El estudio del espectro de Vega usando modelos de atmósfera clásicos

- Principales contribuyentes a la opacidad del continuo y de las líneas en Vega:

  Con unos pocos elementos se puede dar cuenta de la mayor parte de la opacidad en el UV, dominada por las líneas de Fe para casi todos los tipos espectrales y por la opacidad del continuo de algunos metales, que varían según sea el tipo espectral. La contribución de un ion a la opacidad ligado-libre depende de su estructura atómica y de su abundancia. Como paso preliminar, hemos hallado la abundancia de los 30 primeros elementos en sus 3 primeros estados de ionización para una estrella como Vega, usando el modelo preferido por Castelli & Kurucz 1994 (T_{eff} = 9550 K y log g = 3.95) usando las ecuaciones de Saha y Boltzmann. Hemos supuesto abundancias fotosféricas solares de Anders & Grevesse (1989).

  A continuación, hemos calculado espectros sintéticos visibles y UV cercanos que incluían la opacidad producida sólo por H y espectros incluyendo además la opacidad del continuo de cada uno de los iones con abundancias relativas al H mayores de 10^{-6}: He I, C II, N I, N II, O I, O II, Na II, Mg II, Al II, Si II, S II, Ca II, Fe II y Ni II. Hemos usado abundancias solares para cada elemento excepto el Fe, ya que hemos adoptado inicialmente [M/H] = −0.5 (y por tanto [Fe/H] = −0.34). Comparamos entre sí los espectros derivados incluyendo distintos iones, deduciendo así la relevancia de la opacidad del continuo de cada ion respecto a los flujos observados. La absorción ligado-libre y la de las líneas del H dominan la opacidad a longitudes de onda menores que Lα. Para longitudes de onda mayores que unos 1500 Å, el H neutro y el ion H^- dominan la opacidad ligado-libre. Si y C contribuyen significativamente a la opacidad del continuo entre 1200 y 1450 Å, mientras que los demás iones producen una disminución del flujo inferior al 1.5 % en todas las regiones.

  En cuanto a la absorción de las líneas debidas a cada ion, domina la del Fe II, siendo más o menos la mitad de la absorción total de las líneas para Vega. En conclusión, para modelar el espectro UV de una estrella como Vega es necesario tener en cuenta las opacidades de H, C, Si y Fe detalladamente.

- Estimación de la temperatura efectiva y el diámetro angular (D_{ang}) de Vega usando las regiones visible y UV e IR cercana:

A continuación, intentamos determinar T_{eff} y D_{ang} a partir del espectro visible, UV cercano e IR cercano, tomando la gravedad obtenida a partir de datos de *Hipparcos*: $\log g = 3.98 \pm 0.02$ (Allende Prieto & Lambert 1999). Para ello, hemos comparado el flujo calculado a partir de modelos de Kurucz (convertido en flujo recibido usando D_{ang}) respecto al flujo observado. En estas regiones, la absorción de los metales es pequeña, por lo que se pueden calcular estos dos parámetros independientemente de la composición química.

Hemos realizado un ajuste χ^2 entre los espectros observados y calculados en tres regiones espectrales: entre 1600 y 2150 Å, entre 2200 y 3000 Å y entre 4150 y 8480 Å, excluyendo las líneas de Balmer. Hemos pesado cada χ^2 según la incertidumbre aproximada de los flujos observados. Usando SYNSPEC, hacemos una malla interpolando los flujos obtenidos usando modelos de Kurucz con T_{eff}'s distintas. Hemos excluido las regiones donde hay dificultades especiales, como cerca del salto de Balmer (3000-4150 Å), porque Hayes avisa sobre errores significativos en esta región y el efecto de la rotación es importante (Gulliver et al. 1994). En esta fase se usaron las abundancias de Qiu et al. (2001) y [Fe/H] = −0.54. Los pares (T_{eff},D_{ang}) de los mejores ajustes se muestran en la Tabla 4.1. El ajuste es claramente mejor usando la calibración de Bohlin que usando la de INES. Observamos que no hay ningún modelo de atmósfera que reproduzca bien a la vez el espectro visible y el UV calibrado por INES, pero sí lo hay al considerar la calibración de Bohlin. Además, como se ve en la Tabla 4.1, los valores de T_{eff} y D_{ang} de la literatura son casi siempre consistentes con los de la calibración de Bohlin, pero no con los valores obtenidos con la calibración de INES. Como la calibración de M&F está en la misma escala de flujo que la de Bohlin, hemos tomado como espectro UV la media de las calibraciones de Bohlin y de M&F.

Usando el flujo anterior y ajustando la región espectral entre 2200 y 8500 Å (sin incluir la zona de 3000 a 4150 Å ni las líneas de Balmer), obtenemos el resultado siguiente:
$T_{eff} = 9620^{+49}_{-63}$ K, $D_{ang} = 3.27 \pm 0.05$ mas,
donde las barras de error fueron derivadas perturbando los parámetros del mejor ajuste hasta que la variación de flujo excediera las barras de error asignadas al espectro observado.

Se llevó a cabo el mismo análisis usando nuevos modelos de atmósfera (Castelli & Kurucz 2003) calculados sin "overshooting", con funciones de distribución de opacidad revisadas (ODFNEW), para chequear el efecto sobre los colores del "overshooting" convectivo, obteniendo:

T_{eff} = 9575 K, D_{ang} = 3.271 mas,
con un ajuste ligeramente mejor y valores consistentes con los de la literatura. Adoptando T_{eff} y [M/H] obtenidos usando el Método del Flujo Infrarrojo (Alonso, Arribas & Martínez-Roger 1994), buscamos el valor de D_{ang} para el mejor ajuste al espectro observado en el UV cercano y visible, obteniendo de nuevo 3.27 mas.

Hemos calculado el flujo en alta resolución en tres regiones espectrales seleccionadas al azar entre 1550 y 3050 Å, donde los efectos de la rotación rápida y de la opacidad del continuo del Si y el C sobre el flujo son muy limitados. Se han usado los parámetros en baja resolución derivados comparando espectros sintéticos usando modelos de Kurucz con el espectro observado, obteniendo una desviación estándar aproximadamente el doble que las del espectro de baja resolución, pero el espectro sintético reproduce la forma del espectro observado bastante bien.

Hemos realizado un test preliminar del efecto de la rotación rápida sobre el flujo de Vega y la calidad del ajuste de este espectro al observado en torno a la línea O I λ6158.19 Å, obteniendo un buen ajuste con los parámetros preferidos por Gulliver et al. (1994).

- Estimación de las abundancias de Si y C a partir del continuo UV:

  Vimos en este capítulo que los principales contribuyentes a la opacidad del continuo en el UV para Vega son Si y C. Usando los parámetros atmosféricos derivados en la sección anterior, intentamos derivar las abundancias de Si y C usando el flujo UV. Para ello, hemos calculado una malla de espectros sintéticos de 1270 a 1380 Å y de 1460 a 1550 Å con distintas abundancias de C y de Si. El mejor ajuste se obtiene con [Si/H] $= -0.90^{+0.57}_{-2.10}$ y [C/H] $= 0.03^{+0.34}_{-0.48}$, con una desviación cuadrática media $\sigma = 3\%$, aproximadamente la incertidumbre del espectro UV observado. Las fuentes de error más relevantes son la incertidumbre en la abundancia de He (supuesta ± 0.1 dex) y en T_{eff}. Los valores obtenidos por Qiu et al. (2001) a partir del análisis de líneas visibles fueron [Si/H] $= -0.59 \pm 0.06$ y [C/H] $= -0.06 \pm 0.13$.

  Las grandes barras de error en las abundancias obtenidas a partir del continuo UV se deben a la respuesta débil del continuo UV a cambios en las abundancias de los metales debido al papel predominante de la opacidad del hidrógeno en una atmósfera tan templada. Además, hay regiones donde no podemos obtener un ajuste bueno, lo que impide derivar con precisión abundancias por este método. Algunas de las discrepancias están asociadas con líneas de Si I y C I profundas (por ejemplo, a $\sim$ 1560

Å y $\sim$ 1660 Å), que mejoran al introducir el efecto del no-ETL, no tenido en cuenta por nuestros modelos. Sin embargo, hay líneas profundas de otras especies (como el Fe II) que se reproducen bien en ETL. También se observa un mal ajuste entre 1380 y 1460 Å, cuya razón no está clara. Respecto a las líneas de Balmer, el ajuste mejora mucho al usar el flujo revisado de Vega basado en espectros de STIS (Bohlin & Gilliland 2004).

- Estimación de las abundancias a partir de líneas espectrales del visible:

  Para hacer una comparación consistente entre las abundancias UV y las obtenidas a partir de líneas de la región visible, hemos seleccionado una serie de líneas con incertidumbre del log gf $\leq$ 25 % tomadas de Przybilla (2002). Hemos excluido las líneas de He porque son demasiado débiles, y el doblete resonante de Na I ya que el efecto del no-ETL en el *core* de estas líneas es importante. Hemos calculado las anchuras equivalentes (AE) integrando el flujo de las líneas y hemos considerado parámetros de ensanchamiento clásicos.

  En las tablas 4.4 y 4.5 se muestra AE para cada línea espectral y las abundancias derivadas usando distintos modelos de atmósfera. La diferencia media de $\sim$ 0.1 entre las abundancias de Fe obtenidas a partir de líneas de Fe I y Fe II puede deberse a los efectos del no-ETL en la formación de las primeras.

  Usando las abundancias obtenidas a partir de las líneas espectrales, encontramos la abundancia media de cada elemento. Encontramos que las abundancias de C, N y O para Vega son similares a las del Sol, mientras que las de Mg, Al, Si, Ca, Cr y Fe están entre -0.3 y -0.7 dex comparadas con la solar, consistente con Vega como estrella λ Boo suave.

Cap. 5: El estudio del espectro de Proción usando modelos de atmósfera clásicos

- Principales contribuyentes a la opacidad en Proción:

  Se ha llevado a cabo con Proción un proceso muy parecido al de Vega para determinar los principales contribuyentes a la opacidad del continuo. Hemos usado un modelo de atmósfera de Kurucz con los primeros parámetros propuestos por Allende Prieto et al. (2002), con $T_{eff} = 6512$ K y $\log g = 3.96$, para calcular las abundancias de los 30 primeros elementos en sus tres primeros estados de ionización usando las ecuaciones de Saha y de Boltzmann. Hemos supuesto abundancias fotosféricas solares (Anders & Grevesse 1989), excepto para el Fe, para el que hemos adoptado [Fe/H] $= -0.05$. Obtenemos los siguientes iones con abundancias relativas a H mayores que 10^{-6}: He I, C I, N I, O I, Ne I, Na II, Mg I, Mg II, Al I, Si I, S I, A I, Ca II, Fe I, Fe II y Ni I.

  Después, comparamos los flujos UV cercano y visible incluyendo la opacidad del continuo producido sólo por H con la opacidad producida por H y cada uno de los iones más abundantes en Vega, obteniendo la importancia de la opacidad del continuo para cada ion. Para longitudes de onda menores que ~ 2150 Å, vemos que el H neutro, el ion H^-, el Fe I y el Mg I dominan la opacidad ligado-libre, pero para $\lambda > 3000$ Å sólo son importantes los iones de H. A longitudes de onda más cortas, los siguientes iones disminuyen el flujo en más del 0.5 %: C I, Si I, Ca I y Al I.

- Estimación de la temperatura efectiva y el diámetro angular:

  Como hicimos para Vega, hemos fijado la gravedad y la metalicidad de los modelos de atmósfera de Kurucz en nuestros primeros cálculos a los valores de Allende Prieto et al. (2002; $\log g = 3.96$ y [M/H] $= -0.21$, teniendo en cuenta que [Fe/H] $= -0.05$) y hemos hallado T_{eff} y D_{ang} a partir de las observaciones en el IR cercano y el visible. Para ello, hemos calculado una malla de flujos emitidos usando modelos de Kurucz con distinta T_{eff}, transformados en flujos recibidos usando D_{ang}. Éstos los hemos comparado con flujos observados en regiones donde la absorción debida a metales es pequeña, lo que nos permite obtener T_{eff} y D_{ang} independientemente de la composición química.

  Hemos usado tres regiones espectrales en los cálculos: de 3200 a 3800 Å, de 5300 a 6500 Å y de 6600 a 8800 Å, cada una con el mismo peso en el ajuste. No incluimos la región de 3800 a 5300 Å porque no hemos podido ajustarla al espectro observado, y tampoco por debajo de 3200 Å porque

la absorción ligado-libre debido a iones metálicos es importante. Hemos minimizado la χ^2 de la diferencia entre el flujo sintético y el observado, obteniendo los siguientes parámetros: $T_{eff} = 6590^{+61}_{-56}$ K y $D_{ang} = 5.47 \pm 0.08$ mas, con una desviación estándar total $\sigma = 1.45$ %. Usando la paralaje medida por *Hipparcos*, obtenemos una distancia d = 3.497 ± 0.011 pc. Si usamos este valor y nuestro diámetro angular, obtenemos el siguiente radio para Proción: $R = 2.056 \pm 0.018\ R_{\odot}$. Introduciendo la masa derivada por Allende Prieto et al. (2002), obtenemos la siguiente gravedad superficial: $\log g = 3.96 \pm 0.06$, consistente con el valor adoptado.

Al comparar nuestros parámetros con los obtenidos por otros autores, se observa que nuestro D_{ang} es compatible con todos los demás valores. El valor de T_{eff} obtenido usando el método del flujo IR es compatible con nuestro resultado. Los otros dos valores no parecen ser compatibles, aunque tres de los valores de flujo bolométrico que usan (véase Fuhrmann et al. 1997) son mucho más viejos que el otro y posiblemente no son muy precisos. Si usamos el diámetro angular de Kervella et al. (2004), T_{eff} se transformaría de 6530 a 6566 K, bastante próximo a nuestro valor.

También es importante tener en cuenta las correcciones en el radio y el diámetro angular que se obtienen al usar simulaciones 3D, debido a los diferentes oscurecimientos del limbo (OL) resultantes. Por ejemplo, Allende Prieto et al. (2002) encuentran que el cambio en OL al usar simulaciones 3D produce una disminución del diámetro angular y un incremento de T_{eff} para Proción, además de cambiar la distribución espectral de energía, que podría explicar la incapacidad de nuestros modelos para reproducir el espectro en algunas regiones, como entre 3800 y 5300 Å.

Hemos calculado un espectro de resolución intermedia de Proción entre 3200 y 3800 Å a partir del espectro de alto poder resolutivo del atlas UV (ver Apéndice). Hemos usado los parámetros estelares recién obtenidos, con abundancias solares para los elementos distintos del hierro. Al comparar el espectro sintético con el observado en tres zonas de la región mencionada escogidas al azar, obtenemos desviaciones estándar no mucho mayores (aproximadamente el triple) que las del espectro de baja resolución.

- Estimación de abundancias químicas a partir del continuo UV:

  Hemos visto que los contribuyentes más importantes a la opacidad del continuo UV por encima de 2150 Å para Proción son el Mg y el Fe. Con los parámetros estelares adoptados, determinamos las abundancias

de estos elementos usando el flujo UV. Hacemos una malla de flujos entre 2200 y 3000 Å con distintos valores de las abundancias de Mg y de Fe.

Al no considerar algunas regiones con problemas excepcionales, obtenemos el mejor ajuste al espectro observado para [Mg/H] = $0.00^{+0.37}_{-0.26}$ y [Fe/H] = -0.04 ± 0.17, con $\sigma_{\rm rms} = 10\%$. Al usar toda la región de 2200 a 3000 Å, se obtiene el mejor ajuste con: [Mg/H] = $0.00^{+0.37}_{-0.26}$ y [Fe/H] = -0.16 ± 0.17, con $\sigma_{\rm rms} = 20\%$. Las barras de error tienen en cuenta la incertidumbre en el flujo observado, supuesto del 3%, en las regiones con mayor sensibilidad a cambios en la abundancia, que son entre 2200 y 2400 Å para el Mg y entre 2650 y 3000 Å para el Fe.

También hemos estimado el efecto sobre el flujo de un cambio en $T_{\rm eff}$ y la abundancia de Fe (consistente con la metalicidad del modelo de atmósfera). Obtenemos un incremento casi uniforme del flujo al aumentar $T_{\rm eff}$, mientras que al aumentar la abundancia de Fe el flujo se incrementa en algunas regiones y disminuye en otras, aumentando la diferencia entre los máximos y mínimos de flujo.

- Estimación de abundancias químicas a partir de líneas espectrales en la región visible:

  Volvemos a calcular las abundancias de forma independiente para garantizar que el análisis es totalmente consistente con nuestro estudio UV. Se han estudiado los siguientes iones: Mg I, Cr I, Cr II, Mn I, Fe I y Fe II. Hemos medido AE para estas líneas (con el código MOOG) usando el atlas fotométrico del espectro de Proción (Griffin & Griffin 1979), excepto para las líneas de Fe, para las que hemos usado las AE de Allende Prieto et al. (2002). Observamos que las abundancias derivadas a partir de las líneas son compatibles con las obtenidas por otros autores y con las obtenidas a partir del continuo UV.

Cap. 6: El estudio del espectro de Vega usando modelos estelares con rotación rápida

- Modelos estelares con rotación rápida:

  Hemos desarrollado un método para calcular el flujo de Vega teniendo en cuenta las desviaciones de la simetría esférica debidas a la rotación, usando las mismas suposiciones que Pérez Hernández et al. (1999). Se considera una velocidad de rotación angular constante y el potencial gravitatorio de un punto con la misma masa, por lo que la superficie de la estrella resulta ser una superficie de Roche, lo que simplifica el modelado de la estrella.

  Se definieron algunas cantidades normalizadas que sólo dependen de la colatitud θ. Estas son:

  - el *radio relativo*, definido como $x(\theta) = \mathrm{R}(\theta)/\mathrm{R_p}$.
  - la *gravedad efectiva*, definida como $g_n(\theta) \equiv \frac{\mathrm{R_p^2}}{\mathrm{GM}} g(\theta)$.
  - la *temperatura efectiva normalizada*, definida como $t_n^4(\theta) \equiv \frac{\mathrm{T_{eff}^4}(\theta)}{\mathrm{T_{polar}^4}}$.

  También se definió la *velocidad de rotación angular normalizada* como $\tilde{w} \equiv \frac{\Omega}{\Omega_c}$, donde la velocidad angular crítica se define como $\Omega_c^2 \equiv \frac{8\mathrm{GM}}{27\mathrm{R_p^3}}$. Para una estrella que gira a la velocidad crítica, $\mathrm{R_{equat}} = 1.5\ \mathrm{R_p}$. Usando la paralaje de Hipparcos y el diámetro angular que obtuvimos para Vega y suponiendo que un polo de la estrella apunta hacia nosotros, obtenemos $\mathrm{R_{equat}} = \mathrm{D_{ang}(rad)} \cdot \mathrm{d}/2 = 2.73 \pm 0.05\ \mathrm{R_\odot}$, mientras que para una estrella A0 V típica $\mathrm{R_{equat}} = 1.87\ \mathrm{R_\odot}$ (Gray 1992), lo que sugiere que Vega gira rápidamente.

  Para una estrella con una envoltura totalmente radiativa como Vega, la ley de oscurecimiento gravitatorio nos da la relación $t_n^4(\theta) = g_n(\theta)$. Después de algunos cálculos, obtenemos que el espectro recibido es:

$$\mathrm{F}(\lambda) = \frac{c}{\mathrm{d}^2 \cdot \lambda^2} L_\nu(\tilde{w}, i), \tag{1}$$

  donde L_ν viene dado (según la fórmula de Collins 1965) por:

$$L_\nu(\tilde{w}, i) = 2R_p^2 \int_0^{\pi/2} \int_0^{\pi} I_\nu(\theta, \phi) x^2(\theta) \sin\theta f(\theta, \phi) d\theta d\phi, \tag{2}$$

  donde I_ν lo calculamos con SYNSPEC y:

$$f(\theta, \phi) = \sin\theta \sin i \cos\phi + \cos\theta \cos i - \frac{8\tilde{w}^2 x^3(\theta) \sin\theta \cos\theta}{27 - 8\tilde{w}^2 x^3(\theta) \sin^2\theta} (\sin i \cos\phi \cos\theta - \sin\theta \cos i). \tag{3}$$

- Cálculos preliminares de parámetros estelares:

  En primer lugar, hemos hecho tests para calcular parámetros preliminares: la inclinación del eje de rotación con respecto a la línea de visión (i) y la temperatura polar (T_{polar}) de Vega. Para ello, hemos seleccionado 6 líneas espectrales que cubren un amplio rango de longitud de onda, sin solapamiento importante y con gran variedad de anchuras equivalentes, pero sin ser demasiado débiles ni demasiado profundas. Además, hemos incluido una línea de la región donde el efecto de la rotación rápida en el continuo es mayor según Gulliver et al. (1994): Ca II λ3158.87 Å. Hemos fijado [M/H] = -0.7 en los primeros modelos de atmósfera. Hemos usado la abundancia de He de Grevesse & Sauval (1998): N(He)/N(H) = 0.085 y el diámetro angular de García-Gil et al. (2005): D_{ang} = 3.27 mas, compatible con casi todos los valores de la literatura. Al comparar el flujo sintético usando un modelo sin rotación con los parámetros de nuestro mejor ajuste al flujo observado, obtenemos un flujo calculado mayor que el observado en un 4-5% para la línea de Ca, mientras que es menor en un 1-2% para las otras líneas, resultado similar al obtenido por Gulliver et al. (1994).

  Hemos calculado una malla de flujos sintéticos con distintos valores de i y T_{polar}, fijando las abundancias obtenidas a partir de las líneas con modelos de atmósfera clásicos (García-Gil et al. 2005), $v_{equat} \cdot \sin i$ = 23 km s^{-1} (Gray 1980), v_{turb} = 2.0 km s^{-1} (Castelli & Kurucz 1994) y un perfil gaussiano con FWHM = 0.2 Å, consecuente con la resolución del espectro observado. Hemos minimizado la χ^2 del ajuste entre el espectro sintético y el observado para cada línea (adoptando un error típico mayor para la línea de Ca), obteniendo: i = 6.59 grados y T_{polar} = 9576 K, con χ^2 = 0.092.

- Cálculo de parámetros del modelo:

  Usando los valores anteriores de i y T_{polar}, hicimos una malla de flujos junto a seis líneas de Fe con distintos valores de [M/H], de v_{turb} y de $v_{equat} \cdot \sin i$. Tres de estas líneas son relativamente profundas, así que la abundancia de Fe calculada a partir de ellas depende fuertemente de v_{turb}, mientras que las otras tres son más débiles, por lo que son menos dependientes de v_{turb}. A partir de las gráficas de la abundancia de Fe en función de la microturbulencia para cada línea, obtenemos: v_{turb} = 2.11 $\pm$ 0.13 km s^{-1} y log ϵ_{Fe} = 6.71, luego [M/H] = -0.96 ± 0.03. Fijando esos parámetros, obtenemos $v_{equat} \cdot \sin i = 21.65 \pm 0.32$ km s^{-1}.

- Cálculo de abundancias y nuevos valores de i y T_{polar}:

Usando los parámetros de la líneas hallados en la sección anterior, hemos calculado i,T_{polar} y las abundancias de Ca, O, Si y N de Vega. Para ello, hemos calculado una malla de flujos con distintos valores de los parámetros anteriores. Minimizando el valor de χ^2 del ajuste entre el espectro observado y el sintético, hemos obtenido: i = 5.33 grados y T_{polar} = 9802 K, con log ϵ_{Ca} = 5.86, log ϵ_O = 8.66, log ϵ_{Si} = 7.01 y log ϵ_N = 7.82, con χ^2 = 0.040.

Como el flujo del continuo calculado es distinto que el observado, sobre todo en el caso de la línea N I λ7442.30 Å, hemos determinado de nuevo las abundancias normalizando los flujos. Hemos obtenido: log ϵ_{Ca} = 5.77, log ϵ_O = 8.70, log ϵ_{Si} = 7.08 y log ϵ_N = 7.96. Usando estas abundancias, hemos calculado de nuevo los parámetros, obteniendo: i = 5.33 grados y T_{polar} = 9807 K, con χ^2 = 0.061. Estos valores implican v_{equat} = 233 km s^{-1}, T_{equat} = 8240 K, $\tilde{w}$ = 0.84, log g_{polar} = 4.08 y log g_{equat} = 3.77. Hay que destacar que el ajuste empeora poco al variar en 50 K la temperatura polar variando i de una manera determinada, como se muestra a continuación:

- para T_{polar} = 9757 K: i = 5.54 grados, con χ^2 = 0.066,
- para T_{polar} = 9857 K: i = 5.16 grados, con χ^2 = 0.065,

donde χ^2 es poco mayor que el del mejor ajuste.

- Comparación del resultado con el obtenido usando modelos clásicos:

  En el Cap. 4, calculamos abundancias químicas para Vega usando tanto líneas espectrales como usando el continuo UV utilizando modelos de atmósfera clásicos. Hemos comparado las abundancias relativas al Fe (para que sea consistente la comparación, ya que hemos usado distintos modelos estelares en cada caso) obtenidas a partir de líneas espectrales usando rotación rápida con las abundancias sin usar rotación. A partir de esta comparación, obtenemos los siguientes resultados:

  - las abundancias relativas de N y O son casi las mismas usando modelos con rotación rápida que usando modelos sin rotación,
  - hay una diferencia de 0.2-0.3 dex en las abundancias relativas de Si y Ca entre los modelos con rotación rápida (con mayor abundancia) y los modelos sin rotación.

  La comparación de temperaturas efectivas obtenidas con modelos con rotación rápida y sin rotación no es sencilla, ya que T_{eff} depende de θ para

modelos con rotación rápida. Se puede hacer un intento de comparación promediando T_{eff} obtenido con modelos de rotación rápida, pesándolo con el flujo y el área proyectada en la línea de visión:

$$< T_{eff} >= \frac{\int T_{eff}(\theta)\frac{dL}{d\theta}dS}{\int \frac{dL}{d\theta}dS} = \frac{\int_0^{\pi/2} T_{eff}(\theta)\frac{dL}{d\theta}\sin\theta\cos\theta\, d\theta}{\int_0^{\pi/2} \frac{dL}{d\theta}\sin\theta\cos\theta\, d\theta}. \qquad (4)$$

Con los valores de $T_{eff}(\theta)$ obtenidos para el mejor ajuste, obtenemos $< T_{eff} > = 9210$ K. Este valor es claramente menor que los obtenidos en la literatura. Sin embargo, al usar esta T_{eff} para calcular la anchura equivalente de las líneas utilizando un modelo de atmósfera sin rotación con las abundancias obtenidas con modelos de rotación rápida, los valores salen relativamente parecidos a los observados, por lo que $< T_{eff} >$ puede considerarse una aproximación razonable de T_{eff} de un modelo sin rotación necesario para reproducir las líneas espectrales observadas usando las abundancias obtenidas con modelos de rotación rápida.

Conclusiones y trabajo futuro

El trabajo principal de esta tesis ha sido el estudio cuantitativo de los espectros ultravioletas y visibles de Vega y Proción. Resumimos en este capítulo las principales conclusiones.

Hemos compilado espectros observados de Vega y Proción procedentes de archivos y los hemos complementado con nuevas observaciones. Para Vega, hemos considerado distintas calibraciones de los espectros UV de baja dispersión obtenidos con el satélite IUE. La comparación del flujo observado (teniendo también en cuenta el flujo visible e IR cercano) con nuestros cálculos, considerando en detalle las opacidades de los metales, favorece la escala de flujo del telescopio espacial Hubble (HST) frente a la de INES, ya que la calidad del mejor ajuste es claramente mejor en el UV para la primera escala. Como no hay espectros UV de alta dispersión en la escala del HST, hemos usado espectros en la calibración de INES corregida su escala de flujo a la del HST. Hemos usado el espectro de Hayes (1985), con una pequeña incertidumbre de flujo, como espectro visible de baja dispersión, y dos espectros tomados desde el Observatorio McDonald de Texas como espectros visibles de alta dispersión.

Para Proción, hemos obtenido nuevos espectros con STIS, a bordo del HST. Estos espectros tienen un mayor poder de resolución y una precisión espectrofotométrica similar a los datos espectrofotométricos UV disponibles para el Sol. Hemos comparado diferentes espectros visibles de Proción con el espectro de STIS para escoger entre ellos, concluyendo que los flujos de Burnashev y Glushneva son los más parecidos en la región de solapamiento, así que hemos usado la media de ambos como espectro visible de resolución intermedia. Hemos usado un espectro de alta dispersión tomado desde el observatorio McDonald para derivar abundancias a partir de las líneas espectrales. Para el IR, hemos adoptado el catálogo espectrofotométrico de Moscú, que muestra un flujo similar al espectro visible usado en la región de solapamiento.

Hemos identificado los contribuyentes principales a la opacidad del continuo en Vega comparando el flujo sintético usando los iones más abundantes con el flujo usando sólo H, obteniendo: H, H^-, C I y Si II. Estos iones (excepto el H y el H^-) sólo contribuyen significativamente a la opacidad en el UV para $\lambda < 1500$ Å. Teniendo esto en cuenta, hemos derivado la temperatura efectiva (T_{eff}) y el diámetro angular (D_{ang}) de Vega (adoptando la metalicidad y gravedad preferidas) comparando los flujos obtenidos usando distintos modelos de atmósfera con el espectro visible, IR cercano y UV cercano observados, obteniendo valores similares a los de la literatura.

Con los valores de T_{eff} y de D_{ang} derivados para Vega, hemos determinado

las abundancias de Si y de C comparando los flujos sintéticos con el observado en el UV en regiones donde la opacidad del continuo producida por estos elementos es importante. Entonces, hemos derivado estas y otras abundancias químicas a partir de líneas espectrales del visible, obteniendo un valor similar para el C. Sin embargo, la abundancia de Si obtenida es diferente, lo que puede deberse a la gran incertidumbre de esta abundancia al derivarla a partir del continuo.

Hemos llevado a cabo un estudio similar de Proción A. Como esta estrella tiene menor $T_{\rm eff}$, es mayor el efecto de la opacidad de los metales sobre su flujo emitido. Usando el método de Vega, encontramos que las especies que más contribuyen a la opacidad del continuo UV son: H, H^-, C I, Mg I, Al I, Si I, Ca I y Fe I. Hay que considerar la opacidad de estos iones para $\lambda < 3000$ Å, aunque el Fe y el H también contribuyen a longitudes de onda mayores.

Hemos usado las regiones IR cercana y visible para derivar $T_{\rm eff}$ y $D_{\rm ang}$ usando el mismo método que para Vega. Hemos derivado las abundancias químicas para muchos elementos de Proción A. Hemos obtenido las abundancias de Fe y Mg a partir del flujo UV en la región donde su opacidad del continuo es importante. También las hemos derivado a partir de líneas del visible, obteniendo resultados compatibles. Hemos hallado además las abundancia de otros elementos usando líneas del visible, y nuestros resultados son compatibles con los de otros autores.

La compatibilidad de las abundancias obtenidas a partir del continuo UV y a partir de las líneas espectrales del visible para los principales contribuyentes a la opacidad del continuo es un resultado importante de la tesis. Hemos desarrollado un método independiente para derivar abundancias aparte del estudio de las líneas espectrales.

Finalmente, hemos llevado a cabo un estudio del espectro de Vega usando modelos estelares con rotación rápida y hemos comparado el flujo calculado con el observado. Hemos usado varias líneas espectrales de distintos elementos que cubren un rango amplio en longitud de onda y con diferentes anchuras equivalentes. Hemos estimado la temperatura polar ($T_{\rm polar}$) y la inclinación del eje de rotación (i) ajustando los flujos calculados con distintos parámetros atmosféricos al flujo observado.

Hemos usado 6 líneas de Fe con anchuras equivalentes diferentes (y por tanto distinta sensibilidad de la abundancia de Fe a la microturbulencia) para derivar la microturbulencia, la velocidad de rotación proyectada y la metalicidad. Hemos obtenido $v_{\rm equat} \cdot \sin i = 21.65$ km s^{-1}, $v_{\rm turb} = 2.11 \pm 0.13$ km s^{-1} y [M/H] $= -0.96 \pm 0.03$. Los dos primeros valores están de acuerdo con trabajos previos, mientras que la metalicidad es ~ 0.2 dex menor que la obtenida usando modelos sin rotación.

Usando estos valores para los modelos con rotación rápida, hemos vuelto a

derivar las abundancias, T_{polar} e i, obteniendo: $i = 5.33$ grados and $T_{polar} = 9802$ K, $\log \epsilon_N = 7.96$, $\log \epsilon_{Ca} = 5.77$, $\log \epsilon_O = 8.70$ y $\log \epsilon_{Si} = 7.08$.

Hemos comparado las abundancias relativas al Fe con las de modelos sin rotación. Están de acuerdo para el N y el O, pero son 0.2-0.3 dex mayores para el Si y el Ca al usar modelos con rotación rápida. El bajo valor de i (5.33 grados) es consistente con otros trabajos. T_{polar} (9802 K) es algo mayor que los valores usuales de T_{eff} de la literatura (9400-9700 K). Sin embargo, la temperatura efectiva ecuatorial (8240 K) es muy baja comparada con ella, y la temperatura fotosférica media sobre la superficie observada es menor que en otros trabajos, lo que explica parcialmente las diferentes abundancias y la baja metalicidad obtenidas usando nuestros modelos con rotación rápida.

A continuación resumo el trabajo futuro relacionado con esta tesis doctoral que planeamos llevar a cabo. En primer lugar, hay que mejorar nuestros ajustes de los espectros sintéticos al espectro observado de Proción, ya que es insatisfactorio en algunas regiones espectrales. Para llevar a cabo esto, se necesita un estudio más detallado de Proción. La comparación del flujo observado con el obtenido usando simulaciones de atmósfera 3D de Proción con nuestros parámetros preferidos nos daría una idea de la importancia de este efecto.

También es importante extender este estudio a estrellas de tipo más tardío, porque la contribución de la opacidad de los metales a su flujo es mayor y, por lo tanto, estas estrellas son más difíciles de modelar. Nuestra experiencia con el estudio de Vega y Proción nos ayudará a llevar a cabo un trabajo similar con este tipo de estrellas.

En este trabajo, hemos realizado un estudio preliminar del efecto de no considerar ETL sobre el flujo de Vega y Proción. Sin embargo, hemos limitado el escaso estudio al cálculo de poblaciones de niveles, fijando la estructura atmosférica. Un estudio más detallado de éstas y otras estrellas de tipo espectral tardío teniendo en cuenta el cambio en la estructura atmosférica producido al no usar ETL nos permitirá especificar con mayor precisión los parámetros estelares y nos ayudará a entender mejor la estructura y la evolución estelares, comparando el resultado con modelos evolutivos.

Apéndice: atlas UV cercano de Proción

El atlas del espectro UV cercano de Proción fue tomado con el espectrógrafo STIS a bordo del HST merced a una propuesta de nuestro grupo incluida en el ciclo 11. Se usaron las redes G230B (con 6 inclinaciones que cubrían de 2200 a 3050 Å, aproximadamente) y G430M (con 4 inclinaciones que cubrían de 3022 a 4080 Å), el 9 de septiembre de 2002, realizándose dos exposiciones para cada inclinación. Usamos el atlas como espectro de resolución intermedia calibrado en flujo. La relación S/R es alta, de al menos 200.

Entre 2200 y 3050 Å las diferencias de longitud de onda entre píxeles vecinos es de 0.15 Å, y de ahí en adelante de 0.28 Å, luego la resolución espectral es peor. La precisión del flujo absoluto es ∼5 % y la del flujo relativo es ∼2 %, debido a factores tales como la estabilidad instrumental, la evolución de la eficiencia de la transferencia de carga y la calibración fotométrica.

Hemos reducido los espectros calibrándolos en longitud de onda y calculando las diferencias de velocidades radiales de cada una de las dos exposiciones de cada inclinación y de inclinaciones consecutivas con la rutina *fxcor* de IRAF. Después, hemos interpolado los espectros en las regiones de superposición con la rutina *spline* de IDL y hemos promediado los espectros que se superponen. El resultado es un espectro continuo de resolución intermedia calibrado en flujo que ocupa todas las longitudes de onda comprendidas entre 2200 y 4080 Å.

Acknowledgements

First of all, I must thank my thesis supervisors. Thanks to Ramón J. García López, who has found time, in spite of being quite busy with other obligations, when I needed him to help me elaborate and correct the thesis and other related business, giving me ideas, tips and encouraging me to continue. Thanks also to Carlos Allende Prieto, who I have kept a fluid communication with, in spite of the distance, by e-mail and during the periods when I have visited Austin. I have learnt from him how to use some programs necessary for the thesis, and how to manage in a different 'world' such as Texas.

I also thank the grant program for Ph. D. studies of the Instituto de Astrofísica de Canarias (and his director, Professor Francisco Sánchez) for the scholarship and later contract received and the formation obtained during the doctorate courses, quite useful in order to improve my knowledge of Astrophysics, which was scarce when studying at University. I am also in doubt with the Universidad de La Laguna and the lecturers whose classes I attended: Basilio Ruiz Cobo, Inés Rodríguez Hidalgo and Charo Villamariz. Thanks also to the project 'Chemical Evolution of the Local Group' (PNAYA 2001-0436), which allowed me to attend conferences and visit Austin during some formation periods. The comments of the panel members (Basilio Ruiz Cobo and Artemio Herrero) of my DEA's report, and those of Charo Villamariz, the revisor of my thesis from the IAC, were also very useful.

My thanks also to the lecturers of the UAM Carlos Eiroa and M. Ángeles Díaz Beltrán, who wrote the recommendation letters that allowed me to do the doctorate at the IAC.

I am also grateful to the Department of Astronomy of the University of Texas at Austin. They made my stays very nice, not only at the University, with the help of the stellar spectroscopy group (especially David Yong and David Lambert), but also outdoors, during the entertaining talks at 'The Crown and the Ancor' and the funny volley-ball games organized by Michael Endl.

I also appreciate the help of the hot stars' group of the IAC, especially Sergio and Miguel, on the modeling of stellar atmospheres and spectral synthesis. My thanks to Ivan Hubeny for his colaboration in the article about the study of the near-UV spectrum of Vega, and to Ralph Bohlin for his revision of it. I do not forget Nuno Santos, Garik Israelian, Michel Mayor, Rafael Rebolo and the other authors of the article about the comparison of abundances in stars with and without planets for letting me colaborate with them. For the study of Vega using fast rotating models, the talks with Fernando Pérez Hernández have been decisive.

My thanks also to my office mates of the 'Corralón', who have helped me solve doubts about the thesis and other business related to the doctorate, and my friends of the IAC (some of them also office mates), with whom I have had good times at the cafeteria, at the court or outside the IAC, and who have made my stay in Tenerife nice. Moreover, my friends not related to the IAC have been also important, because they have shown their interest on the course of my thesis.

Finally, but not less important, I thank my familly, especially my parents, my brother and my sister, the support given to me to continue with the thesis and the interest shown about its course, in spite of not knowing very well what it was about.

Alejandro Manuel García Gil

Abstract

In this thesis we present a quantitative analysis of near ultraviolet, optical and near infrared spectra of the stars Vega and Procyon, with the purpose of the determination of their physical parameters as well as their surface chemical abundances.

We have compared different observed spectra with our calculations considering in detail metal opacities to discriminate between them. This aspect is especially important in the ultraviolet, since there is a controversy about which is the best flux scale: that of the Hubble Space Telescope (HST) or that of INES, calibrated directly from the International Ultraviolet Explorer (IUE) satellite. The comparison of synthetic near-UV, visible and near-IR fluxes with those observed favors the HST flux scale over the INES scale. We have also obtained new medium-resolution spectra of Procyon with STIS on board HST and high-resolution spectra of Vega from McDonald Observatory.

We have derived the effective temperature and the metallicity from model atmospheres in Local Thermodynamic Equilibrium (LTE), fixing the surface gravity, by comparing synthetic fluxes with that observed in regions where the continuum opacity from other elements different from hydrogen is not important, which is usually valid in the visible region.

Using the earlier derived parameters, we have identified the main contributors to the continuum opacity in Vega and Procyon. The chemical abundances of these main contributors have been investigated by comparing synthetic fluxes with that observed in the ultraviolet in regions where the continuum opacity produced by these elements is important. We have also derived chemical abundances from spectral lines in the visible and compared the results with those obtained using the ultraviolet region.

We have finally carried out a study of Vega's spectrum using rapidly rotating stellar models, comparing the computed fluxes with the observed one. We have thus obtained new physical parameters (rotational velocity, inclination of

the rotation axis, polar and equatorial temperature and gravity, metallicity and microturbulence) and photospheric chemical abundances. The high rotational velocity and low inclination obtained are consistent with other works that take into account rotation, while the microturbulence and projected equatorial velocity obtained compare well with the results where the effect of fast rotation on the stellar surface and on the emitted flux was not considered. Different values of gravity, effective temperature and some abundances are obtained when taking into account the effect of rotational velocity in detail.

UNESCO codes: 2101.10, 2101.11, 2101.12, 2103.03

Contents

Contents in Spanish v

Acknowledgements xxxix

Abstract xli

1 Introduction 1
- 1.1 *Line and continuum opacity* . . . 1
- 1.2 *UV stellar spectrum* . . . 2
- 1.3 *Difficulties to reproduce the observed solar and stellar UV spectrum* . . . 5
- 1.4 *Vega and Procyon as cases of study* . . . 5
- 1.5 *Vega as a fast-rotating star* . . . 7

2 Atomic data and tools to study spectra 9
- 2.1 *Model atmospheres* . . . 9
- 2.2 *Spectral synthesis* . . . 11
- 2.3 *Atomic data and line lists* . . . 12
- 2.4 *Minimization procedure* . . . 13

3 Observed spectra 17
- 3.1 *Observed spectra of Vega* . . . 17
  - 3.1.1 UV spectra . . . 17
  - 3.1.2 Visible and near-IR spectra . . . 21
- 3.2 *Observed spectra of Procyon* . . . 22
  - 3.2.1 Near-UV spectrum . . . 22
  - 3.2.2 Visible spectra . . . 22
  - 3.2.3 Near-IR spectrum . . . 24

4 The study of Vega's spectrum using classical model atmospheres **29**
4.1 *Main contributors to the opacity in Vega* 30
4.2 *Estimation of parameters of Vega by using visible, near-IR and near-UV regions* 32
4.3 *Estimation of Si and C abundances from the UV continuum* 40
4.4 *Estimation of abundances from spectral lines in the visible range* 44

5 The study of Procyon's spectrum using classical model atmospheres **51**
5.1 *Main contributors to the opacity in Procyon* 52
5.2 *Estimation of effective temperature and angular diameter* . 52
5.3 *Estimation of chemical abundances from the UV continuum* 57
5.4 *Estimation of chemical abundances from spectral lines* . . 59

6 The study of Vega's spectrum using rapidly rotating stellar models **63**
6.1 *Rapidly rotating stellar models* 64
6.2 *Preliminary calculation of stellar parameters* 68
6.3 *Calculation of model parameters* 71
6.4 *Calculation of abundances and new values of i and $T_{\rm polar}$* . 73
6.5 *Comparison of the result with that from classical models* . 76

7 Conclusions and future work **83**
7.1 *Conclusions* 83
7.2 *Future work* 85

8 Appendix: near-UV atlas of Procyon **87**

Bibliography **103**

1

Introduction

Whiteness and all grey Colours between white and black, may be compounded of Colours, and the whiteness of the Sun's Light is compounded of all the primary Colours mix'd in a due Proportion.
Prop. V. Theor. IV, "Opticks", Sir Isaac Newton

1.1 Line and continuum opacity

Most of the optical light from stars is shaped in a relatively thin layer of the stars' atmosphere, called photosphere, by different sources of line opacity (produced by bound-bound transitions) and continuum opacity (produced by bound-free or free-free transitions). In the stars we are interested in (late-type stars) emission lines are rare, and we will not discuss them.

Spectral lines were first discovered in the Sun about two centuries ago (Wollaston 1802). Joseph Fraunhofer (1817, 1821, 1823) extended the study of spectra to other astronomical objects, discovering the *Fraunhofer* lines in them and noticing the common source of the light coming from the Sun and the planets and the different spectra of the Sun and other bright stars. Nowadays, high signal-to-noise ratio (S/N) high-resolution spectra of stars are available. These observations are enough to provide a very precise radial velocity determination of stars for kinematical studies, or the projected rotational velocity. Other measurements such as chemical abundances can be obtained from the strength (or similarly the equivalent width EW) of spectral lines, but it is also necessary to know what physical conditions exist in the atmosphere. For that purpose

model atmospheres are constructed based on first principles and a number of simplifications (see the discussion in §2.1).

The study of the continuum flux can be used to obtain the effective temperature of stars. For instance, the infrared flux method (IRFM) can be used to derive it by only using photometric measurements in the IR, bolometric corrections and the calculation of model stellar atmospheres (see, e.g. Alonso, Arribas & Martínez-Roger 1994). It can be used for other determinations, like obtaining surface gravity and metallicity or the detection of companion stars and disks, or the measurement of chemical abundances by considering the continuum absorption of the elements whose abundance is to be computed. These determinations also require the calculation of model atmospheres. In the case of abundance determination, very few studies have explored this possibility, because very detailed model atmospheres and atomic data and high-quality spectrophotometric stellar observations are necessary. This is one of the aims of this thesis.

1.2 UV stellar spectrum

Most studies since the invention of the telescope have only taken into account visible radiation for photometric or spectroscopic observations of astronomical objects. This seems natural, because this is the only range that we can directly see, but other ranges of the electromagnetic spectrum contain very useful information of the Universe, so they can not be forgotten. However, only the visible and radio wavelengths and some regions of the infrared and the ultraviolet (UV) spectrum are able to go through the Earth's atmosphere and reach the ground due to atmospheric absorption (see Fig. 1.1), so the other spectral regions were an absolute mystery until the advent of the space era. The first satellite used to study spectroscopically the near-UV was the *International Ultraviolet Explorer* (IUE), launched in the 1970's decade. However, a precise calibration of their instruments could not be carried out until some years later, and the stellar model atmospheres containing sufficient numbers of spectral lines as there are in the UV were not calculated until the end of the decade (e.g. Kurucz 1979).

In spite of these difficulties, understanding the formation of the UV spectrum of individual stars is essential in order to quantitatively determine stellar abundances for a number of chemical elements that only produce measurable features in the UV domain such as the light elements B and Be, or the neutron capture element Ge. Let us define the notation that will be used for abundances:

$$[\mathrm{A/H}] \equiv \log[\mathrm{N(A)/N(H)}] - \log[\mathrm{N(A)/N(H)}]_{\odot}, \tag{1.1}$$

where N(A) is the number abundance of element A.

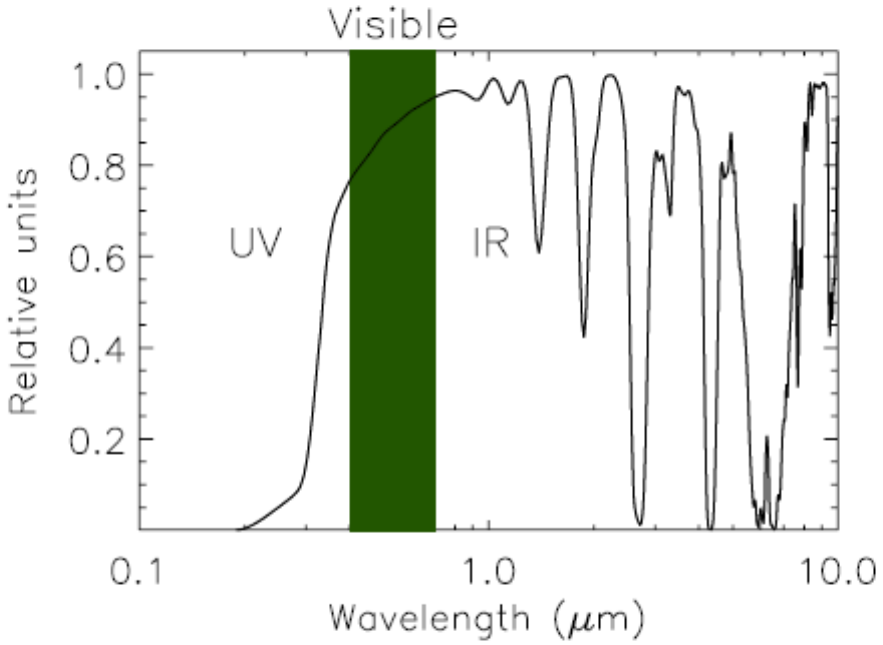

FIGURE 1.1— Portion of radiation transmitted through the Earth's atmosphere, where optical and near-UV transmission were taken from Nitschelm (1988) and near-IR transmission from the UKIRT web pages (`http://www.jach.hawaii.edu/UKIRT/`).

The case of B and Be abundance evolution is remarkably interesting. Standard big bang nucleosynthesis calculations do not predict a significant production of Be and B (see, e.g., Walker et al. 1991), which are thought to be produced by spallation reactions between cosmic rays and CNO nuclei (see Ramaty, Kozlovsky & Lingenfelter 1996 and Ramaty et al. 1997 for recent discussions on the theoretical yields). Models of inhomogeneous big bang nucleosynthesis suggest that observable amounts of Be and B could be produced (e.g., Malaney & Fowler 1989; Kajino & Boyd 1990; Jedamzik et al. 1994), but this possibility has been questioned on theoretical grounds (e.g., Terasawa & Sato 1990; Reeves et al. 1990). The existing data do not indicate the presence of an observational B or Be "plateau" in extreme metal-deficient stars which could be representative of the primordial B and Be abundance. A study of Be and B abundances in metal-poor stars ($-3 \leq$ [Fe/H] ≤ -1) shows a constant boron-to-beryllium ratio of $\sim$20, and the relation between boron (or beryllium) and iron abundance has a slope of $\sim$1 (García López et al. 1998). The simplest interpretation is that B and Be are made by the same nucleosynthetic process: spallation of CNO nuclei by collisions with protons and α-particles.

Apart from Ge, other important elements produced by neutron capture, like Os and Pt, have their strongest atomic transitions in the UV. The abundance distributions in Galactic halo stars indicate the extent of early Galactic nucleosynthesis and the nature of the earliest progenitor stars. Of particular interest is the scatter in the mean level of the n-capture element to iron abundance ratios in stars of very low metallicity ([Fe/H] < -2.0). The chemical calculation in the metal-poor halo star BD +17 3248 (Cowan et al. 2002) indicates that the abundances of the lighter n-capture elements, including Ge, fall below the scaled solar r-process curve that fits well the abundances of heavier r-process elements, a result similar to that seen in another very-metal-poor star: CS 22892-052. This abundance pattern might be produced by two r-process types (with one for the heavier and one for the lighter n-capture elements), perhaps from supernovae occurring at different frequencies, or neutron star binaries, or some combination of those.

A proper understanding of the spectra of individual stars is also crucial to interpret integrated light from galaxies and other stellar systems. The UV radiation field, besides affecting directly the abundances obtained from UV lines, has an important effect on the construction of atmospheric models through the energy balance. Theoretical atmospheric structures computed under the assumptions of radiative equilibrium and local thermodynamical equilibrium are routinely employed in the analysis of spectra from astronomical objects. Consequently, an error in the UV opacities translates into wrongly derived physical properties, namely, chemical composition and atmospheric parameters for indi-

vidual stars, or into wrongly derived ages for galaxies.

1.3 Difficulties when trying to reproduce the observed UV spectrum

A possible UV opacity source missing from the calculations has been proposed to explain an early reported failure to match the observed solar UV spectrum. It has been suggested that missing line opacity (with an important contribution from faint lines) could be responsible for a quasi-continuum absorption of 10 % or more for $\lambda < 4000$ Å (e.g. Vernazza, Avrett & Loeser 1976; Holweger 1970). Continuum metal absorption has also been suggested to provide that extra opacity (Bell, Paltoglou & Tripicco 1994; Bell, Balachandran & Bautista 2001). However, several recent studies of UV spectra of other stars suggest that there is a reasonable agreement between theoretical models (Kurucz 1992) and observations (e.g. Fitzpatrick & Massa 1999; Allende Prieto & Lambert 2000; Peterson et al. 2001). The analysis of the solar spectrum by Bell, Balachandran & Bautista (2001) concluded that even when using the most recent calculations of line and continuum opacities, classical model atmospheres predict too much UV flux. Nonetheless, this result has been challenged by independent calculations by Allende Prieto et al. (2003), who found that LTE modeling can reproduce closely the observed solar flux at wavelengths longer than about 2600 Å, and uncertainties in the atomic line data fully account for the differences between computed and observed fluxes. High quality observations of stars with atmospheric parameters different from solar present a promising way to solve the controversy.

1.4 Vega and Procyon as cases of study

One of the stars we deal with in this work is Vega (α Lyr, HD 172167, A0 V). This star has been studied very deeply for its condition of standard flux star. It is, however, not straightforward to model for several reasons. For instance, the satellite IRAS detected an infrared excess above what was expected from the stellar photosphere at $\lambda \geq 12$ μm, attributed to a dust and gas disk that was actually observed later (Walgate 1983; Wilner et al. 2002). Besides, it is a fast rotator seen pole-on (Gulliver et al. 1994). This rapid rotation is not uncommon for a A0 V star like Vega (Gray 1992), but produces a gradient in temperature difficult to model in the stellar surface. It is possibly variable (Vasil'Yev et al. 1989), with results by that date that argue for and against variability, although recent IR measurements do not find any flux variability (Price et al. 2004). Moreover, it has a peculiar abundance pattern, similar to that of λ Boo stars (Ilijić et al. 1998), that is, with a relative underabundance

of Fe-like elements with respect to the Sun, but solar proportions of C, N, O, and S. Estimations of physical parameters from the literature and from our study are shown in chapters 4 and 6.

Despite these difficulties, Vega is one of the few dwarf stars that can be used to test detailed calculations of UV irradiances: both precise UV spectrophotometry and independent measurements of its angular diameter are available. Visible high resolution and high signal-to-noise ratio (S/N) spectra of Vega are also readily obtained from the ground. Besides, the disk is expected to make no detectable contribution to the star's visible and UV spectrum, and it has been found that the influence of fast rotation is only important for the shape of spectral lines, with a small effect on the continuum limited to the spectral region in the vicinity of the Balmer jump (Gulliver et al. 1994).

The other star we deal with is Procyon (α CMi, HD61421, F5 IV-V). Its parallax measured by *Hipparcos* is very precise: $\Pi = (285.93 \pm 0.88) \times 10^{-3}$ arcsec, so its derived distance is: d = 3.497 ± 0.011 pc. Its mass can be constrained by using orbital parameters to $M = 1.42 \pm 0.06\ M_\odot$ (Allende Prieto et al. 2002), because it has a DQZ white dwarf companion (Procyon B), with $T_{eff} = 7740 \pm 50$ K and $M = 0.602 \pm 0.015\ M_\odot$ (Provencal et al. 2002). The measured orbital period, from an updated astrometric orbit from photographic plates obtained at different observatories between 1912 and 1995, is $P = 40.82 \pm 0.06$ yr (Girard et al. 2000). The same authors measured the angular separation of the pair using the IR cold coronograph at the NASA IR Telescope Facility and the WFPC2 on board the HST to obtain both masses: $M = 1.497 \pm 0.037\ M_\odot$ for Procyon A and $M = 0.602 \pm 0.015\ M_\odot$ for Procyon B. The age of Procyon A is very tightly constrained to the range 1.66-1.73 Gyr (Allende Prieto et al. 2002) by interpolating solar metallicity isochrones (Bertelli et al. 1994) to match the pair (M_V, $B - V$). Alternatively, matching the observed radius and mass would shift the age estimate to 2.0 Gyr. These ages are significantly shorter than the nuclear timescale of 3.9 Gyr adopted by Provencal et al. (1997), implying a mass for the progenitor of Procyon B larger than previously estimated. Eggenberger, Carrier & Bouchy (2005) have recently carried out asteroseismic measurements, favouring a mass of 1.497 $M_\odot$ and an age of 1.72 ± 0.30 Gyr.

Procyon A is cooler than Vega (see different determinations of T_{eff}, as well as metallicity and gravity in chapter 5) and therefore it has more line and continuum opacity in the UV and is harder to model. However, Procyon is similar to Vega in an important sense: it can be used to test detailed calculations of UV irradiances: both precise UV spectrophotometry (taken following a proposal made by our group to use the STIS instrument onboard HST) and independent measurements of its angular diameter are available. Furthermore, visible low and high resolution and high signal-to-noise ratio (S/N) spectra of

Procyon are also readily obtained from the ground.

1.5 Vega as a fast-rotating star

Gray (1988) was the first researcher suggesting that Vega is a rapid rotator seen pole-on as the solution to the problem of its luminosity excess: its absolute luminosity in V is 0.7 magnitudes too high compared to other stars of the same spectral type and similar $uvby\beta$ indices, as predicted by the rotating models from Collins & Sonneborn (1977), which take into account the diameter increase and the decrease of temperature and gravity from the poles to the equator. The problem of the luminosity excess was first pointed out by Petrie (1964) from his absolute magnitude calibration of Hγ equivalent widths. Gray suggested that a rotational velocity between 0.9 and 1.0 of the critical velocity (implying a rotational velocity somewhat in excess of 300 km s^{-1}) would explain the flux excess. This velocity is high, but not unusual for early A-type stars, which usually rotate quite fast. That rotational velocity implies, given the estimated projected equatorial velocity $v_{\rm equat} \cdot \sin i$ of $\sim$20 km s^{-1}, that the inclination of the rotational axis of Vega is $\sim$4 degrees or less. This thesis is also supported by the fact that the angular diameter of Vega is larger than expected for a slowly rotating A0 V star (Hanbury Brown et al. 1967).

Furthermore, the weak line profiles seen in high-resolution high S/N spectra have their bottom clearly flat, with a trapezoidal appearance, while strong lines exhibit normal rotationally broadened profiles (Gulliver et al. 1991). Gulliver et al. (1994) studied in more detail the effect of rapid rotation on Vega and showed that the variation of $T_{\rm eff}$ and log g (and then the emitted flux) from the poles (near the center of the disk for Vega) to the equator (near the stellar limb for Vega) could explain the appearance of the weak lines, since the lower temperatures at the equator/limb produce a higher contribution to the outer edges of the profiles, i.e., a "limb-strengthening". They used high-dispersion ultrahigh S/N spectra of Vega, ATLAS9 model atmospheres (Kurucz 1993) and SYNTHE synthetic spectra (Kurucz & Avrett 1981) to model Vega as a rapidly rotating pole-on star and considering the distortion of the equipotential surfaces with rotation. A low-dispersion observed spectrum from 1200 to 10500 Å was used: IUE UV observations from 1200 to 3300 Å (Bohlin 1990) and visible and near-IR observations from 3300 to 10500 Å (Hayes 1985). Gulliver et al. (1994) obtained the best fit using the following parameters, where formal errors are included: an inclination $i = 6.0 \pm 0.7$ degrees, polar effective temperature $T_{\rm polar} = 9595 \pm 20$ K, and log $g_{\rm polar} = 3.80 \pm 0.03$ dex for a fixed $v_{\rm equat} \cdot \sin i$ = 21.8 km s^{-1}, so the equatorial rotational velocity is $v_{\rm equat} = 210$ km s^{-1} and the equatorial effective temperature is $T_{\rm equat} = 9325$ K. The quality of the fit

for the pole-on model reproduces the low-resolution observations as well as the preferred standard Kurucz model (which is a non-rotating model), with T_{eff} = 9550 K, log g = 3.95 and metallicity (which will be defined in the following chapter) [M/H] = −0.5 (Castelli & Kurucz 1994), except in the region 2850-3700 Å, where the pole-on model improves the fit. They also fit two flat-bottomed line profiles, finding best fit values of $v_{\rm equat} \cdot \sin i = 21.8 \pm 0.2$ km s^{-1}, $T_{\rm polar}$ = 9695 ± 25 K, log $g_{\rm polar} = 3.75 \pm 0.02$ dex, and $i = 5.1 \pm 0.3$ degrees, so $v_{\rm equat}$ = 245 km s^{-1} and $T_{\rm equat}$ = 9300 K, with a much higher fit quality than using non-rotating models. Although both results are incompatible using formal errors, the authors claim that they are compatible when using realistic error estimates.

Finally, recent high-resolution mid- and far-IR images of the debris disk of Vega from the satellite *Spitzer* (Su et al. 2005) show a circular, smooth and larger than thought before disk, which supports the hypothesis of Vega as a pole-on rotating star. The radius of the disk is at least 43" (330 AU), 70" (543 AU), and 105" (815 AU) in extent at 24, 70 and 160 μm, respectively.

2

Atomic data and tools to study spectra

2.1 Model atmospheres

We have based our spectroscopic analyses on the model atmospheres developed by Kurucz (1979, 1993) and Castelli & Kurucz (2003). These models have been widely used in studies of individual stars and in population synthesis codes, and form a grid defined by three parameters: the effective temperature, the surface gravity and the metallicity. They are built on the approximations of static homogeneous and plane-parallel atmosphere in LTE and take into account line-blanketing. Convection is considered by means of the mixing-length theory.

Opacities from about 58 million atomic lines and diatomic molecules are included. The distribution functions of line opacities, temperatures, pressures, electron densities and particle densities are tabulated in 64 steps of depth for model atmospheres with the following parameters: 56 effective temperatures in the interval between 2000 and 200,000 K, 21 values of the surface pressure spanning 10 orders of magnitude, 1212 wavelength intervals between 10^2 and 10^5 Å, microturbulence velocities of 0, 1, 2, 4 and 8 km s^{-1} and scaled solar abundances of [+1.0] to [−5.0] and [+0.0, no He]. These distribution functions are used as input for the program that computes the model atmospheres, ATLAS9. There is a more recent opacity sampling version of Kurucz's model atmosphere code called ATLAS12 (Kurucz 1993). Mean Rosseland opacities are also tabulated for each case.

The metallicity M/H of a model atmosphere implies that all elements with Z>2 are coupled to iron in solar proportions. It is usually assumed that [M/H]

= [Fe/H]. However, the iron abundance in the Sun considered in the Kurucz's models (1993) was adopted from Anders & Grevesse (1989): $\log \epsilon_{\rm Fe,Kurucz}$ = 7.67 ± 0.03, which differs from the meteoritic iron abundance. In this work, $\log \epsilon_{\rm X}$ is defined as usual:

$$\log \epsilon_{\rm X} \equiv \log[{\rm N(X)/N(H)}] + 12. \tag{2.1}$$

We adopt the following as the solar photospheric abundance that we use in spectral syntheses: $\log \epsilon_{\rm Fe,meteoritic}$ = 7.51 ± 0.01, so we obtain: [M/H] = [Fe/H] − 0.16, where hereon [Fe/H] is no longer the metallicity written in model atmospheres, but the iron abundance compared to the solar one used for spectral syntheses, to be compatible with the iron abundance used in the model atmospheres.

A microturbulence of 2 km s^{-1} is assumed in the models. Besides, there are systematic errors in the cooler models, because the opacities of the molecular lines are incomplete. In some cases, we have computed fluxes using new model atmospheres (Castelli & Kurucz 2003) that were calculated with overshooting turned off (resulting in a steeper rise in temperature with depth in the region where the optical continuum is formed; Castelli, Gratton & Kurucz 1997), and using updated values for the solar elemental abundances and revised opacity distribution functions (ODFNEW). The reason for this new analysis is to check the effect of convective overshoot and new opacities on the colors.

Another grid of model atmospheres (NextGen; Hauschildt, Allard & Baron 1999) is used by some researchers for 3000 K $\leq T_{\rm eff} \leq$ 10000 K. Most of the models are calculated under the assumption of LTE. Large differences were expected at $T_{\rm eff}$ < 5000 K between these and Kurucz's model atmospheres, because of differences between the equations of state and the treatment of molecular opacities in ATLAS12 and PHOENIX, the program that computes NextGen model atmospheres. An actual comparison (Bertone et al. 2004) concludes that the atmospheric parameters obtained from fitting synthetic to observed spectra using ATLAS9 model atmospheres are, in general, sensibly more similar to those from empirical calibrations (a factor of 2 lower σ of flux residuals) than those obtained using NextGen.

Another important grid is OSMARCS, firstly developed by Gustafsson et al. (1975) and Bell et al. (1976). Later, an opacity sampling (OS) version of the original opacity distribution function (ODF) was implemented by Plez, Brett & Nordlund (1992), assuming a static, spherically symmetric model atmosphere in LTE. The most recent version is mentioned in Gustafsson et al. (2003). It is a grid for cool (2500 K $\leq T_{\rm eff} \leq$ 8000 K, and $-1.0 \leq \log g \leq 5.0$ in cgs units) and metal poor stars ($-5.0 \leq$ [Fe/H] ≤ 1.0). The parameters of this grid are

M, R, T_{eff}, log g and CNO abundance. Metal and molecular lines are taken into account.

Recently, new 3D time-dependent, inhomogeneous model atmospheres in LTE have been developed (Asplund et al. 2000). They applied realistic ab-initio 3D, radiative-hydrodynamical convection simulations. In contrast to classical analysis based on hydrostatic 1D model atmospheres, the procedure contains no adjustable free parameters (such as the mixing length or the micro- and macro-turbulence) but the treatment of the numerical viscosity in the construction of the 3D model atmosphere for stability purposes.

There are several reasons why Kurucz's model atmospheres have been used in this work. Firstly, the grid is very complete and contains the photospheric parameters that we need for our stars, while OSMARCS is limited to cool stars and the NextGen grid finishes very close to the parameters of Vega. Furthermore, 3D model atmospheres are very difficult to compute and there is no grid available at this time. Finally, Kurucz's model atmospheres take into account the most important sources of opacity, so the flux extracted from them is reliable, which partially explains that most researchers use them to compute stellar fluxes.

2.2 Spectral synthesis

The calculations of synthetic fluxes were carried out with the program SYNPLOT, an IDL wrapper of the FORTRAN code SYNSPEC (Hubeny & Lanz 2000, which computes the spectrum emitted by a stellar atmosphere or a ring of an accretion disk) and ROTINS (which computes the rotational and instrumental broadening). SYNSPEC assumes that the model atmosphere is given, either calculated by TLUSTY (Hubeny & Lanz 2003), used in this work to calculate level populations not assuming LTE, or taken from the literature, as for instance from the Kurucz grid of models (Kurucz 1992). The program reads a general line list and dynamically selects lines which contribute to the total opacity, based on physical parameters of the actual model atmosphere. SYNSPEC then solves the radiative transfer equation, wavelength by wavelength, in a specified wavelength range, and with a specified wavelength resolution. This equation, for radiation passing through an infinitesimal length of material ds, states that:

$$\frac{dI_\nu}{ds} = \eta_\nu - \kappa_\nu I_\nu \tag{2.2}$$

for plane-parallel and stationary atmospheres, where I_ν is the specific intensity of radiation, η_ν is the emissivity and κ_ν is the extinction coefficient. The wavelength points generally are not equidistant. Instead, the calculations are firstly

carried out in the center of each two neighboring lines. The program then adds a certain number of points, equidistantly spaced between these two, such that the interval between the points does not exceed some prespecified value. This procedure assures that neither any line center nor any continuum window is omitted.

For the continuum opacity, the following sources were considered: photoionizations from all explicit levels, free-free opacity for all explicit ions (the ones that most contribute to opacity) and electron scattering. In principle, the line and continuum opacity sources used in calculating a model stellar atmosphere and in calculating the detailed spectrum should be identical. However, the few model atmospheres used in this thesis allowing for some departures from LTE were calculated with fewer opacity sources (lines and continua) than the opacity sources used when calculating synthetic spectra. The rationale for this approach is that the atmospheric structure (i.e. the run of temperature and number densities) can be calculated by considering approximate opacities, while the emergent spectrum has to be computed in detail.

The result consists on the flux emitted at the surface of the star (more specifically, the first moment of the specific intensity, H_ν) between the specified wavelengths and the identification of lines when indicated. The astrophysical flux is F = 4H, and the physical flux, which will be used in what follows, is $F = 4\pi H$.

2.3 Atomic data and line lists

To interpret properly the observations we need to consider realistic opacities. Photoionization cross-sections are taken from the Opacity Project's TOPBASE (Cunto et al. 1993) for most of the important species. These data are precise, although the exact position of the predicted resonances may be affected by significant errors in the R-matrix calculations. This problem is circumvented by smoothing the photoionization cross-sections to the appropriate resolution (see Bautista, Romano & Pradhan 1998, and Allende Prieto et al. 2003). We have used the recipe from Bautista, Romano & Pradhan (1998), which consists on a smoothing with a Gaussian profile with $\sigma = 0.03E$, where E is the energy of the ionizing photon. Fig. 2.1 shows two examples: the ground levels for Na I and Ca I. When the cross-section, as for Na I, is a slowly-changing function, the Gaussian-smoothed cross-section (dots) preserves the original shape, but when strong resonances are present (e.g. Ca I), using the processed cross-sections reduces the effect of errors in the exact location of the resonances, accounting well for the total opacity. For some important species not included in the new TOPBASE library, MODION atomic models have been used (see

`http://tlusty.gsfc.nasa.gov/` for more details), which contain from very simple to quite complete structures of some ions, from where we have taken: H I, He I, C II, N I, O II and Si I.

Line opacity is also important. Wavelengths and strengths of millions of atomic and molecular lines are needed to model with accuracy the detailed shape of the UV spectrum in late-type stars. We considered different sources for the atomic line data, finding that a linelist based on data compiled by Kurucz and distributed with SYNPLOT provided the best results, so this list has been used, except for a few particular lines, in which updated Stark line damping parameters extracted from VALD[1] (*Vienna Atomic Line Database*, Kupka et al. 1999) have been used. Damping constants for collisions with neutral hydrogen (a mayor contributor to the line width of spectral lines in stellar atmospheres) are also in VALD from very precise (a few percent) calculated cross-sections from P. S. Barklem and collaborators (see, e.g. Barklem, Piskunov & O'Mara 2000).

In addition to the photoionization cross-sections, radiative rates are needed when making NLTE calculations. Radiative transition probabilities were adopted from the NIST database (http://physics.nist.gov/cgi-bin/AtData/main_asd), and complemented with the Opacity Project calculations. The necessary collisional rates were calculated based on general formulae due to van Regemorter (1962), Mihalas (1972), and Auer & Mihalas (1973), and suplemented with the laboratory data when available (Nahar & Pradhan 1997; Nahar 1999). Most of the necessary data had already been compiled[2].

2.4 Minimization procedure

We used the Amoeba routine of IDL for the minimization of the χ^2 statistics for the fit of synthetic to observed spectra. This procedure develops a multidimensional minimization of a function Func(x), where x is a n-dimensional vector, by using the Nelder-Mead *downhill simplex* algorithm (Nelder & Mead 1965), which only requires function evaluations. Some studies about its convergence have been carried out (see, e.g., Lagarias 1998). McKinnon (1998) gave a family of strictly convex functions and a starting configuration in two dimensions for which the Nelder-Mead method converge to a non-minimizing point, so some authors (e.g. Price et al. 2002) have tried to make a convergent variant of the Nelder-Mead algorithm.

To explain how this method works, let us start defining a *simplex*. A *simplex* is a geometric figure, in N dimensions, with N+1 points (or vertex) and all their

[1] Van der Waals parameters are similar, so we have maintained them

[2] available at **http://hebe.as.utexas.edu/at/at.cgi**

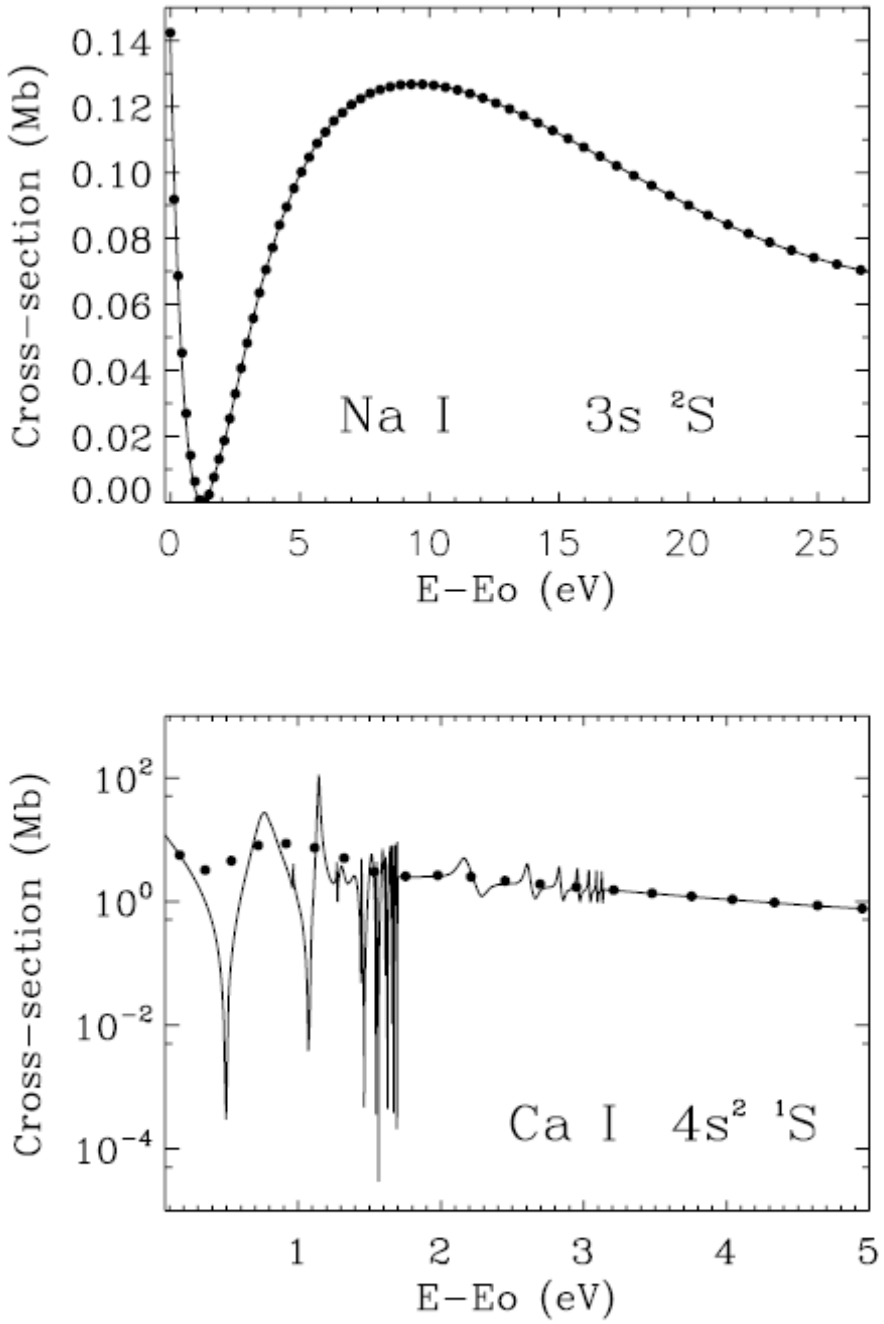

FIGURE 2.1— Detailed (solid line) and resonance-averaged (filled circles) cross-section for the ground states of Na I and Ca I, where 1 megabarn (Mb) = 10^{-18} cm^2. These two cases exemplify a smooth cross-section and a complex resonance structure.

interconnecting segments, faces, etc. For instance, a two-dimensional *simplex* is a triangle. Besides, in this method, only non-degenerated *simplex* are used. We start with a vector of N independent variables, which constitutes the *simplex* of N+1 points. The method then evaluates the function-to-minimize at each point and obtains a new *simplex* that is one of the following four: a reflexion of the point with the greater value over the other points, a reflexion and expansion of the point with the greater value over the other points, a contraction of the point with the greater value along one dimension or a contraction along all the dimensions towards the point with the lowest value.

Moreover, it is necessary to specify the maximum number of iterations and the tolerance, or the fraction between two consecutive values of the function-to-minimize where the routine must stop. The result is the n-dimensional vector in which the function is minimum within some uncertainty related to this tolerance.

3

Observed spectra

THIS chapter describes the sources of observed spectra that we started considering to be useful for the thesis. Later on, by studying them in depth, we discarded or combined some of them, as explained in this and later chapters. For both stars (Vega and Procyon), we consider low-resolution spectra in the visible, the near-UV and the near-IR regions. The aim of this is to find basic physical parameters (the angular diameter, the parameters of model atmospheres, that is, the effective temperature, the metallicity and the surface gravity, and the abundances of the main contributors to the continuum absorption), because it is not necessary to study spectral lines in detail to derive them, but we need a long wavelength region with absolute flux calibration. We also consider high-resolution visible spectra (not flux calibrated) of the stars to derive chemical abundances using spectral lines. For Vega, high-dispersion near-UV observed spectra have also been considered to test the quality of the fit between the synthetic spectra (using the parameters derived from low-resolution flux comparisons) and the observed spectra.

3.1 Observed spectra of Vega

3.1.1 UV spectra

Since the HST had not taken near-UV spectra of Vega covering a long wavelength range, the most useful near-UV observed spectra of Vega for our purpose were those taken with the IUE satellite. We have found the following three calibrations of the average low-dispersion IUE spectrum of Vega:

- Bohlin's calibration[1] (Bohlin 1996). 8 standard stars (4 pure H white dwarfs, DA's, among them) are used to calibrate FOS (*Faint Object Spectrograph*) observations, formerly on board HST. The zero level of the flux scale is tied to the average over the V band for Vega as measured by Hayes (1985). The uncertainty in the absolute fluxes for Vega in the broadband FOS calibration are 1-2 % in the optical and increasing to 3-4 % at 1200 Å (Bohlin 1996). By comparing their FOS and IUE fluxes, a correction factor is determined, which is applied to each wavelength of a IUESIPS (the earlier version of NEWSIPS, which is the processing software developed for calibrating the IUE data set) spectrum of Vega to place the data in the HST flux scale. This set of standard spectra has been updated and improved by new STIS and NICMOS observations (both on board HST; Bohlin, Dickinson & Calzetti 2001) [2].

- Massa & Fitzpatrick's calibration (Massa & Fitzpatrick 2000, hereafter M&F); it takes into account systematic errors in NEWSIPS spectra as a function of the observation epoch and the temperature of the amplifying camera (THDA), and applies a correction factor to place the fluxes into the HST scale.

- INES; this is not a calibration of IUE data processed with NEWSIPS (*New Spectroscopic Image Processing System*; see Garhart et al. 1997), but a new full processing of the raw data, improving the spectrum extraction to diminish the error sources present in NEWSIPS (improving the noise model, the extraction method, the homogenization of the wavelength scale, and the flagging of the extracted spectra calibrated in flux). The spectra were calibrated using a DA, G191B2B, whose virtually featureless spectrum is relatively simple to model. The absolute flux scale relies on that of the UV satellite OAO-2 (González-Riestra, Cassatella & Wamsteker 2001).

The three versions above are based on low-dispersion large-aperture IUE spectra, but the particular individual spectra considered in the average, and some parts of the processing (chiefly, the flux calibration) differ among them. These spectra have a large spectral coverage with a resolution of $\sim$ 6 Å. We combined several IUE spectra (the same IUE spectra from both servers, but with a different calibration) from the INES and Multimission Archive at Space

[1] `http://kahuna.stsci.edu/instruments/observatory/cdbs/calspec.html`

[2] The spectrum that we use in this thesis is not the one obtained with STIS and recently published (Bohlin & Gilliland 2004), but the earlier one, since this one was not yet published at the time this study was carried out

Telescope Sience Institute (MAST) servers[3] to produce the INES and M&F versions, respectively. The list of individual spectra is provided in Table 3.1. Before combining the MAST-IUE spectra to produce the M&F version, the fluxes were processed with the software kindly provided by these authors. Bohlin's spectrum was directly obtained from the STScI web pages, as provided by R. Bohlin[4].

As we can see in Fig. 3.1, Bohlin's and M&F fluxes (which share the same flux scale) are ∼10% higher than the INES fluxes for Vega. This difference is high, but roughly consistent within the error bars with the global differences reported by González-Riestra, Cassatella & Wamsteker (2001) between FOS and IUE spectra for the INES reference star G191B2B. However, they noticed an almost linear reduction from a difference of ∼7 % at 1500 Å to ∼6 % at 3000 Å, while we find larger differences for Vega in the ranges 1500 to 1700 Å and 2000 to 2500 Å. Fig. 3.1 reveals that the M&F flux is higher than Bohlin's at ∼1800 and ∼2000 Å. The feature in the M&F version at ∼2000 Å coincides with the border between the short and long-wavelength cameras, where the uncertainty in the flux is higher. For that at ∼1800 Å, we can not give a satisfactory explanation.

We also compared Bohlin's and INES fluxes for the eight primary standard stars on which the HST fluxes are based (G191B2B, GD153, GD71, HZ43, HZ44, BD +28 4211, BD +33 2642, and BD +75 325). We used all the IUE spectra available for these stars from the INES database, selecting only those pixels labeled with good quality and with flux errors lower than 20%. Bohlin's flux is again higher than the INES one at all wavelengths and for all the stars, with the exception of the SWP spectrum of BD +75 325. The mean relative difference in flux for the other seven stars is $(F_{Bohlin} - F_{INES})/F_{INES} = 0.066 \pm 0.005$, which is again consistent with the global differences reported by González-Riestra, Cassatella & Wamsteker (2001). When studying the wavelength dependence, an increment of the difference is seen at ∼2000 Å and from 2200 to 2500 Å, where the difference is over 8%, while in the other regions it is 5-7%, quite consistent with the larger differences observed in Vega's case between 2000 and 2500 Å.

Finally, we have considered high-dispersion IUE spectra. These spectra have a large spectral coverage with a resolution ∼ 0.2 Å. Table 3.1 lists the high-resolution spectra considered, all of them from the INES calibration, because the M&F calibration can not be used with high-dispersion spectra.

[3] `http://ines.vilspa.esa.es/ines/` and `http://archive.stsci.edu/iue/`, respectively
[4] URL is `ftp://ftp.stsci.edu/cdbs/cdbs2/calspec/`

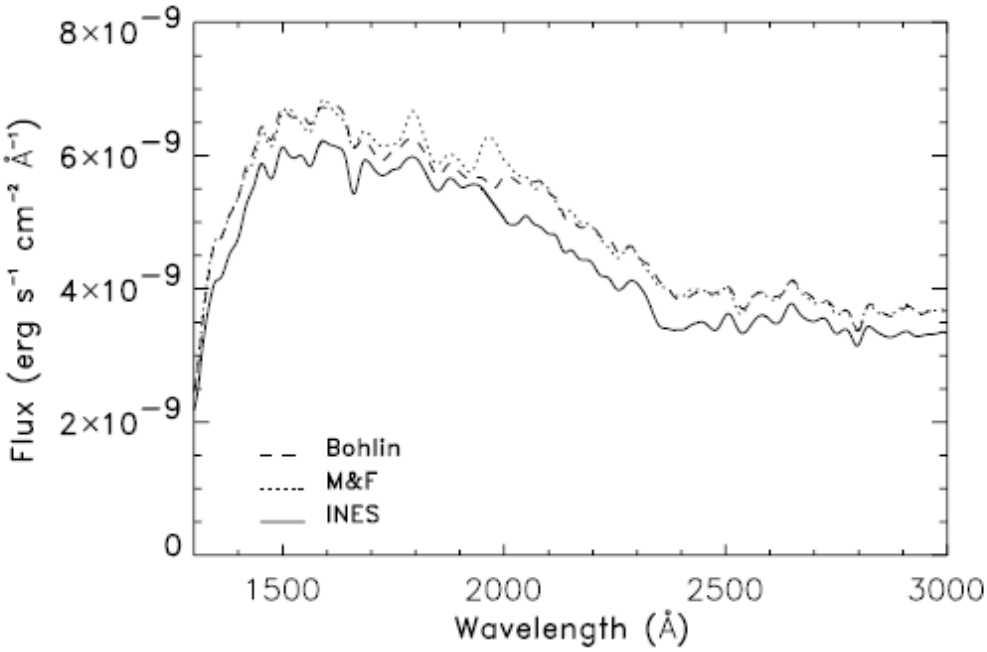

FIGURE 3.1— Comparison of the observed fluxes in the UV obtained with different calibrations of the IUE data smoothed by convolution with a Gaussian profile with FWHM = 25 Å (see text for details).

TABLE 3.1— Spectra averaged to calculate the calibrated spectrum of Vega with different dispersion and wavelength ranges. M&F fluxes are obtained from the MAST-IUE web page and INES fluxes from the INES web page (see text).

Calibration	Dispersion	Camera name	Wavelength range (Å)	Spectrum numbers
M&F and INES	low	SWP	1150-2000 Å	27024, 29864, 30548, 30549, 32906, 32907
M&F and INES	low	LWP	1850-3300 Å	07010, 07038, 07888, 07889, 07902, 07903, 07904, 10347, 10348
INES	high	SWP	1150-2000 Å	01188, 24504, 32870, 32887, 33633, 38411, 42521, 45285
INES	high	LWR	1850-3300 Å	07585, 08630
INES	high	LWP	1850-3300 Å	07490, 12617, 17648, 21295, 23642

3.1.2 Visible and near-IR spectra

Visible spectrophotometry provides additional information that cannot be neglected. For the study of Vega's spectrum using classical atmospheric models, we consider the data compiled by Hayes (1985) combining six different sources of ground-based measurements. This spectrum has a flux uncertainty of just about 1-2% in the optical and covers a wavelength range from 3300 to 10500 Å. The flux is tabulated in steps of 25 Å. These are both the bandwidth and step sizes reported by Terez and Terez (1979), who measured Vega's flux in the entire region critically evaluated by Hayes. The other sources considered by Hayes provide fluxes measured over smaller spectral ranges with bandpasses from 10 to 100 Å, and approximate corrections to obtain the average flux over each bandwidth. Based on this information, it seems therefore appropriate to compare these data to calculated fluxes smoothed to a resolution of at least 50 Å.

For the study of Vega's spectrum using rapidly rotating models, we have used the spectrum recently obtained with the Space Telescope Imaging Spectrograph (STIS). The absolute flux was measured with high accuracy from the near-UV to the near-IR on the HST white dwarf flux scale (Bohlin & Gilliland 2004). It is a low-dispersion spectrum (R $\sim$ 500) with very high signal-to-noise ratio (S/N $\sim$ 1000).

We have used two different optical high-dispersion spectra, with different resolving power, obtained by our group at McDonald Observatory (Mount Locke, Texas), acquired with the *2dcoudé* cross-dispersed echelle spectrograph (Tull et al. 1995) coupled to the Harlan J. Smith 2.7m Telescope. The first spectrum is part of the Spectroscopic Survey of Stars in the Solar Neighborhood (S^4N; Allende Prieto et al. 2004) and is the average of observations secured in May 1 and 2, 2001. It has a resolving power ($R \equiv \frac{\lambda}{\delta\lambda}$) of $\sim 6 \times 10^4$, covering in full the optical range, extending into the near IR. As the spectrograph provides full coverage only from about 3600 Å to ~5100 Å in a single exposure for this resolution, with increasingly larger gaps between redder orders, two overlapping settings were used to circumvent the problem. The second spectrum was obtained at the focal station F1, and has R $\sim$ 173000, S/N = 400-500, covers the range from ~4400 to ~7600 Å with some small gaps, and was obtained in June 9–12, 2000. The spectral coverage is much smaller at F1, and 10 tilts of the grating/prisms were needed to achieve the final coverage. The CCD registered pieces of ~16 adjacent orders.

For both the high- and intermediate-resolution spectra, the detector was TK3, a thinned 2048 $\times$ 2048 Tektronix CCD with 24 μm pixels, and we used grating E2, a 53.67 gr mm^{-1} R2 echelle from Milton Roy Co. For the spectrum

with R $\sim$ 6 $\times$ 10^4, we used slit #4, which has a central width of 511 μm (or approx. 1.2 arcsec on the sky). For the spectrum with R $\sim$ 173000, we used slit #2, which has a central width of 145 μm, and partially masked the collimator. A careful data reduction was applied to both spectra, using IRAF[5], which consisted of overscan (bias) and scattered-light subtraction; flatfielding; extraction of one-dimensional spectra; wavelength calibration; and continuum normalization.

3.2 Observed spectra of Procyon

3.2.1 Near-UV spectrum

We have used spectroscopic data acquired by the STIS instrument on board HST, which have been very accurately flux calibrated (Bohlin, Dickinson & Calzetti 2001). The spectroscopic coverage goes from $\sim$ 2200 to $\sim$ 4080 Å. The details of this spectrum are given in Chapter 8. It has been used to discriminate between different flux-calibrated visible spectra, to derive abundances from the UV continuum opacity and as a test to see how well this medium-resolution observed flux is reproduced by our best-fitting computed flux obtained by reproducing the optical, near-UV and near-IR spectrophotometric flux.

3.2.2 Visible spectra

We have looked for spectrophotometric catalogs containing Procyon data in the CDS web page[6]. We have found the following catalogs:

- The Pulkovo Spectrophotometric Catalog of Bright Stars (Alekseeva et al. 1996, hereafter Pulkovo spectrum): It is a combination of numerous observations made by Pulkovo astronomers at different observing sites, with a range from 3200 to 10800 Å, a resolution of 50 Å and an accuracy not lower than 1.5-2.0 %.

- The Sternberg Spectrophotometric Catalog (Glushneva et al. 1984, hereafter Sternberg spectrum): The observations were made at the Crimean Station of the Sternberg Astronomical Institute during 1970-1984 using a spectrophotometer installed at the 48-cm and 60-cm Zeiss reflectors. It covers the range from 3225 to 7625 Å with a step of 50 Å. The average accuracy of the catalog data is 3.2 %.

[5]IRAF is distributed by the National Optical Astronomy Observatories, which are operated by the Association of Universities for Research in Astronomy, Inc., under cooperative agreement with the National Science Foundation

[6]`http://cdsweb.u-strasbg.fr/`

- The Stellar Spectrophotometric Catalog by Burnashev (Burnashev 1985): Contains spectra in the spectral region 3200-8170 Å by steps of 25 Å. It is a compilation of different spectrophotometric catalogs. Procyon is included in three catalogs: Spectrophotometry of Bright Stars by Glushneva (Glushneva et al. 1982, hereafter Glushneva spectrum), Stellar Spectrophotometric Catalog by Kharitonov (Kharitonov, Tereshchenko & Knyazeva 1978, hereafter Kharitonov spectrum) and Burnashev's observations at the Crimean Observatory.

The difference in absolute flux between some of these visible spectra is large, so we try to discriminate between them by comparing the fluxes with the HST spectrum in the overlapping region. A comparison between the different visible spectra of Procyon from 3500 to 4050 Å (including the HST spectrum to discriminate between them) is shown in Fig. 3.2. The Sternberg spectrum is not shown for clarity. It is very similar to the Glushneva spectrum, except between $\sim$ 3700 and 3850 Å and $\sim$ 3950 and 4000 Å, where the Sternberg flux is $\sim$ 10 % lower. The best agreement with the STIS spectrum is found for Burnashev's and Glushneva's fluxes, so the mean of both was used as the visible observed spectrum.

Although the visible photometric atlas of Procyon by Griffin & Griffin (1979) covers a longer spectral range (from 3140 to 7470 Å in steps of 5 mÅ), we have used the optical spectrum of Allende Prieto et al. (2002) as high-resolution spectrum to derive chemical abundances from spectral lines, because it has a better S/N and is ready to use from the web[7]. It was observed from McDonald Observatory on 1999 January 30 and 31. The Harlan J. Smith 2.7 m telescope and the 2dcoudé spectrograph (Tull et al. 1995), at the focal station F1 were used, delivering a FWHM resolving power of $R \simeq 2 \times 10^5$. Five different spectral setups, selected by tilting the E2 grating, provided almost complete spectral coverage from 4559 to 5780 Å (with a spectral resolution between 20 and 30 mÅ), and different exposures (up to 10 for a single setup) were co-added to reach S/Ns per pixel in the range 550-2000. A comparison between both high-resolution visible spectra is shown in Fig. 3.3. They are very similar in the common region. The comparison between the STIS spectrum and the spectrum by Griffin & Griffin (1979) smoothed to the resolution of the former and multiplied by the absolute mean flux, because it is normalized to the continuum, is shown in Fig. 3.4 for a small region centered close to the line H_{10}. It can be seen the similarity between both spectra.

[7] http://hebe.as.utexas.edu/

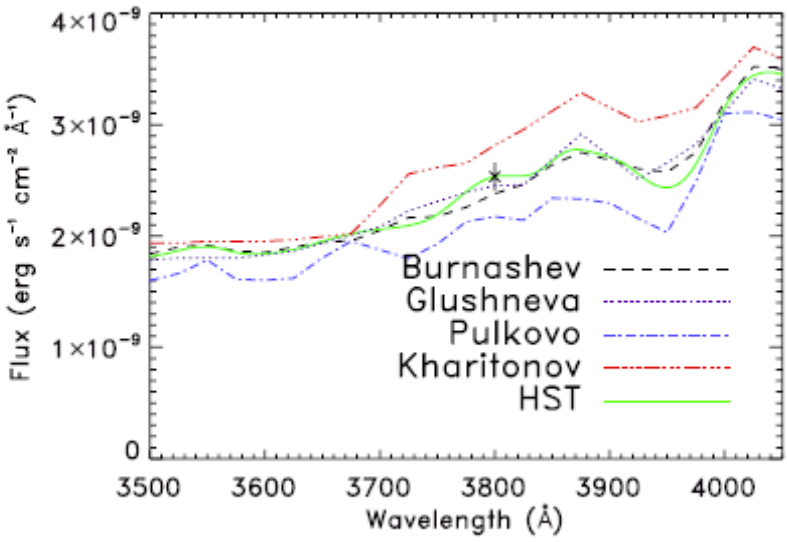

FIGURE 3.2— Comparison between different visible observed spectra of Procyon from the ground and that obtained by the HST (with an error bar) in the overlapping region.

3.2.3 Near-IR spectrum

For the red and near-IR spectrum (wavelengths longer than 6600 Å), the Moscow Spectrophotometric Catalog (Glushneva et al. 1991) has been used. It covers the range from 5975 to 10825 Å, with a step of 50 Å. The observations were made at the Crimean Station of the Sternberg Astronomical Institute during 1978-1990 using the near-IR spectrophotometer installed at the 48-cm and 60-cm Zeiss reflectors. There is a good agreement with the visible observed spectrum in the overlapping region, as is shown in Fig. 3.5, except for the region between ∼7200 and 7300 Å, where the near-IR flux is higher.

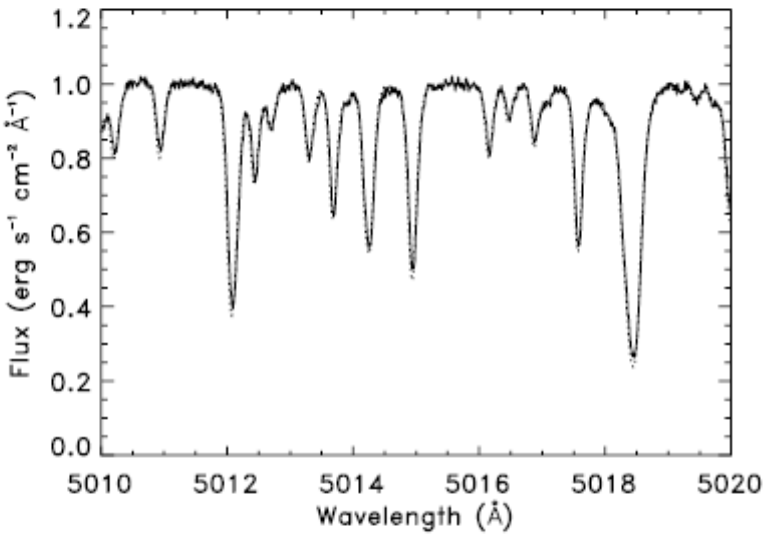

FIGURE 3.3— Comparison between two different high-resolution spectra of Procyon: the spectrum taken by Griffin & Griffin (1979), with solid line, and the spectrum by Allende Prieto et al. (2002) with dotted line.

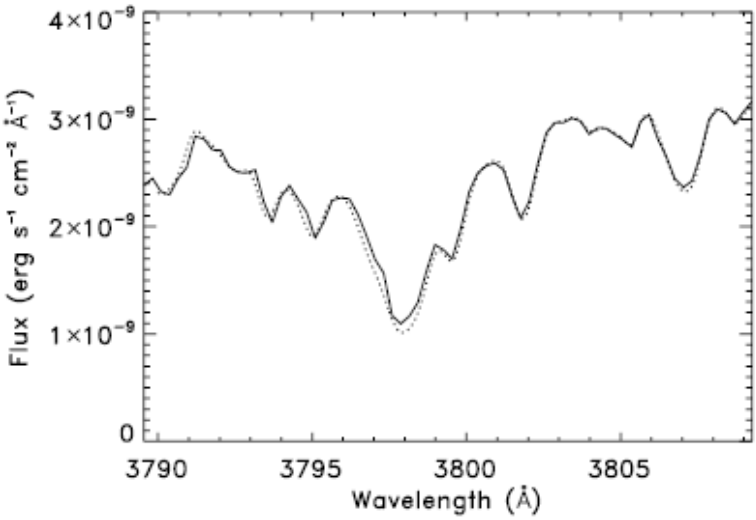

FIGURE 3.4— Comparison between two different observed spectra of Procyon: the spectrum taken with STIS (solid line) and the spectrum by Griffin & Griffin (1979) smoothed to the same resolution, with dotted line.

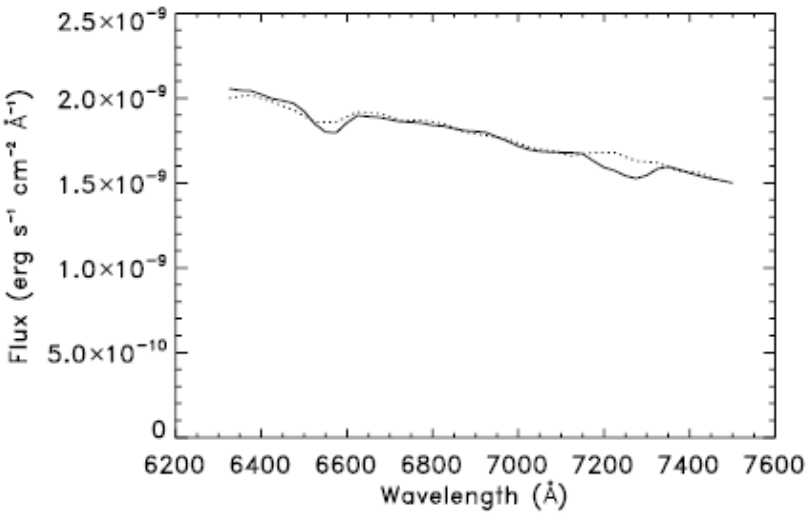

FIGURE 3.5— Comparison between the observed spectrum of Procyon that we have used in the visible range (the average of Burnashev's and Glushneva's flux; solid line) and the spectrum that has been used in the IR region (taken from the Moscow Spectrophotometric Catalog; dotted line) in the overlapping region. Both are very similar, except between ∼7200 and 7300 Å, where the Moscow Catalog's flux is higher.

4

The study of Vega's spectrum using classical model atmospheres

It's an intricate and complex Message. The transmitting civilization is eager for us to receive it. Maybe all this is one small volume of the Encyclopedia Galactica. The star Vega is about three times more massive than the Sun and about fifty times brighter. Because it burns its nuclear fuel so fast, it has a much shorter lifetime than the Sun

"Contact", Carl Sagan

THIS chapter describes the work carried out using classical model atmospheres to derive some physical parameters and chemical abundances of Vega. In §4.1 we calculate the most abundant ions present in the atmosphere of Vega as a preliminary step to derive the most important contributors to the continuum opacity in Vega. The most relevant ions contributing to the line opacity have also been identified. In §4.2 we use low-dispersion visible, near-IR and near-UV spectra of Vega (in regions where the continuum opacity due to elements different to H is not relevant, and fixing the surface gravity and the metallicity) to derive its effective temperature and angular diameter using the different IUE calibrations available in order to decide which one/s is/are the most reliable near-UV spectrum. We have derived these parameters calculating the flux obtained using Kurucz's model atmospheres in SYNPLOT for each set of parameters and matching these spectra to that observed. Once obtained a reliable low-dispersion spectrum, we have re-derived the effective temperature and angular diameter of Vega. Some tests have been carried out in order to

see the relevance of the result: we have re-derived the parameters using another set of model atmospheres, compared our parameters with those derived by other authors, compared the synthetic spectrum using the parameters of our best fit with a high-dispersion spectrum and made a preliminary test to see whether the effect of seen pole-on a rapid rotator with the parameters from other authors can account for the shape of the observed lines. In §4.3 we derive the abundances of the most relevant contributors to the continuum opacity matching synthetic low-dispersion spectra to that observed in the regions of the UV where the effect of continuum absorption is higher, fixing the parameters derived in the section before. We have also derived the error bars of the determination in order to see the relevance of the result and have tried to explain the reasons why the observed flux is not well reproduced by that synthetic in some wavelength regions, trying to explain the differences in some regions using departures from LTE. In §4.4 we have used the high-dispersion visible spectrum to derive the abundances of some elements (among them, those obtained in the section before) from spectral lines, comparing them with those derived from the UV low-dispersion spectrum and with those obtained from the literature.

4.1 Main contributors to the continuum and line opacity in Vega

A few particular elements may contribute significant opacity in the UV. Iron is known to dominate line absorption virtually for all spectral types. Continuum absorption from other metals may also be significant or even dominant. The main contributors to the UV continuum opacity change with the spectral type and, therefore, it is important to evaluate which metals are relevant and provide reasonable estimates of their abundances to calculate realistic UV fluxes. The capability of an ion to contribute bound-free opacity depends on its atomic structure and its abundance. As a preliminary step, ion abundances for the lightest thirty elements in the first three stages of ionization were computed for a star like Vega, using a model atmosphere with the parameters preferred by Castelli & Kurucz (1994; an effective temperature $T_{\rm eff} = 9550$ K and gravity $\log g = 3.95$) and Saha and Boltzmann equations. The number of ionized atoms per unit volume N_1 respect to the number of neutral atoms N_0 is, according to Saha's equation:

$$\frac{N_1}{N_0} = \frac{(2\pi m)^{3/2}(kT)^{5/2}}{h^3 P_e}\frac{2u_1(T)}{u_0(T)}e^{-\frac{I}{kT}} \tag{4.1}$$

where u_1/u_0 is the ratio of the partition functions of ions to neutral atoms (using a polynomial approximation of the partition functions, truncating the summation according to the Debye radius of the ion, which depends on electron

pressure or density, where the partition function is $u(\mathrm{T}) = \sum g_i \exp(-\chi_i/k\mathrm{T})$, with g_i the statistical weight 2J+1 and χ_i the excitation potential, both for level i); m is the electron mass; k is Boltzmann constant; I is the energy difference between the ground level and the continuum; T is the temperature; P_e is the electron pressure and h is the Planck constant. At this point we simply assumed solar photospheric abundances from Grevesse & Sauval (1998).

Next, we computed synthetic visible and near-UV spectra including continuum opacity produced by H only (including bound-bound H opacity, i.e. hydrogen lines, as part of continuum opacity) and each of the most abundant ions in Vega. We studied all the ions with abundances relative to H larger than 10^{-6}: He I, C I, C II, N I, N II, O I, O II, Na II, Mg II, Al II, Si II, S II, Ca II, Fe II and Ni II. A contribution could be missed if it corresponds to an ion with a low abundance but an unusually high photoionization cross section, but we believe our list is complete. For these calculations, the atmospheric parameters of Castelli & Kurucz (1994) were used as well as solar abundances, except for Fe, for which we adopt [Fe/H] = −0.34, to be consistent with the model atmosphere: [M/H] = −0.5 (see the discussion in chapter 2). We compared the derived spectra that include continuum opacity due to H plus any given ion, F(X,H), with the spectrum that includes only neutral H continuum opacity, F(H), in Fig. 4.1. Contributors producing at least a decrease of 0.5 % in the flux in some part of the region considered are included, except for He I, which would also appear in the figure at wavelengths below 1400 Å with a maximum of ∼1.5 %, but has not been included for clarity, and neutral H, because it can not be included due to the criterion adopted. From this comparison, we deduced the relevance of each ion's continuum opacity to the observed fluxes. Hydrogen bound-free and line absorption dominate the opacity blueward of the wing of Lα at about 1500 Å, shaping the near-UV and optical spectrum of Vega. At wavelengths longer than about 1500 Å, neutral hydrogen and the H^- ion dominate the total bound-free opacity. Si and C contribute significantly to the continuum opacity between 1200 and 1450 Å.

Fig. 4.2 shows the continuum and line absorption due to each ion. The UV spectrum of solar-like stars contain many Fe I lines. At the temperatures in Vega's photosphere, iron is almost completely ionized ($\mathrm{N_{FeI}/N_{FeII}} \sim 10^{-4}$), and the atomic line absorption is mainly produced by Fe II (around half the total absorption of lines and most of the absorption due to Fe lines). Molecules are virtually nonexistent at these warm temperatures. All the fluxes shown in Fig. 4.2 include a contribution to the total opacity by electron scattering. Although Thomson scattering is wavelength independent, the vertical structure of the atmosphere produces a maximum absorption due to this effect at about 1300 Å, where it effectively reduces the emerging flux by about 4 %, and over 1 %

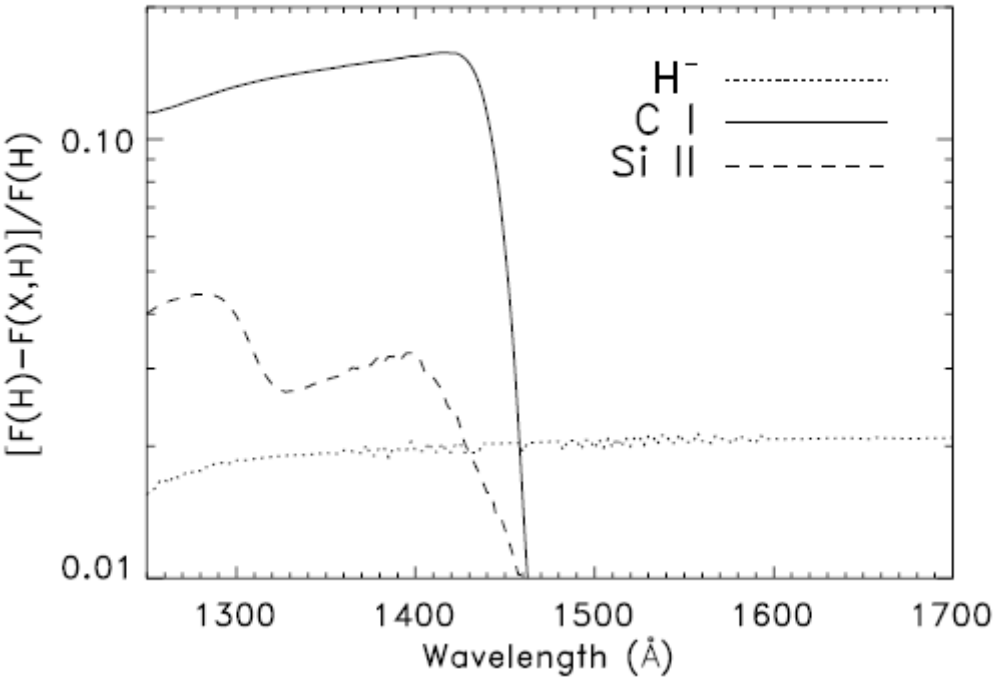

FIGURE 4.1— Relative difference in logarithmic scale between the flux computed by considering neutral H and each ion X explicitly (F(X,H)) and the flux obtained by just taking into account neutral H explicitly (F(H)) using SYNSPEC with Kurucz's model atmospheres. The change in neutral H opacity is also considered in the line labeled as H^-, because the number of protons is constant, and therefore the abundance of neutral H diminishes when including H^-. Note the importance of C I below 1450 Å, and that of H^- above this wavelength.

for $\lambda < 2000$ Å. In conclusion, to model the UV spectrum of a star like Vega it is necessary to account for H, C, Si, and Fe opacities in as much detail as possible.

4.2 Estimation of the effective temperature and angular diameter of Vega by using visible, near-IR and near-UV regions

Allende Prieto & Lambert (1999) estimated a set of fundamental parameters for a large sample of nearby stars, using Hipparcos parallaxes to accurately constrain their positions in the color-magnitude diagram. Comparison with evolutionary calculations by Bertelli et al. (1994) allowed them to provide masses, radii, gravities and effective temperatures for 17,219 stars. Their analysis yields $\log g = 3.98 \pm 0.02$ for Vega. Given the high accuracy in the determination of gravity and its low relevance on the computed fluxes according to some tests

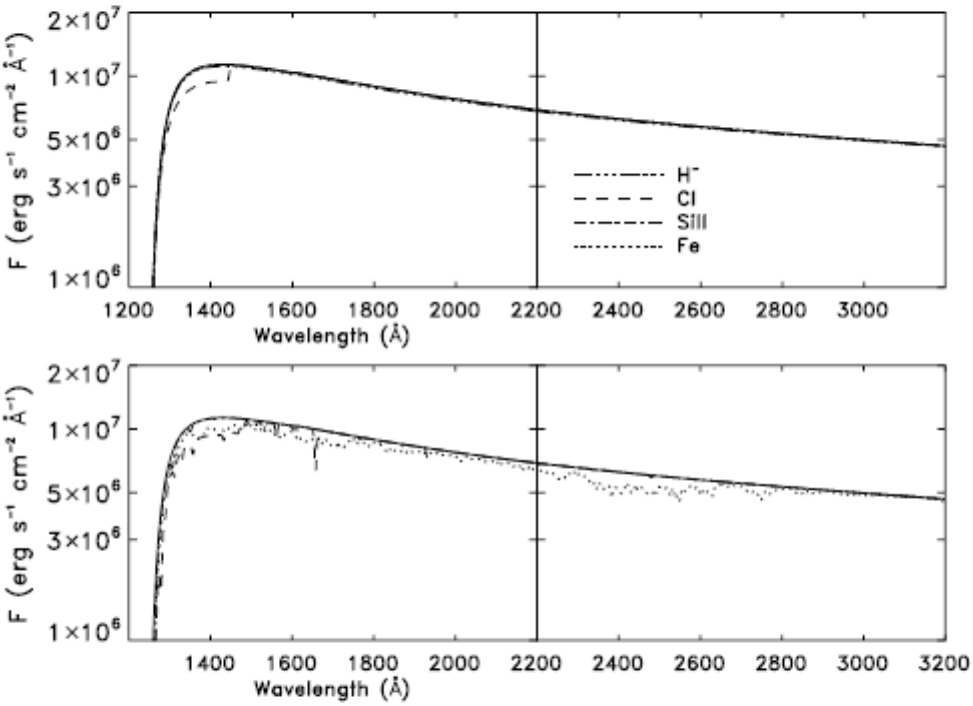

FIGURE 4.2— *Top*: Emergent flux when only the continuum absorption produced by H^-, C I, Si II and Fe is considered. The other ions contribute much less to the opacity and are not included for clarity. *Bottom*: Emergent flux when the total (continuum+metal line) opacity is considered. The curve corresponding to H^- has been omitted in the right panels for clarity. The solid line is the flux when only neutral H opacity is considered.

that we have carried out, we will adopt this value. We will attempt to determine the effective temperature and the angular diameter (D_{ang}) considering limb darkening from the observations in the optical, near-UV and near-IR. This can be achieved by comparing the computed emitted flux using SYNPLOT with Kurucz's model grids (which have [M/H], $\log g$ and T_{eff} as independent parameters), transformed to computed received flux by using the angular diameter and parallax, to the observed flux. In these regions, metal absorption is modest, which allows us to study these two parameters independent of the details of the chemical composition.

We minimized the sum of χ^2 statistics between observed and computed spectra in three wavelength regions: between 1600 and 2150 Å between 2200 and 3000 Å and between 4150 and 8480 Å, excluding Balmer lines. The χ^2 statistics were weighted according to the approximate uncertainty in the observed fluxes inferred from Bohlin's analysis in the UV and Hayes' in the visible range (4% from 1600 to 3000 Å and 2% from 4150 to 8480 Å). Using SYNSPEC (see Chapter 2), we computed a grid of fluxes based on interpolated Kurucz's model atmospheres with T_{eff} running between 9350 and 9650 K in steps of 50 K. As the model atmospheres are available in steps of 250 K, we linearly interpolated all the relevant quantities as a function of the optical depth. We matched selected spectral regions, excluding the segments where special difficulties exist. In particular, the spectrum in the vicinity of the Balmer jump (3000–4150 Å) was discarded because Hayes advises about significant errors in this region and the effect of fast rotation is important (Gulliver et al. 1994). At this stage, a solar He abundance was used and the metal abundances of Vega are taken from Qiu et al. (2001), including [Fe/H] $= -0.54$, so we have considered a Kurucz's model atmosphere with [M/H] $= -0.7$, using the same conversion factor as in chapter 2. The best-fitting pairs (T_{eff}, D_{ang}) and the quality of the fit are displayed in Table 4.1. The fit is clearly better in the near-UV (especially between 2200 and 3000 Å) using Bohlin's calibration than using the INES one. Fig. 4.3 confronts the observed flux (using Bohlin's calibration in the top panel and the INES calibration in the bottom panel) and the computed flux that best matches it. In that figure, the computed flux is clearly lower than the observed one for $\lambda < 1900$ Å and $4150 < \lambda < 4500$ Å when using the parameters of the best fit with INES calibration, and it is clearly higher than the observations for $2200 < \lambda < 3000$ Å, so most of the observed spectrum below 4500 Å is poorly reproduced by the synthetic spectrum of the best fit when using the INES calibration. This can be explained when taking into account that INES UV flux is lower than Bohlin's, but the same visible observed flux has been used. Taking into account that the effect of T_{eff} on the flux is larger at low wavelengths, but the effect of D_{ang} is uniform with wavelength, it is necessary

to decrease T_{eff} and to increase D_{ang} in order to decrease the UV flux fixing the visible one. Considering the fact that the spectrum behaves quite smoothly when changing one parameter of the model atmosphere used and the fact that the flux obtained from one Kurucz's model atmosphere matches both the visible and Bohlin's calibration quite well, it is impossible to obtain a good fit to the INES calibration and the visible spectrum at the same time, but there is a good fit in some part in the middle of the near-UV region, being the slope of the synthetic spectrum different to that of the observed spectrum. This is the reason why we have assumed that the HST flux scale is more reliable than the INES one.

A comparison between these parameters for Vega and those taken from the literature is made in Table 4.1. The selected literature values do not include analyses of UV spectra from IUE. T_{eff} runs the gamut between 9430 and 9660 K and D_{ang} between 3.225 and 3.28 mas. These values are consistent with the parameters obtained with Bohlin's calibration (or with M&F corrected fluxes, given that both are on the same scale). However, the angular diameter derived from the analysis of the INES spectrum is significantly higher than the literature values. In addition, there are only two T_{eff} determinations that are consistent with the result associated with the INES calibration: the extreme value found by Moon & Dworetsky (1985) and that by Ciardi et al. (2001). As the difference in the absolute flux for Vega between INES and the other calibrations amounts to more than 10% for Vega, we have derived an average UV spectrum as the mean of Bohlin's calibration and M&F's, not taking into account INES. Using this flux, we have matched again the region between 2200 and 8500 Å (without the zone between 3000 and 4150 Å and without the Balmer lines). We have not used the region below 2200 Å because the typical deviation of the fit of Bohlin's calibration for Vega is much higher than that of the region over that wavelength, which suggests that our synthetic fluxes can not reproduce the observed flux at those wavelengths. Moreover, as shown in Chapter 3, there are large differences at ~1800 and at ~2000 Å (this one probably due to the uncertainty of the observed flux at the border of the cameras) between the different spectra of Vega in the HST flux scale, so the error bars of the observed flux will be high below ~2200 Å, and the quality of the fit between computed and observed spectra would be low. We have obtained the following result:

$T_{eff} = 9620^{+49}_{-63}$ K, $D_{ang} = 3.272 \pm 0.05$ mas

where the error bars of our T_{eff} and D_{ang} estimates were derived by perturbing the best-fitting parameters until the flux variation exceeded the error bars assigned to the observed spectrum.

The same analysis (fixing $\log g = 3.98$ and $[M/H] = -0.7$ in model atmospheres and using the same abundances as in the calculation before) was

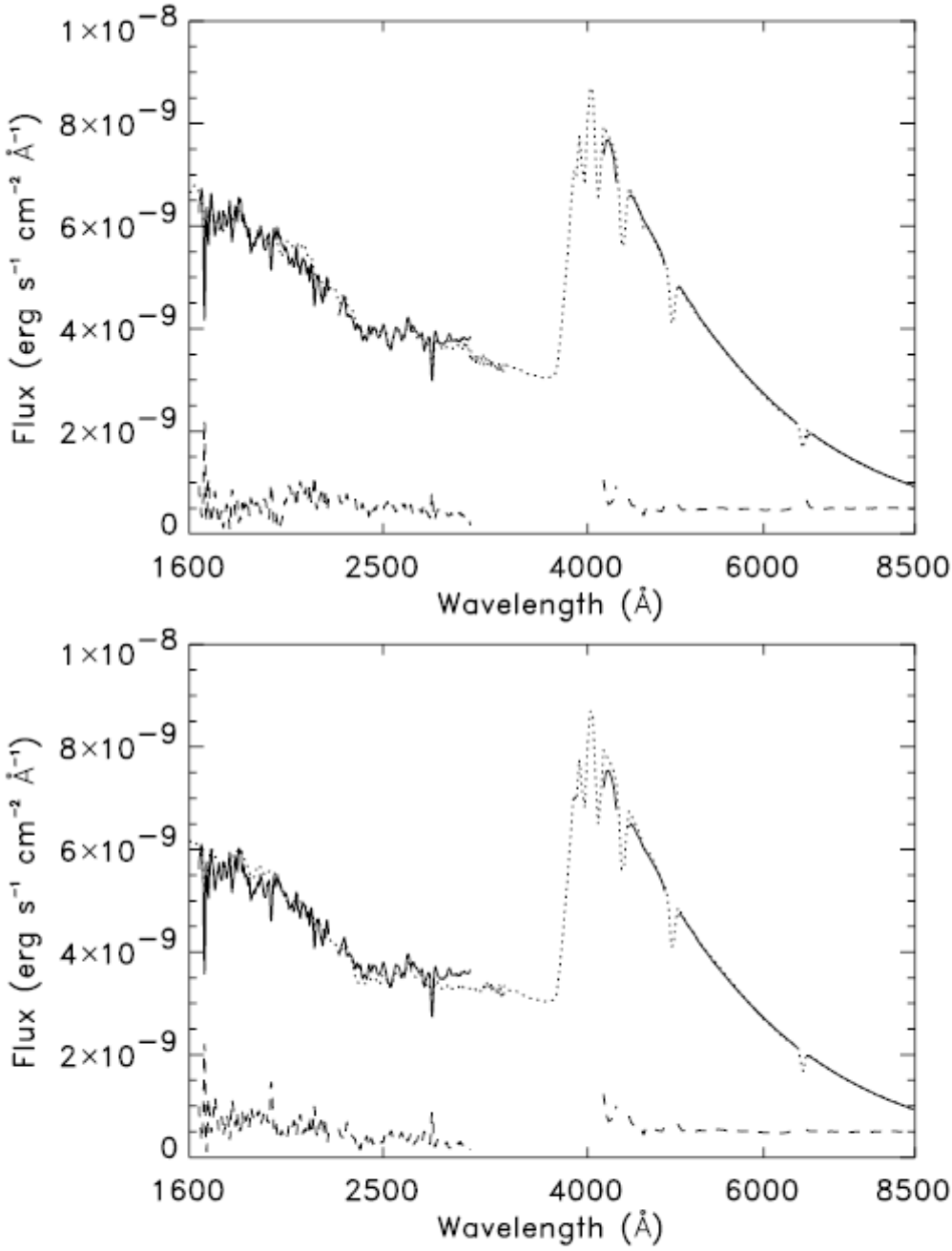

FIGURE 4.3— Best fit between the observed flux of Vega (dotted line) calibrated by Bohlin (top panel) and INES (bottom panel), and the computed flux (solid line). The residuals (observed minus computed flux shifted for clarity to 0.5×10^{-9}) are also shown (dashed line). The stellar parameters associated with the adopted model atmosphere are shown in Table 4.1. The other Kurucz's model parameters used are log $g = 3.98$ and [M/H] $= -0.7$. Abundances were taken from Qiu et al. (2001), except for He and Fe, for which solar abundance and [Fe/H] $= -0.54$ were used, respectively.

TABLE 4.1— Parameters and errors of the best fit between synthetic and observed spectra of Vega using different calibrations. σ_{1622}, σ_{2230} and σ_{4085} are the typical deviation of the fit between 1600 and 2150 Å, between 2200 and 3000 Å and between 4150 and 8480 Å, respectively.

Calibration	T_{eff} (K)	D_{ang} (mas)	σ_{1622}	σ_{2230}	σ_{4085}
Bohlin's	9631	3.272	4.9 %	2.9 %	1.3 %
INES	9458	3.324	5.9 %	5.7 %	1.4 %

TABLE 4.2— Parameters for Vega according to the literature.

Reference	T_{eff} (K)	D_{ang} (mas)	[M/H] (dex)
Code et al. (1976)[1]	9660 ± 140	3.24 ± 0.07	-
Moon & Dworetsky (1985)[2]	9430 ± 200	-	-
Alonso, Arribas & Martínez-Roger (1994)[3]	9610	3.24 ± 0.07	−0.25
Castelli & Kurucz (1994)[4]	9550	-	−0.5
Fitzpatrick & Massa (1999)[5]	9600 ± 10	3.26 ± 0.01	−0.73 ± 0.06
Ciardi et al. (2001)[6]	9553 ± 111	3.28 ± 0.01	-
Mozurkewich et al. (2003)[7]	9657 ± 119	3.225 ± 0.032	-
This work[8]	9620^{+61}_{-56}	3.27 ± 0.05	−0.7

[1]Obtained from interferometric angular size measurements and its absolute flux distribution using optical fluxes from the ground and UV fluxes from the OAO-2 satellite

[2]Based on uvbyβ photometry, with error estimation from Qiu et al. (2001)

[3]Using the Infrared Flux Method (IRFM) to calibrate the absolute flux of stars with interferometric measurements of angular size

[4]Parameters of the Kurucz's model producing the synthetic spectrum that best matches the observed one (in the visible and the UV, with Bohlin's calibration, and near-IR). A solar He abundance has been adopted, with no reddening and with a microturbulence of 2 km s^{-1}

[5]The uncertainties given are 1σ internal errors for the fittings of the synthetic spectrum derived from Kurucz's models to the observed one (in the visible, the near-IR, and the near-UV, with the M&F calibration)

[6]Angular diameter obtained from interferometry at 2.2 μm

[7]Angular diameter obtained from optical interferometry

[8]Using Kurucz (1992) model atmospheres

carried out using new model atmospheres (Castelli & Kurucz 2003) which were calculated with overshooting turned off (resulting in a steeper rise in temperature with depth in the region where the optical continuum is formed; Castelli, Gratton & Kurucz 1997), and using updated values for the solar elemental abundances and revised opacity distribution functions (ODFNEW). The reason for this new analysis is to check the effect on colors of convective overshoot and the parameters thus obtained were:

T_{eff} = 9575 K, D_{ang} = 3.271 mas,
where σ_{2230} = 2.4 % and σ_{4085} = 0.7 %. These values provide a slightly better fit, but are nonetheless consistent with those obtained using older model atmospheres and also with most values from the literature.

Fig. 4.4 compares the observed and calculated fluxes, including the interpolation of calculated fluxes when using ODFNEW model atmospheres with these T_{eff} and D_{ang} values and the C and Si abundances from section 4.3. There is a slight difference between the synthetic spectra in the region between $\sim$ 1400 and $\sim$ 1900 Å, where the flux of the ODFNEW models is higher, except at $\sim$ 1560 Å, where there is no change. For instance, the fit is better at $\sim$ 1450 Å using ODFNEW models.

Adopting the T_{eff} and [M/H] values from Alonso, Arribas & Martínez-Roger (1994) from the Infrared Flux Method, we searched only for the value of D_{ang} leading to the closest match to the observed spectrum in the near-UV and the visible ranges, obtaining again a value of 3.27 mas. Using this angular diameter, the fit to the observed flux is very satisfying in the near-UV and visible spectral ranges, which reinforces the validity of our method. We discuss the UV fluxes below.

A high-resolution spectrum using the interpolated Kurucz (1992) model atmospheres with T_{eff} = 9620 K and log g = 3.98, and an angular diameter of 3.27 mas, has been computed and compared with the high-resolution IUE observed spectrum in three 100 Å-wide spectral regions randomly selected between 1550 and 3050 Å, where the effects of rapid rotation and Si and C continuum opacities on the flux are very limited. To calculate the spectrum, we have used the following projected rotational velocity: $v_{equat} \cdot \sin i$ = 23 km s^{-1}, as proposed by Gray (1980) for Vega, and we have smoothed the resulting spectrum to the spectrograph resolution: 0.2 Å. The standard deviations between the computed and the observed spectra are: 8.5 % in the region centered at 1668 Å, 9.9 % at 2174 Å and 6.9 % at 2550 Å, which, although are higher (about twice) than the values derived from the low-resolution spectra (4.9 % from 1600 to 2150 Å and 2.9 % for wavelengths over 2200 Å, see Table 4.1 for Bohlin's calibration), reproduce the shape of the high-resolution observations quite well. Fig. 4.5 compares the computed and the observed fluxes in three 20 Å-wide windows,

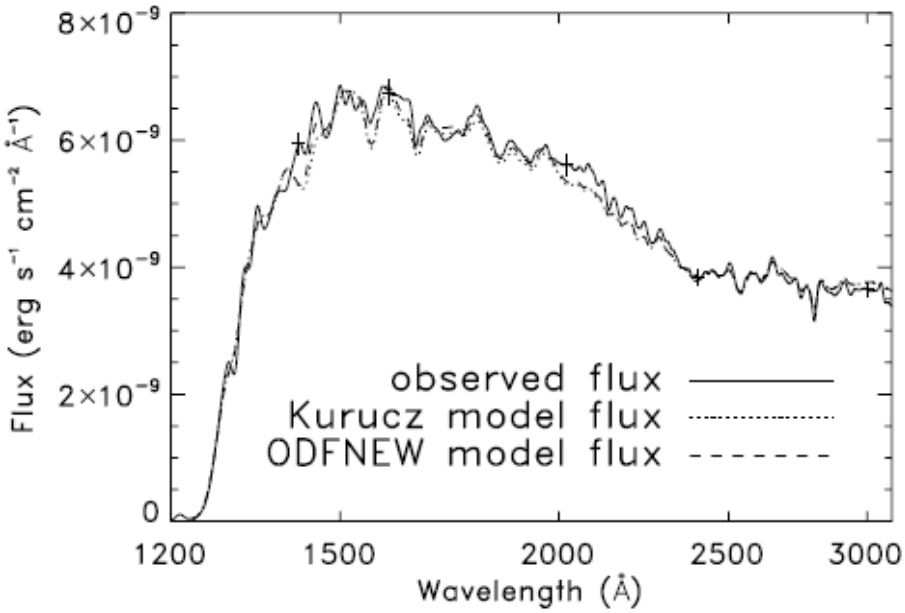

FIGURE 4.4— Comparison between the observed spectrum of Vega (mean of Bohlin's and M&F, with error bars) and the computed spectrum using a Kurucz's model atmosphere with the following parameters: $T_{\rm eff}$ = 9620 K, $\log g$ = 3.98, [M/H] = −0.7, [Si/H] = −0.90 and [C/H] = 0.03 and the computed spectrum using an ODF model atmosphere with the following parameters: $T_{\rm eff}$ = 9575 K, $\log g$ = 3.98, [M/H] = −0.7, [Si/H] = −0.90 and [C/H] = 0.03. The adopted angular diameter is 3.27 mas.

one in each region.

A preliminary test taking into account the rapid rotation on the emergent flux of spectral lines was also performed. Some of the parameters used (T_{polar} = 9595 K and i = 6 degrees) were taken from one of the best fits to the observed flux by Gulliver et al. (1994)[1], following the procedure used by Pérez Hernández et al. (1999) to compute the flux. This procedure assumes uniform rotation and gravitational potential as a mass point. Using these stellar models with the line O I λ6158.19 Å, the synthetic line becomes deeper and deeper and less and less broad when the rotational velocity decreases, obtaining a good fit with a rotation equatorial velocity v_{equat} = 210 km/s, for which $v_{equat} \cdot \sin i$ = 22.0 km/s, consistent with the slow-rotating value. The comparison between the observed line and the computed ones with v_{equat} = 170, 210 and 250 km/s is shown in Fig. 4.6. This effect on the spectral lines is considered in detail in Chapter 6.

4.3 Estimation of Si and C abundances from the UV continuum

We turn to the main issue we are interested in, the analysis of the UV spectrum. In Section 4.1, we concluded that Si and C were important contributors to the UV continuum opacity for a star like Vega. With the adopted atmospheric parameters (gravity derived from the *Hipparcos* parallax, log g = 3.98, the metallicity of the model atmosphere fixed to [M/H] = −0.7 and T_{eff} obtained fitting the optical and near-IR flux, T_{eff} = 9620 K) and D_{ang} also obtained fitting the optical and near-IR flux, D_{ang} = 3.27 mas, we now attempt to constrain the abundances of these elements from the UV flux, fixing the others to those from Qiu et al. (2001). We calculated synthetic spectra from 1270 Å to 1380 Å and from 1460 Å to 1550 Å. The region between 1380 and 1460 Å is not considered because of exceptional problems that we discuss below. We considered Si abundances (from Grevesse & Sauval 1998) between [Si/H] = −1.1 and −0.5 and C abundances between [C/H] = −0.1 and 0.2, to find C and Si abundances varying both at the same time. In Fig. 4.7, we can see the effect of a change of 0.2 dex in the abundances of C (top left) and Si (top right), the effect on the flux of a change of He abundance (solar abundance versus our adopted value, bottom left) and the effect of a change of 100 K in T_{eff} (bottom right), using the atmospheric parameters, D_{ang} and the other abundances as

[1]However, the other parameters used are different. We have used the observed angular diameter (3.27 mas, taken from this thesis) and the distance (7.76 pc, obtained from the Hipparcos parallax) to derive the equatorial radius (2.73 $R_\odot$), and also the polar radius by using the stellar model. We have also used the mass of a typical A0V star (2.4 $M_\odot$) to calculate the surface gravity.

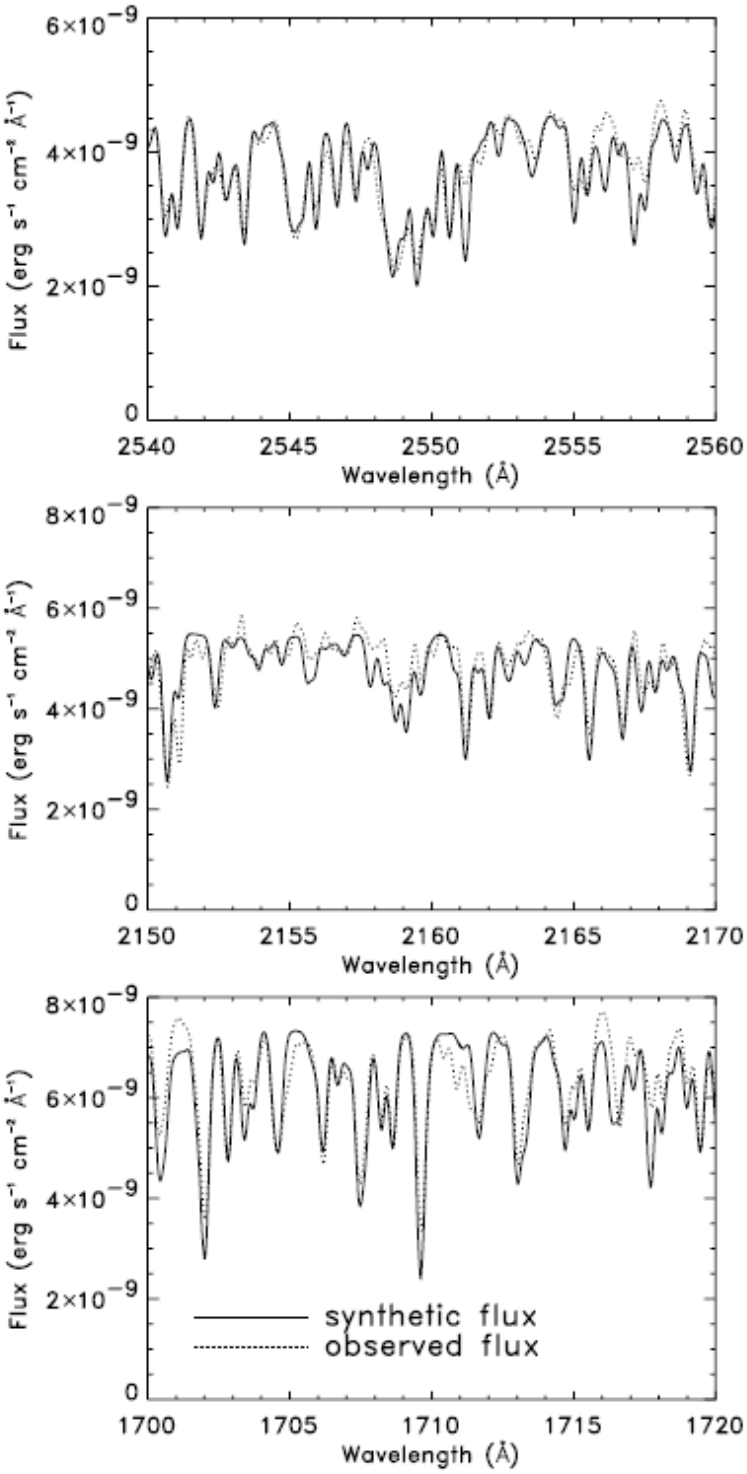

FIGURE 4.5— Comparison between the observed flux of Vega (dashed line, INES increased by a 10 % to take the fluxes to the HST scale) and the computed flux (solid line) at high resolution. The stellar parameters associated with the adopted model atmosphere are $T_{\mathbf{eff}}$ = 9620 K, [M/H] = −0.7 and log g = 3.98. The angular diameter used is 3.27 mas and abundances are taken from Qiu et al. (2001), except for He, for which solar abundance was used.

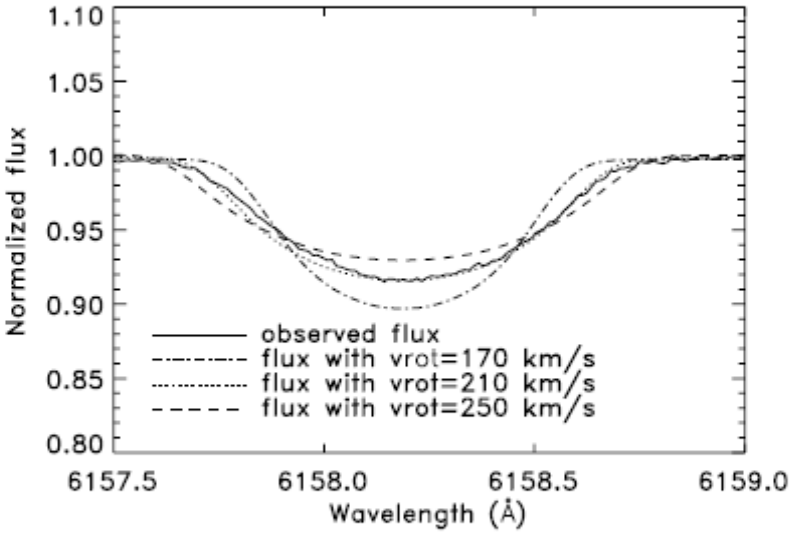

FIGURE 4.6— Comparison of the normalized high-resolution observed flux next to O I λ6158.19 Å and the normalized synthetic fluxes using T_{polar} = 9595 K and i = 6 degrees and different rotational velocities: v_{equat} = 170, 210 and 250 km/s.

commented above.

The best fit to the observations is obtained for [Si/H] = $-0.90\ ^{+0.57}_{-2.10}$ and [C/H] = $0.03\ ^{+0.34}_{-0.48}$, with σ_{rms} = 3%, approximately the same as the uncertainty of the UV observed spectrum of Bohlin's calibration (see §3.1.1), which can be approximated as the uncertainty of our UV observed spectrum. The error bars take into account the uncertainty in He abundance (assumed ±0.1 dex, since it seems reasonable), T_{eff}, the observed flux, and Si abundance (C abundance) when computing the error in C abundance (Si abundance), where the first two error sources are relevant. The values obtained by Qiu et al. (2001) from the analysis of visible lines were [Si/H] = -0.59 ± 0.06 and [C/H] = -0.06 ± 0.13. The reference solar abundances were adopted from the literature (Grevesse & Sauval 1998) and not derived by us following a similar procedure using the UV solar spectrum.

The large error bars in the UV-based abundances are the result of the relatively weak response of the UV continuum to changes in metal abundances, which is primarily a consequence of the dominant role of the hydrogen opacity in such a warm atmosphere. In addition, the existence of several spectral regions where the agreement between observed and computed fluxes is, independently

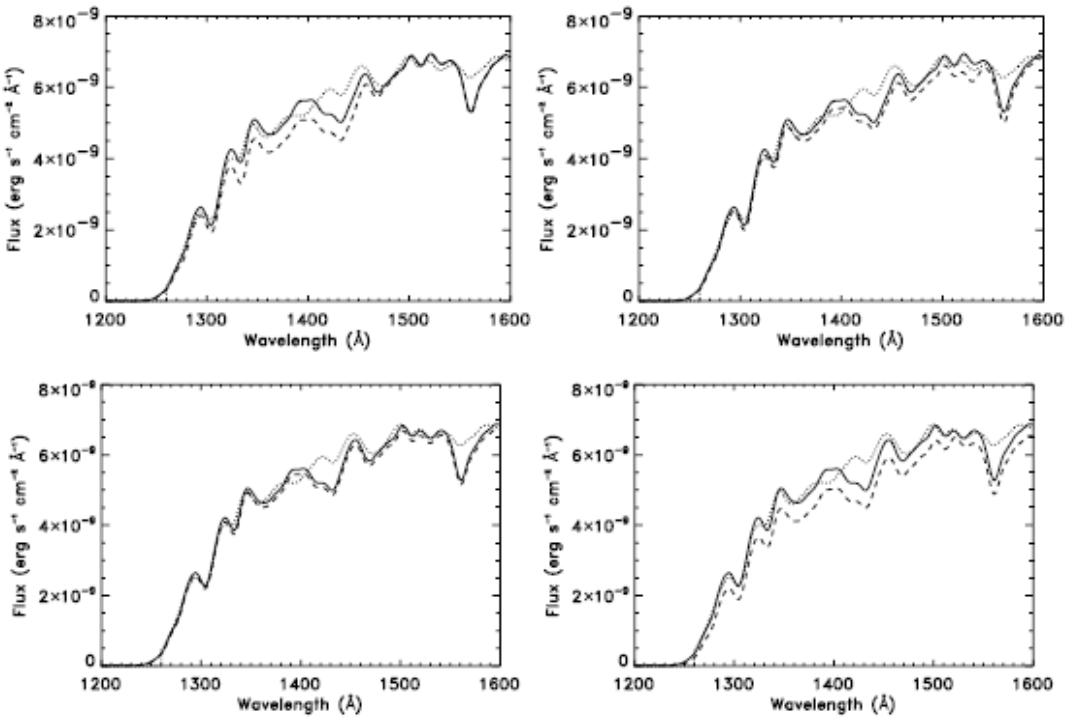

FIGURE 4.7— Comparison between the observed flux of Vega (dotted lines) and different computed fluxes: the computed flux using [C/H] = +0.03 (solid line, top left) and [C/H] = +0.23 dex (dashed line, top left); the computed flux using [Si/H] = −0.90 dex (solid line, top right) and [Si/H] = −0.70 dex (dashed line, top right); the computed flux using solar abundance of He from Grevesse & Sauval (1998): N(He)/N(H) = 0.085 (solid line, bottom left) and He abundance from Kurucz (1992) models: N(He)/N(H) = 0.098 (dashed line, bottom left); and the computed flux using T_{eff} = 9620 K (solid line, bottom right) and T_{eff} = 9520 K (dashed line, bottom right). The stellar parameters associated with the adopted model atmosphere are commented in the text.

of the adopted abundances, poor, has quite a negative impact on our potential to derive abundances from UV fluxes. Some of the most remarkable discrepancies are associated with deep Si I and C I lines (for instance, at $\sim$ 1560 Å and at $\sim$ 1660 Å), most likely because departures from LTE, neglected in our calculations, are important. These departures may contribute somewhat for the solar case, but are expected to be more important for a star like Vega (see, e.g., Hubeny 1981; Hauschildt, Allard & Baron 1999). This effect is known to affect C I, Si I and Si II lines (Wedemeyer 2001, Stürenburg & Holweger 1990) and could also affect the C and Si abundances derived from the UV continuum. However, some deep lines of other species (like Fe II) are well reproduced in LTE. A comparison between these C and Si lines in LTE and NLTE (using TLUSTY to derive the level populations in detailed balance for departures from LTE, maintaining the structure of the model atmosphere) with the observed lines is shown in Fig. 4.8. A list of some of the deepest lines in these regions is given in Table 4.3. The regions between 1380 and 1460 Å and between 2000 and 2200 Å show also a disappointing mismatch between observed and calculated fluxes. The reason for this failure is not clear (although the fit improves when using NLTE, but not enough), and a similar effect is apparent when using revised Vega fluxes based on STIS spectra (Bohlin & Gilliland 2004). The new STIS fluxes agree much better with the computed flux in Balmer lines, thus supporting the exclusion of these lines in our analysis of IUE data. This revised flux is lower than the Hayes fiducial, so it would be necessary a lower $T_{\rm eff}$ and $D_{\rm ang}$ to reproduce this revised flux.

4.4 Estimation of abundances from spectral lines in the visible range

To make a consistent comparison between UV abundances and those derived from spectral lines in the visible region, we have selected a set of clean lines with an uncertainty in log gf smaller than 25% from Przybilla (2002)[2], using his gf values, except for Fe II lines, which log gf values were taken from Allende Prieto et al. (2002). We have excluded from consideration He lines, because they are too weak, and the Na I resonance doublet, because of the important departures from LTE in the core of these lines. We have measured the equivalent width (EW) of these lines by integrating the flux over the whole line using

[2]We prefer to revisit the optical abundances for this star because newer, high-quality data is now available, and because that is the only way to guarantee the analysis is fully consistent with our UV study. The reader should, however, keep in mind that our LTE analysis is more limited than previously published studies such as Przybilla (2002), who studied several species in NLTE

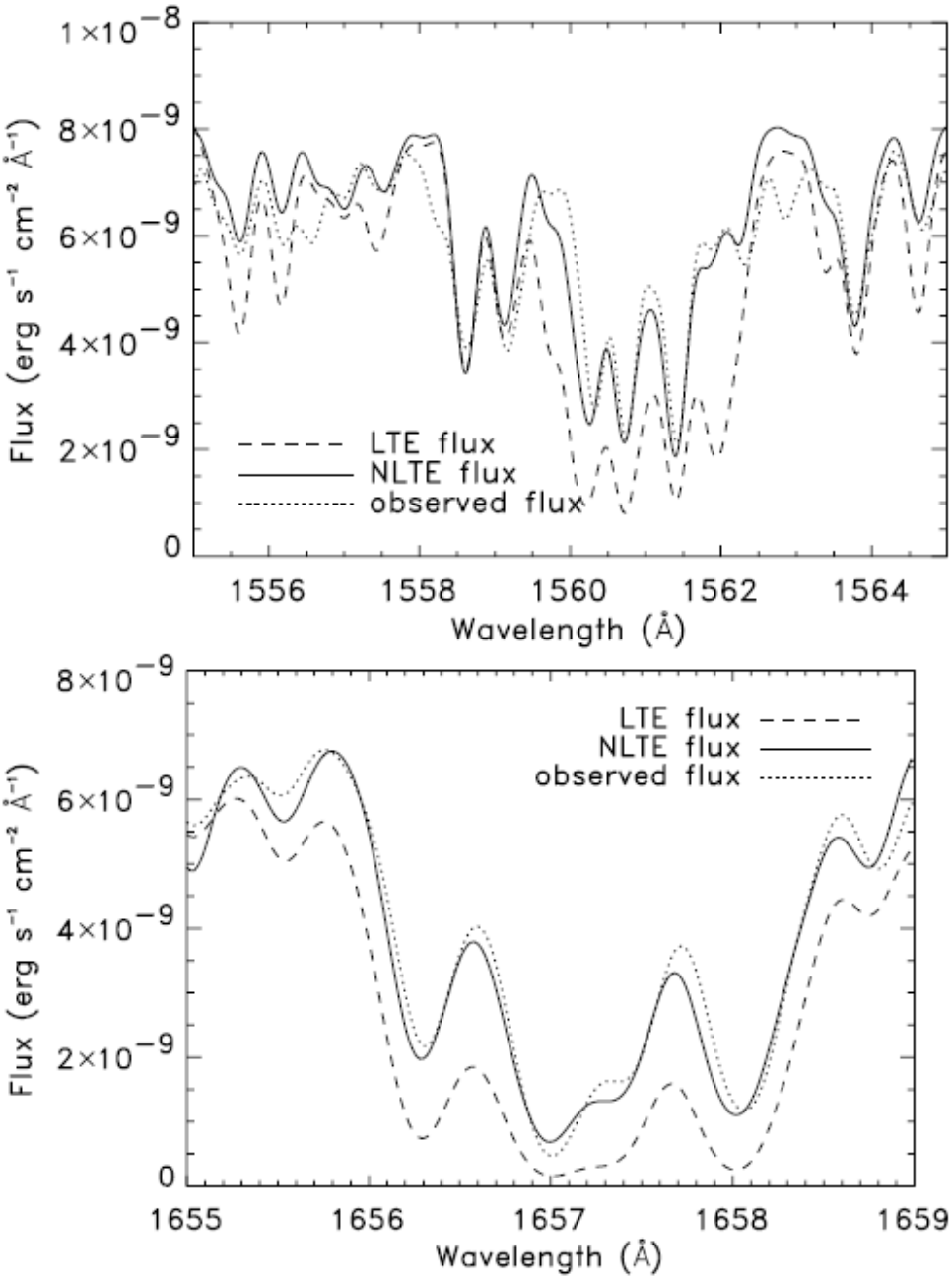

FIGURE 4.8— Comparisons between the observed spectrum of Vega (mean of Bohlin's and M&F) and the computed spectrum around two wavelength regions (which have a poor fit in LTE in low resolution) using a Kurucz's model atmosphere with the following parameters: $T_{\rm eff}$ = 9620 K, $\log g$ = 3.98, [M/H] = −0.7, [Si/H] = −0.90 and [C/H] = 0.03, in LTE and using level populations calculated in NLTE with TLUSTY. The regions are ∼ 1560 Å (top) and ∼ 1657 Å (bottom). The adopted angular diameter is 3.27 mas.

TABLE 4.3— Some of the deepest lines in the regions shown in Fig. 4.8 ($\sim$ 1560 and $\sim$ 1657 Å), where a study of the NLTE effect has been carried out.

Wavelength (Å)	Ion
1555.660	Si I
1556.161	Si I
1558.541	Fe II
1558.692	Fe II
1559.085	Fe II
1559.706	Si I
1560.309	C I
1560.682	C I
1560.709	C I
1561.340	C I
1561.438	C I
1562.002	Si I
1563.790	Fe II
1564.612	Si I
1656.267	C I
1656.929	C I
1657.008	C I
1657.379	C I
1657.907	C I
1658.121	C I

the *splot* procedure within IRAF on the visible spectra taken at McDonald Observatory (see Chapter 2). These EW's were used to derive abundances with MOOG[3]. Classical line damping parameters were used, that is, classical natural line broadening was assumed, as well as Ünsold's approximation for the Van der Waals broadening, while Stark broadening was neglected. The abundances derived using the Stark broadening value from VALD are similar to those derived by neglecting that broadening.

Tables 4.4 and 4.5 show the observed EW of each spectral line (with its uncertainty, derived from the uncertainty of the observed flux) and the abundance (log ϵ_X) derived using model parameters from different sources: Qiu et al. (2001), Przybilla (2002), and ours (in which we have used a microturbulence from Castelli & Kurucz 1994 based on previous spectroscopic works: 2 km s^{-1}). The mean difference of $\sim$ 0.1 dex between iron abundances derived from Fe I and Fe II lines is possibly due to NLTE effects in the formation of the former.

Using the abundances obtained from optical spectral lines, we derived the mean abundance of each element, shown in Table 4.6 with its total uncertainty including the standard deviation and the uncertainties in the line-based abundances due to $T_{\rm eff}$ (9620^{+49}_{-63}K) and to $\log g$ (assumed 3.98 $\pm$ 0.1). The latter uncertainties are in the range 0.01-0.07 dex and 0.01-0.06 dex, respectively. In the same table, we show the original abundances found in the literature using the corresponding stellar parameters and, for C and Si, the values that we derived from the analysis of the UV spectrum. Besides, solar abundances from Grevesse & Sauval (1998) are shown.

We can see from Table 4.6 that C, N, and O abundances for Vega are similar to those of the Sun, while Mg, Al, Si, Ca, Cr, and Fe abundances are between -0.3 and -0.7 dex compared to the solar ones. This is consistent with previous studies (Ilijić et al. 1998), and suggests that Vega is a mild λ Boo star.

[3]To obtain a copy of the latest version (2002) of MOOG via ftp, see Chris Sneden's Web site at http://verdi.as.utexas.edu/moog.html

TABLE 4.4— Chemical abundances obtained from spectral lines in the visible region.

Ion	Wavelength (Å)	Equivalent Width (mÅ)	log ϵ_X with Parameters from Qiu et al. (2001)	log ϵ_X with Parameters from Przybilla (2002)	log ϵ_X with Our Parameters
C I	5052.17	33±4	8.37	8.44	8.47
	5380.34	20±3	8.30	8.37	8.39
	6828.12	7±2	8.25	8.32	8.34
	7111.47	17±5	8.35	8.42	8.44
	7113.18	23±2	8.19	8.26	8.28
	7115.17	23±2	8.34	8.41	8.44
	7116.99	21±2	8.28	8.35	8.37
N I	7423.64	20.5±3	8.11	8.12	8.12
	7442.30	34±3	8.08	8.08	8.09
	7468.31	42±4	8.05	8.04	8.05
O I	5329.68[1]	23±4	8.77	8.77	8.77
	6158.19[2]	57±3	8.81	8.79	8.80
Mg I	4167.27[3]	20±3	7.10	7.19	7.22
	4702.99	30±3	6.96	7.04	7.07
	5183.60[4]	122.5±2	7.40	7.31	7.35
	5528.41	28±2	6.92	7.00	7.03
Mg II	4427.99	5±2	6.88	6.87	6.87
	4433.99	12±2	6.97	6.95	6.95
Al II	4663.05	4.5±2	5.81	5.77	5.77
Si II	4128.07	54±4	7.02	6.97	6.96
	4130.89	68±4	6.85	7.04	7.04
	6347.11[5]	114±4	7.63	7.49	7.42
	6371.37	80±3	7.30	7.22	7.23
Ca I	4226.73	58±3	5.62	5.71	5.76
Cr I	5206.02	11±2	5.24	5.35	5.39
	5208.42	15±2	5.26	5.37	5.41

[1]This is a set of several weak OI lines according to the line list taken from SYNPLOT. However, Przybilla (2002) seems to take an effective gf with the central wavelength of the table, which is what we have used

[2]Comparing the computed triplet with the observed "line"

[3]Using the log gf from Qiu et al. (2001, −0.79); when using the log gf of Przybilla's PhD Thesis (2002, −1.71), a value 0.92 dex higher is obtained

[4]Important NLTE effect

[5]The abundances using damping parameters from VALD are very different, so we have not used this line to derive the abundance of Si

TABLE 4.5— Chemical abundances for Fe obtained from spectral lines in the visible region.

Ion	Wavelength (Å)	Equivalent Width (mÅ)	log ϵ_X with Parameters from Qiu et al. (2001)	log ϵ_X with Parameters from Przybilla (2002)	log ϵ_X with with Our Parameters
Fe I	4187.04	11±2	6.74	6.84	6.87
	4187.79	16±3	6.92	7.02	7.05
	4202.03	31±3	6.89	6.97	7.01
	4404.75	53.5±3	6.81	6.84	6.88
	4459.12	7±2	7.06	7.16	7.19
	4494.56	8±2	6.99	7.09	7.13
	4736.77	5.5±2	7.04	7.14	7.17
	5324.18	15±2	7.02	7.11	7.14
	5367.47	8±2	6.89	6.98	7.01
	5369.96	12±2	7.02	7.10	7.13
	5383.37	14±2	6.92	7.01	7.04
	5410.91	9±2	7.00	7.09	7.12
	5569.62	5±1	6.94	7.03	7.07
	5572.84	7±2	6.85	6.95	6.98
	5586.76	11±2	6.95	7.05	7.08
	5615.64	13±2	6.94	7.03	7.06
Fe II	4173.47	61±3	7.01	6.94	6.95
	4178.87	59±3	6.93	6.86	6.87
	4233.17	103±4	7.45	7.15	7.17
	4303.17	42.5±5	6.82	6.80	6.81
	4351.76	73±5	6.88	6.74	6.76
	4385.39	48±4	7.06	7.03	7.04
	4491.40	39±3	6.89	6.88	6.89
	4508.29	58±3	7.13	7.07	7.09
	4515.33	50±4	6.78	6.75	6.76
	4522.62	71±5	6.88	6.76	6.77
	4555.88	61.5±4	6.92	6.85	6.86
	4576.33	27±4	6.87	6.88	6.89
	4582.83	20.5±3	6.87	6.88	6.89
	4583.83	93±5	7.18	6.94	6.95
	4620.51	14.5±3	6.80	6.82	6.83
	4629.34	56±3	6.82	6.76	6.77
	4656.97	11±3	7.09	7.12	7.13
	4923.92	118.5±5	7.37	7.06	7.08
	5018.45	128.5±3	7.55	7.24	7.28
	5169.00	134±3	7.31	7.01	7.05
	5197.57	54±4	6.81	6.77	6.78
	5234.66	60±5	7.11	7.04	7.05
	5276.00	64±5	6.86	6.78	6.79
	7711.73	12±3	6.70	6.72	6.73

TABLE 4.6— Chemical abundances obtained from spectral lines in the visible compared with those from the literature, from the UV region, and for the Sun.

Ion	log ϵ_X with Parameters from Qiu et al. (2001)	log ϵ_X with Parameters from Przybilla (2002)	log ϵ_X with Our Parameters	log ϵ_X for the Sun, from GS98[1]
C I				
mean	8.30±0.08	8.37±0.08	8.39±0.08	
literature	8.46±0.13	8.23±0.11		8.52
UV continuum			$8.55\ ^{+0.34}_{-0.48}$	
N I				
mean	8.08±0.03	8.08±0.04	8.09±0.04	
literature	8.00±0.02	7.69±0.06 (NLTE)		7.92
O I				
mean	8.79±0.03	8.78±0.02	8.78±0.02	
literature	9.01±0.14	8.57±0.05 (NLTE)		8.83
Mg I				
mean	7.10±0.22	7.14±0.15	7.17±0.16	
literature	6.81 (1 line)	7.02±0.06 (NLTE)		7.58
Mg II				
mean	6.92±0.06	6.91±0.06	6.91±0.06	
literature	6.69±0.05	7.02±0.03		7.58
Al II				
mean (1 line)	5.81±0.03	5.77±0.03	5.77±0.03	
literature	—	5.84 (1 line)		6.47
Si II				
mean	7.06±0.23	7.08±0.13	7.08±0.14	
literature	6.96±0.06	6.94±0.05		7.55
UV continuum			$6.65\ ^{+0.57}_{-2.10}$	
Ca I				
mean (1 line)	5.62±0.09	5.71±0.09	5.76±0.09	
literature	5.41±0.09	5.67±0.11		6.36
Cr I				
mean	5.25±0.06	5.36±0.06	5.40±0.06	
literature	5.19±0.17 (CrII)	5.12±0.04		5.67
Fe I				
mean	6.94±0.11	7.03±0.11	7.06±0.11	
literature	6.94±0.12	6.96±0.08		7.50
Fe II				
mean	7.00±0.23	6.91±0.15	6.92±0.15	
literature	6.93±0.13	6.97±0.12 (NLTE)		7.50

[1]Grevesse & Sauval (1998)

5

The study of Procyon's spectrum using classical model atmospheres

In this chapter we study the star Procyon to derive some physical parameters and chemical abundances using classical model atmospheres. This is the most luminous star in Canis Minoris, with a V magnitude of 0.363 ± 0.03 mag and a color index B-V = 0.421 ± 0.003 mag, as derived from 13 measurements extracted from SIMBAD. It is a subgiant star a bit hotter than the Sun, according to its spectral type: F5 IV-V (Gray et al. 2001), although it is younger than our star. It also has a white dwarf companion.

In §5.1 we compute the most abundant ions present in the atmosphere of Procyon in order to derive the most important contributors to the continuum opacity. In §5.2 we have used low-dispersion visible, near-IR and near-UV spectra (in regions where the continuum opacity due to elements different to H is not relevant, and fixing the surface gravity and the metallicity) to derive its effective temperature and angular diameter. To achieve this, we have calculated the flux obtained using Kurucz's model atmospheres in SYNSPEC for each set of parameters and have matched these spectra to that observed. To see the relevance of the result, we have compared our parameters with those from other authors and have compared the gravity obtained using our derived angular diameter and the mass from the literature with our fixed gravity. We have also compared medium-resolution spectra with that obtained using our best-fitting parameters in some visible regions randomly selected. In §5.3 we have fixed the angular diameter derived before and have used the Kurucz's model atmosphere with our best-fitting parameters, changing the abundances of the chemical species that contribute most to the continuum opacity, to match the

computed to the observed spectrum in the region where they contribute most in the near-UV range. We have also estimated the effect of a change in the effective temperature and in the iron abundance on the flux. In §5.4 we have derived some chemical abundances (those derived in the section before and some others) from spectral lines in the visible range and have compared the result with that obtained in the section before and with the literature.

5.1 Main contributors to the continuum and line opacity in Procyon

The analysis protocol followed with Procyon A is very similar to that used with Vega. As a preliminary step, ion abundances for the 30 first elements in the first three states of ionization were computed using the first model parameters proposed by Allende Prieto et al. without 3D atmosphere simulations (2002; $T_{\rm eff} = 6512$ K, and $\log g = 3.96$ in cgs units) and Saha and Boltzmann equations. At this point we simply assumed solar photospheric abundances (Grevesse & Sauval 1998) when calculating the flux with SYNSPEC, except for Fe, for which we adopted [Fe/H] = −0.05 (Allende Prieto et al. 2002) and therefore [M/H] = −0.21 (see the discusion in chapter 2.

Next, we computed synthetic visible and near-UV spectra including continuum opacity produced by only H and each of the most abundant ions in Procyon. We studied all the ions with abundances relative to H larger than 10^{-6}: He I, C I, N I, O I, Ne I, Na II, Mg I, Mg II, Al I, Si I, S I, Ar I, Ca II, Fe I, Fe II and Ni I. By comparing the spectra derived including continuum opacity due to H plus any given ion to that obtained including only neutral H continuum opacity, we estimated the contribution of each ion to the continuum opacity of the observed fluxes. This is illustrated in Fig. 5.1 for the most important contributors. At wavelengths longer than about 2150 Å, neutral hydrogen, the H^- ion, Fe I and Mg I dominate the total bound-free opacity, and at wavelengths longer than about 3000 Å only the H ions are important. At shorter wavelengths, there are more ions contributing besides H, H^-, Fe I and Mg I, namely C I, Si I, Ca I and Al I.

5.2 Estimation of effective temperature and angular diameter

As we did in an earlier chapter with Vega, we have fixed in our first calculations the gravity and metallicity values to those given by Allende Prieto et al. (2002; $\log g = 3.96$ and [Fe/H] = −0.05, so the metallicity of the model atmospheres used is [M/H] = −0.21, according to chapter 2) and have attempted to determine the effective temperature and angular diameter from comparisons of computed fluxes with the observations in the near-UV, optical and near-IR

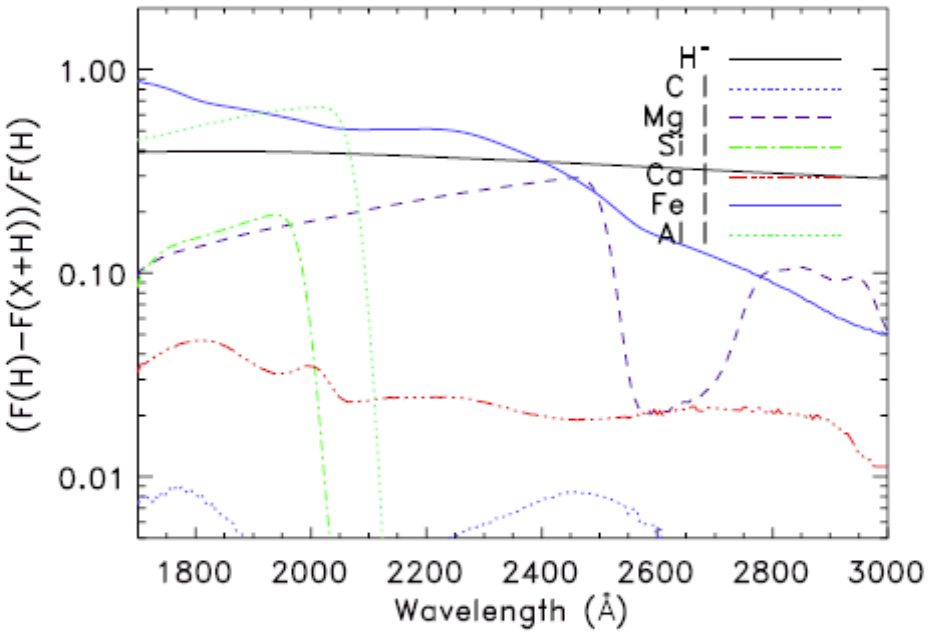

FIGURE 5.1— Relative difference between the flux computed taking into account neutral H and each ion X explicitly (F(X,H)) and the flux obtained by just taking into account neutral H explicitly (F(H)). The change in neutral H opacity is also considered in the line labeled as H^-, because the number of protons is constant, and therefore the abundance of neutral H diminishes when including H^-.

regions. This can be achieved by comparing the computed emitted flux from Kurucz model grids (which have log g, [M/H] and T_{eff} as independent parameters), transformed to computed received flux by using the angular diameter, to the observed flux. We have searched a region where metal absorption is modest, which allows us to study these two parameters fairly independent of the details of the chemical composition.

We minimized the χ^2 statistics by using the Nelder-Mead simplex algorithm and computed a grid of fluxes based on Kurucz's model atmospheres (see chapter 2) with T_{eff} running between 6530 and 6630 K. We matched selected spectral regions, excluding the segments where special difficulties exist. In particular, the spectrum between 3800 and 5300 Å was discarded because we were unable to match it to the observed spectrum, and the region below 3200 Å was also discarded because of important bound-free absorption due to metal ions (see Fig. 5.1). Then, we divided the total range into three regions identified in Fig. 5.2: from 3200 to 3800 Å, from 5300 to 6500 Å and from 6600 to 8800 Å. For the statistics, we used the same weight for each of these regions (because the uncertainty of the observed flux in these regions is similar), obtaining for the best fit: $T_{eff} = 6590^{+61}_{-56}$ K and $D_{ang} = 5.47 \pm 0.08$ mas, with a total standard deviation of 1.45 %, being $\sigma_{3238} = 1.35$ %, $\sigma_{5365} = 1.31$ % and $\sigma_{6688} = 1.70$ % the standard deviation from 3200 to 3800 Å, from 5300 to 6500 Å and from 6600 to 8800 Å, respectively. The error bars of our estimates were derived by perturbing our best-fitting parameters until the flux variation exceeded the error bars assigned to the observed spectrum: 3 % of the observed flux. The parallax measured by *Hipparcos* is very precise: $\Pi = (285.93 \pm 0.88) \times 10^{-3}$ arcsec, so its derived distance is: d = 3.497 ± 0.011 pc. Using the distance value from *Hipparcos* and our angular diameter, we obtain R = 2.056 ± 0.018 $R_\odot$. If we introduce the mass from Allende Prieto et al. (2002), we obtain the following gravity value: log $g = 3.96 \pm 0.06$, which is totally consistent with the assumed value. A comparison between the spectrum computed with these parameters and the observations is shown in Fig. 5.2.

In Table 5.1 it is shown that the angular diameter that we obtain is compatible with all the other measurements from the fit. Some comments are necessary about the measurements of T_{eff}. The value obtained using the IRFM is compatible with our result. The other two measurements (both based on the bolometric flux and the angular diameter) are also compatible with our result, but are just in the edge of our error bars. However, the bolometric flux used by Allende Prieto et al. (2002) and Kervella et al. (2004) ($F_{BOL} = 18.20 \pm 0.43$, in units of 10^{-6} erg cm^{-2} s^{-1}) is taken from Fuhrmann et al. (1997), where three of the four measurements are relatively old and possibly not too accurate. Besides, if we use the angular diameter by Kervella et al. (2004),

TABLE 5.1— Parameters for Procyon according to the literature.

Reference	T_{eff} (K)	D_{ang} (mas)	[Fe/H] (dex)
Allende Prieto et al. (2002)[1]	6530 ± 49	5.51 ± 0.05	-0.05 ± 0.03
AAM96[2]	6579 ± 100	-	-0.05
Kervella et al. (2004)[3]	6530 ± 50	5.45 ± 0.05	-0.05 ± 0.03
This work	6590^{+61}_{-56}	5.47 ± 0.08	-0.05

[1]Angular diameter measured using optical interferometry by Mozurkewich et al. (1991). T_{eff} obtained using the earlier angular diameter, the weighted average of the bolometric fluxes from Fuhrmann et al. (1997) and detailed 3D stellar atmosphere simulations.

[2]Alonso, Arribas & Martínez-Roger (1996): using the IRFM to calibrate the absolute flux of stars with direct measurements of angular size

[3]Angular diameter using interferometric measurements obtained with the VINCI/VLTI instrument. T_{eff} and [Fe/H] taken from Allende Prieto et al. (2002).

then T_{eff} would transform from 6530 to 6566 K, quite closer to the value that we have obtained.

It is also important to take into account the correction in radius and T_{eff} that results when using three-dimensional simulations, due to the different limb-darkening correction (LD) obtained. The LD correction is a scale factor, which depends on the model used, between the angular diameter obtained from the visible data assuming a uniformly bright stellar disk and the actual angular diameter corresponding to a physical diameter (see e.g. Davis, Tango & Booth 2000). For instance, Allende Prieto et al. (2002) find that the different LD obtained when using 3D simulations result in a decrease on the angular diameter and an increase in T_{eff} for Procyon. This fact could also have some effects on the spectral energy distribution, and could explain (at least partially) the unability for the model atmospheres to reproduce the spectrum in some regions, such as from 3800 to 5300 Å.

A medium-resolution spectrum of Procyon between 3200 and 3800 Å has been computed, using the resolving power of the near-UV atlas (see Appendix). The Kurucz (1992) model atmosphere used had $T_{eff} = 6590$ K, $\log g = 3.96$ and $[M/H] = -0.21$ (taken to be consistent with the abundance of Fe derived from spectral lines), but we used solar abundances for the other elements. We have compared the computed spectrum (using $D_{ang} = 5.47$ mas) with the near-UV atlas in three 40 Å-wide regions randomly selected between 3200 and 3800 Å, where continuum opacity is mostly produced by H ions and is within the limits of the atlas. The standard deviations between the computed and the observed spectra are: 4.2 % in the region centered at 3314 Å, 6.1 % in the

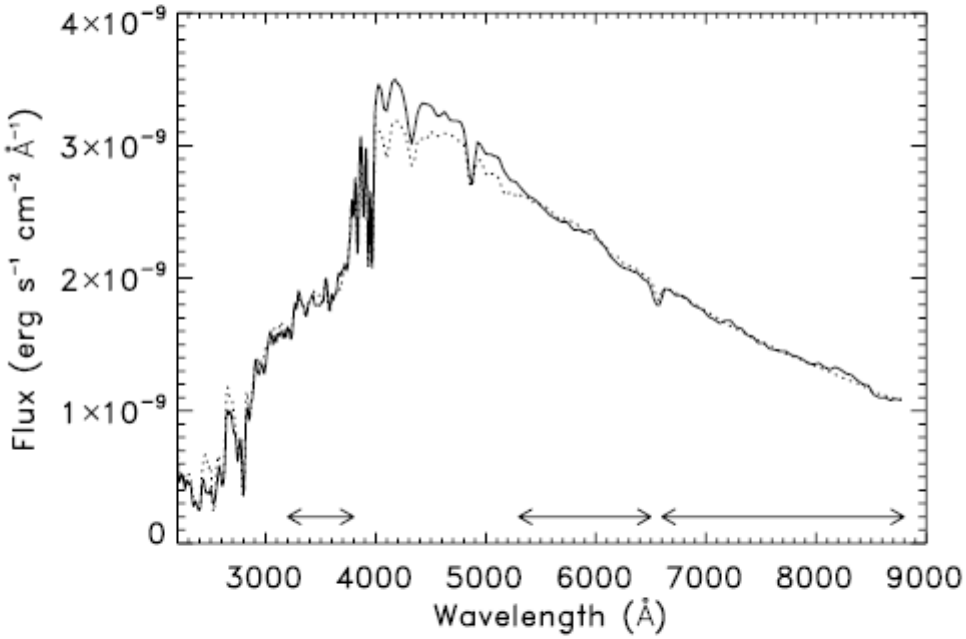

FIGURE 5.2— Comparison of the observed flux (solid line) and the synthetic flux (dotted line) in the near-IR, the visible and the near-UV, using the parameters of the best fit, that is, T_{eff} = 6590 K and D_{ang} = 5.47 mas. The regions used for the fit are marked with arrows.

region centered at 3619 Å and 4.0 % in the region centered at 3756 Å, so the synthetic spectrum reproduce the medium-resolution observed spectrum quite well. Fig. 5.3 compares the computed and the observed fluxes in the three regions.

5.3 Estimation of chemical abundances from the UV continuum

In Section 5.1, we concluded that Mg and Fe were the most important contributors to the UV continuum opacity for wavelengths over 2150 Å for a star like Procyon. With the adopted atmospheric parameters (gravity derived from the *Hipparcos* parallax and both $T_{\rm eff}$ and $D_{\rm ang}$ from fitting the optical and near-IR flux), we now attempt to constrain the abundances of these elements from the UV flux. We calculated synthetic spectra from 2200 Å to 3000 Å. We considered Mg abundances between [Mg/H] = −0.4 and 0.4 and Fe abundances between [Fe/H] = −0.45 and 0.35 dex, to determine the Mg and Fe abundances.

The best fit to the observations is obtained for [Mg/H] = $0.00^{+0.37}_{-0.26}$ and [Fe/H] = -0.04 ± 0.17, with $\sigma_{\rm rms} = 10\%$ when using wavelength regions where there are no problems to match the synthetic to the observed flux: from 2290 to 2350 Å, from 2580 to 2650 Å, from 2720 to 2770 Å and from 2860 to 2920 Å. When using the complete region between 2200 and 3000 Å, the best fit is obtained for [Mg/H] = $0.00^{+0.37}_{-0.26}$ and [Fe/H] = -0.16 ± 0.17, with $\sigma_{\rm rms} = 20\%$, and therefore the fit is much worse and we consequently prefer the other values as the abundances obtained from the continuum. The error bars take into account the uncertainty in the observed flux, estimated as 3%, in the regions with higher sensitivity to changes in the parameters, and the uncertainty in $T_{\rm eff}$. The regions used to find the errors in the abundances derived from the uncertainty in the observed flux, are: from 2200 to 2400 Å for Mg and from 2650 to 3000 Å for Fe. We find the following uncertainties: $^{+0.10}_{-0.13}$ for the Fe abundance and $^{+0.05}_{-0.07}$ for the Mg abundance. The regions used to derive the abundance errors obtained from the uncertainty in $T_{\rm eff}$ were: from 2650 to 3000 Å for Fe and from 2250 to 3000 Å for Mg, obtaining the following uncertainties: $^{+0.14}_{-0.11}$ for the Fe abundance and $^{+0.37}_{-0.25}$ for the Mg abundance.

We have also estimated the effect on the flux of a change in $T_{\rm eff}$ and in Fe abundance (compatible with metallicity). In Fig. 5.4 we show the comparison of the observed flux from the near-UV atlas (see Appendix), the computed flux using the parameters recently obtained ($T_{\rm eff}$ = 6590 K, log g =3.96, [M/H] = −0.21 and $D_{\rm ang}$ = 5.47 mas) and the computed flux using an iron abundance 0.2 dex higher and $T_{\rm eff}$ 100 K lower. An almost uniform increase in the flux difference is shown when using a model atmosphere with $T_{\rm eff}$ 100 K lower. The flux difference is positive for some wavelengths and negative for others

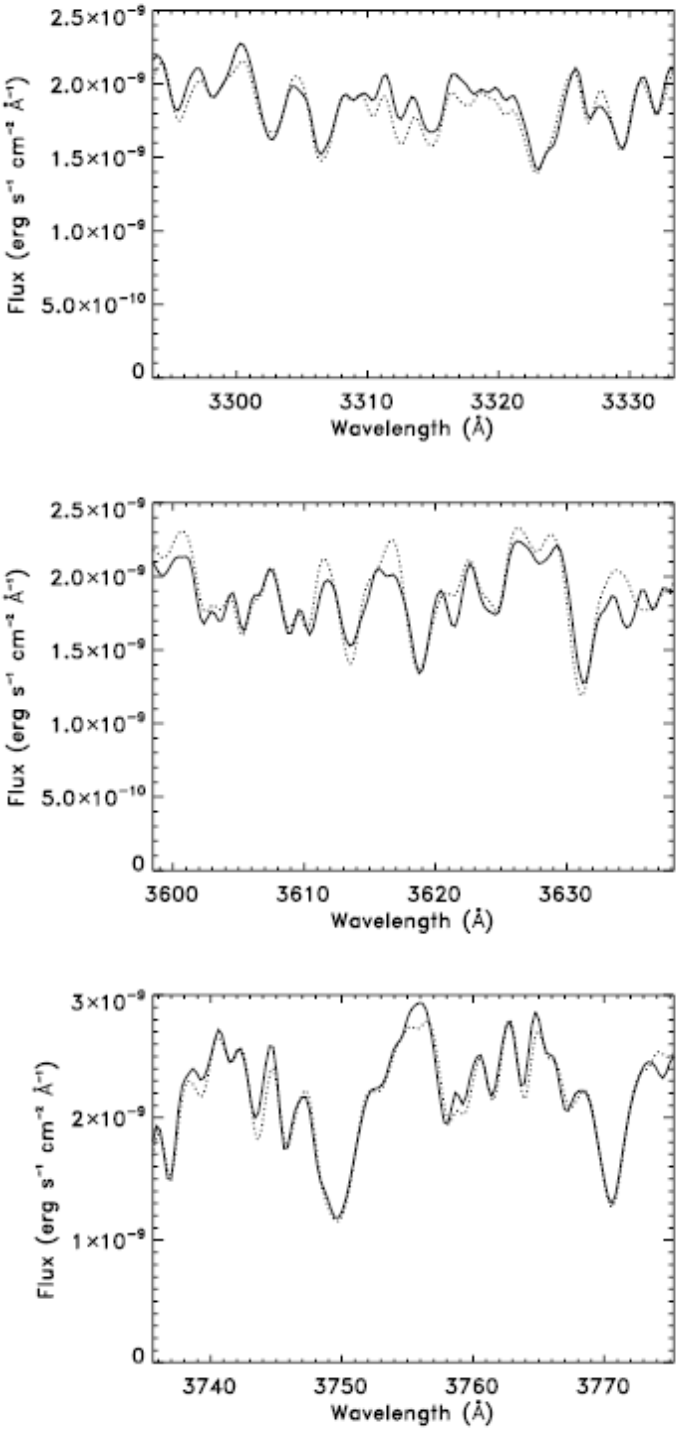

FIGURE 5.3— Comparison of the observed flux (solid line) from the near-UV atlas of Procyon and the synthetic flux (dotted line) at medium resolution, using the parameters of our best fit, that is, $T_{\rm eff} = 6590$ K, $\log g = 3.96$ and [M/H] $= -0.21$ for the Kurucz's model atmosphere and $D_{\rm ang} = 5.47$ mas. We computed the flux using the program SYNSPEC with solar abundances, except for Fe, for which [Fe/H] $= -0.05$ was used.

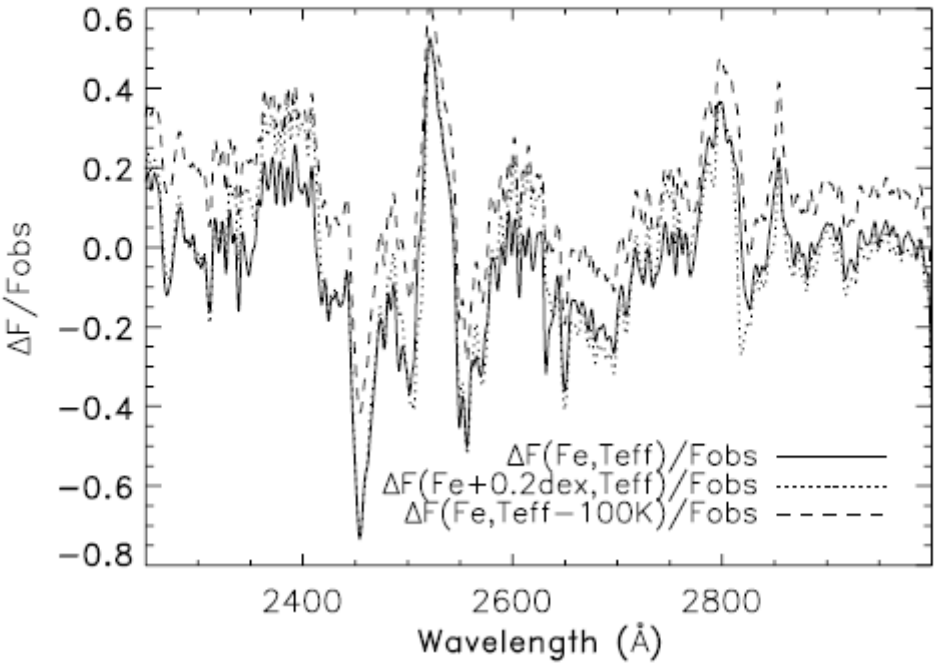

FIGURE 5.4— Relative flux difference (observed flux minus synthetic flux all divided by observed flux) between the observed flux and three synthetic fluxes: using the parameters of the best fit (that is, T_{eff} = 6590 K, log g = 3.96, [M/H] = −0.21, solid line), using Fe abundance 0.2 dex higher (dotted line) and using T_{eff} 100 K lower (dashed line).

when using an iron abundance 0.2 dex higher, increasing the difference between maxima and minima in flux.

5.4 Estimation of chemical abundances from spectral lines in the visible range

We calculated again the chemical abundances of this star from its spectral lines in order to guarantee that the analysis is fully consistent with our UV study. The following ions have been studied: C I, Mg I, Cr I, Cr II, Mn I and Fe II. We measured the equivalent width (EW) of lines from these species from the photometric atlas of Procyon by Allende Prieto et al. (2002). These EW's were used to derive abundances with MOOG. The abundances from each line are shown in Table 5.2. Line data (excitation potential and log gf) were taken from the line list distributed with SYNPLOT (and compiled by Kurucz), except

for Fe lines, for which line data were adopted from Allende Prieto et al. (2002).

The abundances derived from spectral lines and the UV continuum are compared in Table 5.3 with those from the literature. It is shown that the abundances derived from the UV continuum are compatible with the abundances obtained from visible spectral lines. Besides, the abundances that we obtained from spectral lines are compatible with most abundances derived by other authors.

TABLE 5.2— Chemical abundances obtained from spectral lines in the visible region. For Fe I, the number of lines is so high that we have not included it.

Ion	Wavelength (Å)	EW (mÅ)	log ϵ_X
C I[1]	5052.170	77.4	8.70
	5380.340	55.5	8.60
Mg I[2]	4571.096	66.4	7.63
	4702.991	204.5	7.95
	4730.029	44.6	7.86
	5528.405	185.3	7.82
	5711.088	82.9	7.70
Cr I[3]	5204.506	153.0	5.93
	5409.772	113.1	5.73
Cr II[3]	4588.199	111.4	5.66
	4618.803	108.5	5.80
	4824.127	111.5	5.82
	5237.329	82.7	5.57
Mn I[4]	4754.042	101.8	5.58
	4765.846	58.2	5.37
	4766.418	73.9	5.42
	4783.427	109.3	5.61
Fe II[5]	4576.33	102.1	7.51
	4620.51	81.2	7.39
	4629.34	130.8	7.40
	5234.62	124.5	7.49
	5264.80	70.1	7.54
	5414.07	44.3	7.36
	5525.12	22	7.43

[1]The lines used for Vega that are within the range of the spectrum by Allende Prieto et al. (2002)

[2]Not blended lines with EW's larger than 30 mÅ and smaller than 200 mÅ with wavelengths between 4500 and 6000 Å

[3]Not blended lines with EW's larger than 70 mÅ with wavelengths between 4500 and 6000 Å

[4]Not blended lines with EW's larger than 50 mÅ with wavelengths between 4500 and 5000 Å

[5]Lines from Allende Prieto et al. (2002) with EW $<$ 200 mÅ

TABLE 5.3— Chemical abundances relative to the Sun (logarithmic units) obtained from spectral lines in the visible region and from the UV continuum compared with the abundances from the literature.

Ion	This work	KS82[1]	Steffen (1985)	LL87[2]	E93[3]	K
C I						
lines	0.13±0.07	-	−0.03	-	-	
Mg I						
continuum	$0.00^{+0.37}_{-0.26}$	-	-	-	-	
lines	0.21±0.13	−0.04	0.07±0.13	−0.24±0.10	0.07	-
Cr I						
lines	0.16±0.14	−0.10	−0.03±0.07	−0.11±0.20	-	
Cr II						
lines	0.04±0.12	0.03	−0.01±0.09	−0.03±0.24	-	
Mn I						
lines	0.11±0.12	−0.19	0.00±0.10	0.17±0.23	-	
Fe I						
continuum	−0.04±0.17	-	-	-	-	
lines	−0.06±0.07	0.03	0.06±0.07	0.44±0.20	−0.08	

[1]Kato & Sadakane (1982)
[2]Lane & Lester (1987)
[3]Edvardsson et al. (1993)
[4]Kato, Watanabe & Sadakane (1996)

6

The study of Vega's spectrum using rapidly rotating stellar models

In this chapter we study Vega using rapidly rotating stellar models in order to determine some of its physical parameters and to re-derive several chemical abundances. In §6.1 we introduce the theory of the rapidly rotating stellar models that we have used and how to calculate the flux using different stellar parameters. In §6.2 we derive preliminary stellar parameters of Vega (the inclination of the rotational axis with respect to the line of sight and the polar temperature) fixing the other parameters necessary to compute the flux: the metallicity of the model atmosphere, the angular diameter, the projected rotational velocity, the microturbulence and the chemical abundances fixed to the values obtained using classical non-rotating models (except for He), and the mass of a typical A0 V star. The derived parameters are obtained by matching the computed flux to that observed in the vicinity of 6 lines of different elements separated in wavelength. In §6.3 we derived the metallicity and the microturbulence velocity using 6 spectral lines of Fe. The projected equatorial velocity is also calculated averaging the values of the best fits. In §6.4 we fix the parameters obtained in the section before and, matching the computed flux to the same 6 lines as in §6.2, we calculate the abundances of the elements of the lines, the inclination of the rotational axis and the polar temperature of Vega. In §6.5 we compare the parameters obtained in this chapter with those from the literature using non-rotating stellar models. We compare the abundances not only with respect to hydrogen but also with respect to iron, because a relative value of abundances will be more consistent for comparisons. Finally, we try to determine the mean observed effective temperature of our rapidly rotat-

ing star and compare the abundances obtained using non-rotating models with this effective temperature to our abundances obtained using rapidly rotating models.

6.1 Rapidly rotating stellar models

We have developed a procedure to compute the flux of a star accounting for deviations from spherical symmetry due to rotation. We have adopted the same assumptions as Pérez Hernández et al. (1999). The angular rotational velocity is considered constant which, although an important simplification, can report accurate results. The gravitational potential is assumed to be that of a point with the same mass, which is almost certain for the outermost layers of a star. According to that, the surface of the star results to be a Roche surface, simplifying the modeling of the stellar configuration.

The integration of the specific intensities projected onto the line of sight over the part of surface of the star visible to the observer gives the flux for each wavelength. The following parameters are defined:

- The *normalized angular rotational velocity* of the star w, defined as:

$$w \equiv \frac{\Omega}{\Omega_c}, \tag{6.1}$$

where the angular velocity of the star is $\Omega = v_{\rm equat}/{\rm R}_{\rm equat}$ and the critical angular velocity is defined as:

$$\Omega_c \equiv \sqrt{\frac{8{\rm GM}}{27{\rm R}_{\rm p}^3}}, \tag{6.2}$$

where M and $\rm R_p$ represent the stellar mass and polar radius, respectively. Ω_c is the angular velocity for which the centrifugal force and the gravitational attraction are balanced at the equator, and therefore $w \leq 1$ for any stellar configuration. The factor $8/27$ comes from the fact that, for a star rotating at the critical velocity, the centrifugal force at the equator is just compensated by the gravity, that is,

$$\Omega_c^2 {\rm R}_{\rm equat} = \frac{\rm GM}{{\rm R}_{\rm equat}^2}, \tag{6.3}$$

which also implies ${\rm R}_{\rm equat} = 1.5\ {\rm R}_{\rm p}$, as explained by Collins (1963). For Vega, we used the Hipparcos parallax ($\Pi = 128.93 \pm 0.55$ mas, leading to a distance d = 7.76 ± 0.03 pc) and the angular diameter obtained using non-rotating models by our group (${\rm D}_{\rm ang} = 3.27 \pm 0.05$ mas; see chapter 4),

which is consistent with most values from the literature (see comparison in the same chapter), to obtain $R_{equat} = D_{ang}(rad) \cdot d/2 = 2.73 \pm 0.05\ R_\odot$, although a typical A0 V star has $R_{equat} = 1.87\ R_\odot$ (Gray 1992). In this equation, we considered that the observed size is the equatorial diameter, which is a good approximation, since we see Vega almost pole-on. We took the mass of Vega as that of a typical A0 V star: 2.40 $M_\odot$ (Gray 1992) and calculated the polar gravity from its relation with mass and polar radius:

$$\frac{g_{polar}}{g_\odot} = \frac{M/M_\odot}{R_p^2/R_\odot^2}, \tag{6.4}$$

The fact that R_{equat} derived from the parallax and the angular diameter is quite larger than that of a typical A0 V star is what is expected for a rapidly-rotating star. The relation between the observed R_{equat} and the radius of a typical non-rotating A0 V star is ~1.46, a bit lower than R_{equat}/R_p for the critical velocity. It is reasonable that R_p does not change with rotation. Assuming this, the actual relation between both R_{equat}'s suggests that Vega is a rapidly-rotating star with a rotational velocity close to the critical one.

- The *relative radius*, defined as:

$$x(\theta) = r(\theta)/R_p, \tag{6.5}$$

where θ is the colatitude (see Fig. 6.1). For a Roche surface:

$$x(\theta) = \frac{3}{w\sin\theta}\cos\Big\{\frac{1}{3}[\pi + \arccos(w\sin\theta)]\Big\}. \tag{6.6}$$

- The *effective gravity* g_n.
Under the assumptions of constant angular velocity and approximating the gravitational potential by that of a mass point, the effect on the hydrostatic equilibrium equation is to replace the gravitational potential by the *effective potential*:

$$\psi = -\frac{GM}{r(\theta)} - \frac{1}{2}\Omega^2 r^2(\theta)\sin^2\theta. \tag{6.7}$$

Using the definition, we derive the gravity and define the effective gravity:

$$g(\theta) = \|-grad(\psi)\| = \left\|-\frac{\partial\psi}{\partial r}\hat{r} - \frac{1}{r}\frac{\partial\psi}{\partial\theta}\hat{\theta}\right\| = \left(\frac{\partial\psi}{\partial r}\right)^2 + \frac{1}{r^2}\left(\frac{\partial\psi}{\partial\theta}\right)^2 = \frac{GM}{R_p^2}g_n(\theta). \tag{6.8}$$

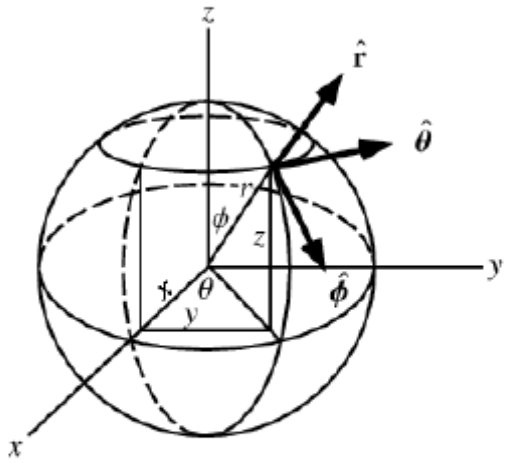

FIGURE 6.1— Spherical coordinate system used in the text.

From Eqs. 6.5, 6.7 and 6.8, g_n results to be:

$$g_n(\theta) = \frac{8}{27}\sqrt{\left(\frac{27}{8x^2} - w^2 x \sin^2\theta\right)^2 + (w^2 x\ \cos\theta\ \sin\theta)^2}. \tag{6.9}$$

- The *normalized effective temperature* is finally defined as:

$$t_n^4(\theta) \equiv \frac{\mathrm{T}_{\mathrm{eff}}^4(\theta)}{\mathrm{T}_{\mathrm{polar}}^4}, \tag{6.10}$$

where the effective temperature $\mathrm{T}_{\mathrm{eff}}(\theta)$ is defined by the Stefan's law: $\mathrm{F} = \sigma \mathrm{T}_{\mathrm{eff}}^4$, where F is the bolometric emergent flux per unit area and σ is the Stefan-Boltzmann constant. If we assume radiative equilibrium and the diffusion approximation (Tassoul 1978), the gravity-darkening law (firstly enunciated by von Zeipel 1924 for a uniformly rotating star) states:

$$\mathrm{F} \propto {\mathrm{T}_{\mathrm{eff}}}^4 \propto g. \tag{6.11}$$

For stars with convective envelopes (Lucy 1967), the law is given by:

$$\mathrm{F} \propto {\mathrm{T}_{\mathrm{eff}}}^4 \propto g^{0.32}. \tag{6.12}$$

We can use a general law of the form:

$$\mathrm{F} = \sigma {\mathrm{T}_{\mathrm{eff}}}^4 = C(w) g^{\beta}, \tag{6.13}$$

where $C(w)$ and the gravity-darkening exponent β are constant for a given rotating star. $\beta \sim 1$ for a star with a fully radiative envelope, as occurs in stars with $\log(\mathrm{T_{eff}}) > 3.9$ and then we will use $\beta = 1$ for Vega. From Eqs. 6.8, 6.10 and 6.13, since t_n and g_n are normalized to be 1 at the pole, so there is no w dependence, we obtain:

$$t_n^4(\theta) = g_n(\theta). \tag{6.14}$$

Making use of these definitions, we proceed to derive the luminosity of the star. In Eq. 6.13, the constant $C(w)$ can be expressed in terms of the intrinsic luminosity, L, by using Stefan's law, $\mathrm{F} = \sigma \mathrm{T_{eff}^4}$, and noticing that L is the integral of F over the stellar surface:

$$\mathrm{L} = \int_A \mathrm{F} d\mathrm{A} = \sigma C(w) \int_A g d\mathrm{A}. \tag{6.15}$$

Hence:

$$C(w) = \frac{\mathrm{L}}{\sigma} \left[\int_A g d\mathrm{A} \right]^{-1}. \tag{6.16}$$

Here the integral is over the whole surface of area A. All the integrals were calculated numerically using an IDL procedure which integrates by the composite trapezoidal rule. A test integrating with a Newton-Cotes formula with 5 points (*int_tabulated* routine of IDL) was made, obtaining almost identical results. Twenty equidistant values were used for each angle: θ and the longitude in spherical coordinates, ϕ.

By integrating over the Roche surface in Eq. 6.16 and using Eqs. 6.10 and 6.13:

$$\mathrm{L} = 4\pi\sigma \mathrm{R_p^2 T_{polar}^4} \int_0^1 \frac{{g_n}^2 x^4}{1 - \frac{8}{27} w^2 x^3 \sin^2\theta} d(\cos\theta). \tag{6.17}$$

Then, we calculate the specific intensity I_ν using the program SYNSPEC with Kurucz's model atmospheres for different angles using the log g from Eq. 6.8 (calculating $g_n(\theta)$ from Eq. 6.9) and $\mathrm{T_{eff}}$ from Eq. 6.10.

The radiation emitted per unit frequency per steradian in the direction defined by the angle from the rotational axis i is then computed in the general case by the expression:

$$L_\nu(w, i) = \int_A I_\nu(\mu) |\mu| d\mathrm{A}, \tag{6.18}$$

where μ is the cosine of the angle between the line of sight and the normal to the surface. For a Roche surface:

$$\mu = \frac{|\mathrm{g} \cdot \mathrm{i}|}{g} = \frac{(1 - \frac{8}{27} w^2 x^3) \sin i \sin\theta \cos\phi + \cos i \cos\theta}{g_n x^2}, \tag{6.19}$$

where i is a unit vector in the direction of the line of sight, and therefore:

$$L_\nu(w,i) = 2R_p^2 \int_0^{\pi/2} \int_0^{\pi} I_\nu(\theta,\phi) x^2(\theta) \sin\theta f(\theta,\phi) d\theta d\phi, \tag{6.20}$$

where

$$f(\theta,\phi) = \sin\theta \sin i \cos\phi + \cos\theta \cos i - \frac{8w^2x^3(\theta)\sin\theta\cos\theta}{27 - 8w^2x^3(\theta)\sin^2\theta}(\sin i \cos\phi \cos\theta - \sin\theta \cos i), \tag{6.21}$$

where we have used the formula from Collins (1965) for a uniformly rotating Roche surface.

We also take into account the wavelength shift due to the projected rotational velocity:

$$v(w,\theta,\phi,i) = -w\ x(\theta)\sqrt{\frac{8g_p \mathrm{R}_p}{27}} \sin\ \theta\ \sin\ \phi\ \sin\ i. \tag{6.22}$$

The computed emitted spectrum is finally transformed to received spectrum at the Earth using the following formula:

$$\mathrm{f}_\lambda = \frac{c}{\mathrm{d}^2 \cdot \lambda^2} L_\nu(w,i), \tag{6.23}$$

where the $1/\mathrm{d}^2$ factor comes from the transformation from emitted to received flux and the c/λ^2 comes from the transformation from flux per wavelength unit to flux per frequency unit, since $\mathrm{c}=\lambda \cdot \nu$:

$$\mathrm{I}_\lambda \mathrm{d}\lambda = \mathrm{I}_\nu \mathrm{d}\nu = -\mathrm{I}_\nu \frac{\mathrm{c}}{\lambda^2} \mathrm{d}\lambda \tag{6.24}$$

We normalized the computed fluxes dividing by the flux calibrated spectra in order to match them to the high-resolution observations. In addition to the basic atmospheric parameters (effective temperature, surface gravity, and overall metallicity), the abundances of particular elements (whose ratio to iron may differ from solar) may affect the spectral energy distribution in the UV because of their continuum opacities (see chapter 4), so our calculation of physical parameters is limited to spectral lines and continuum with $\lambda > 3000$ Å.

6.2 Preliminary calculation of stellar parameters

First of all, we made several tests to calculate preliminary parameters: the inclination of the rotation axis with respect to the line of sight and the polar temperature of Vega. For this purpose, we selected a group of 6 spectral lines

with a wide range of equivalent widths, but not too weak and not too deep; and covering a wide wavelength range with no important blending. The first condition is important because the effect of rapid rotation is different in weak and in strong lines, as described in §1.5. The second condition is also important because the effect on the observed flux of a fast rotator seen pole-on depends on the wavelength of the emitted flux, as seen also in §1.5. Thus we are not introducing systematic effects due to the EW or the wavelength. Besides, these lines are also used to find chemical abundances in this section, so we are neither interested in too weak nor in too strong lines, since abundances obtained from weak lines have large error bars due to noise in the observations, and some very strong lines are affected by departures from LTE, an effect not considered in our models. We also need lines without blending. Moreover, we have included a line (Ca II $\lambda 3158.87$ Å) in the region where the effect of rapid rotation in the continuum is most important according to Gulliver et al. (1994). The lines chosen are shown in Table 6.1. We used classical damping parameters and oscillator strengths from Przybilla (2002), except for Fe lines, which were taken from Allende Prieto et al. (2002).

The metallicity used in these first model atmospheres was [M/H] = -0.7, which is similar to the values obtained in two modern independent determinations: Fitzpatrick & Massa (1999) ([M/H] = -0.73) and Qiu et al. (2001) ($\log \epsilon_{\rm Fe\,I} = 6.94$ and $\log \epsilon_{\rm Fe\,II} = 6.93$, so [M/H] = -0.73 or -0.74), using the relation [M/H] = [Fe/H] $-$ 0.16 from chapter 2. We also used the solar He abundance according to Grevesse & Sauval (1998): $\epsilon_{\rm He}/\epsilon_{\rm H} = 0.085$, while for Kurucz (1992) models: $\epsilon_{\rm He}/\epsilon_{\rm H} = 0.098$. For the angular diameter, the value obtained with non-rotating models in chapter 4 was used: $D_{\rm ang} = 3.27$ mas (compatible with most values from the literature).

We have started by comparing the computed flux using a non-rotating model with the parameters of the best fit and the abundances from spectral lines found in chapter 4. The comparison is shown in Fig. 6.2. It provides a very poor fit for the Ca II line at 3158.87 Å, where the computed flux is 4-5% higher than the observations, in good agreement with the results found by Gulliver et al. (1994). The other computed lines are somewhat lower than the observations by 1-2%.

The high-dispersion computed flux [$F^{\rm high}_{\rm computed}$(absolute)] has been normalized by the observed low-resolution flux [$F^{\rm low}_{\rm observed}$(absolute)] around the line centered at it, obtaining $F^{\rm high}_{\rm computed}$(mean observed = 1). The high-resolution spectrum [$F^{\rm high}_{\rm observed}$(continuum = 1)] is already normalized, but forcing the estimated local continuum to be 1. In order to compare it to the computed flux, we need to normalize it dividing by the flux around the line when de-

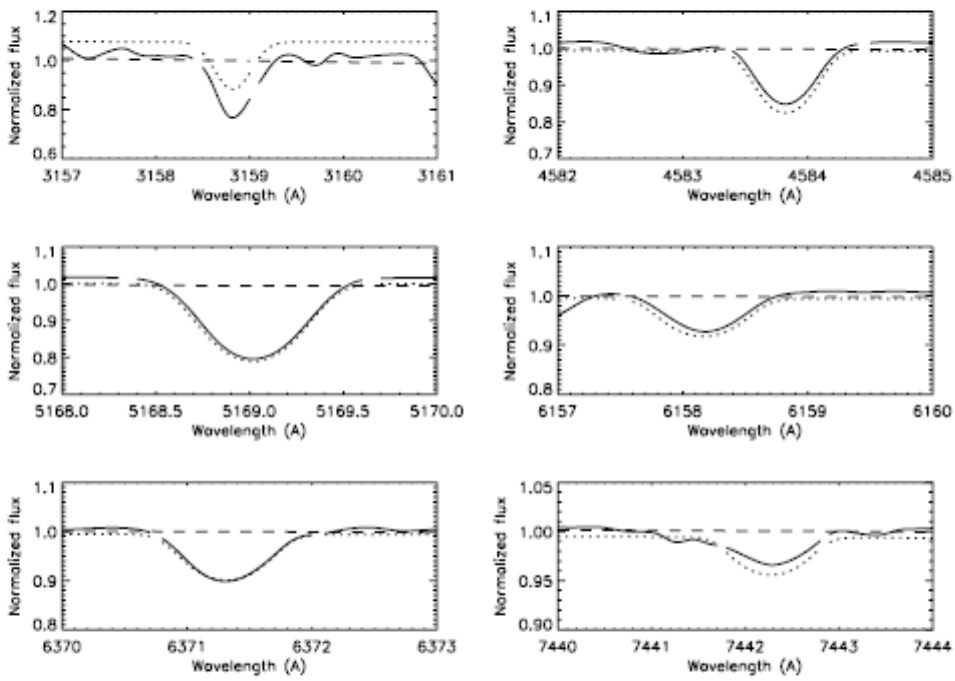

FIGURE 6.2— Comparison of the normalized high-resolution observed flux (solid lines) around 6 spectral lines (Ca II λ3158.87, Fe II λ4583.83, Fe II λ5169.03, O I λ6158.19, Si II λ6371.37 and N I λ7442.30 Å), the low-resolution observed flux normalized at the center of each line (dashed lines) and the synthetic flux (divided by the same normalization constant) for the best fit to the observed one using non-rotating models (dotted lines), taken from chapter 4: $T_{\rm eff} = 9620$ K, $\log g = 3.98$ and [M/H] $= -0.7$. We have applied a rotational profile to the computed flux with $i = 90$ degrees, $v_{\rm equat} \cdot \sin i = v_{\rm equat} = 23$ km s^{-1} (Gray 1980), $v_{\rm turb} = 2.0$ km s^{-1} (Castelli & Kurucz 1994) and a Gaussian profile with FWHM = 0.2 Å, according to the spectral resolution of the observed spectrum.

TABLE 6.1— Lines used to calculate the abundances and parameters (i and T_{polar}) of Vega.

Ion	Wavelength (Å)	EW_{obs} (mÅ)	Abundance (log ϵ_X)
Ca II	3158.87	110[1] ± 15	5.77
Fe II	4583.83	93 ± 8	6.71
Fe II	5169.03	140 ± 8	6.71
O I	6158.2[2]	58 ± 6	8.70
Si II	6371.37	80 ± 6	7.08
N I	7442.30	31 ± 4	7.96

[1]We have obtained the value duplicating the left half of the line, because there is a close line on the right half: Cr II λ3159.095 Å, with a EW of 5-10 mÅ

[2]The three lines of the triplet were used to compute the flux

grading the spectrum to the same resolution as the low-resolution observations [$F^{low}_{observed}$(continuum = 1)], obtaining $F^{high}_{observed}$(mean observed = 1). This is valid when using a wavelength region with similar resolution than that of the low-dispersion spectrum (6 Å), as is our case. We minimized the χ^2 statistics between the computed and the observed spectrum for each line, adopting 2 % as the typical error of the observed flux, except for the Ca II λ3158.87 Å line, for which 4 % was used.

We started estimating preliminary line parameters by fitting computed to observed fluxes for the 6 lines in Table 6.1, interpolating from a grid of synthetic fluxes and minimizing the χ^2 value of the fit. The grid considered T_{polar} = 9750 and 9850 K for i = 5.5 degrees, T_{polar} = 9650 and 9750 K for i = 6.1 degrees, and T_{polar} = 9550 and 9650 K for i = 6.7 degrees. We used the abundances obtained from spectral lines in the visible range using classical atmospheric models (see chapter 4), $v_{equat} \cdot \sin i$ = 23 km s^{-1} (Gray 1980), v_{turb} = 2.0 km s^{-1} (Castelli & Kurucz 1994) and a Gaussian profile with a FWHM of 0.2 Å, according to the spectral resolution of the observed spectrum. The best fit was obtained using the following parameters: i = 6.59 degrees and T_{polar} = 9576 K, with χ^2 = 0.092. The comparison between the observed and the computed spectrum with these parameters is shown in Fig. 6.3.

6.3 Calculation of model parameters

Using these values of i and T_{polar}, we made a grid of fluxes around the six Fe lines of Table 6.2 with [M/H] = −1.0, −0.85 and −0.7, $v_{equat} \cdot \sin i$ = 21 and 22.5 km s^{-1} and v_{turb} = 1.7, 1.9, 2.1 and 2.3 km s^{-1}. Three of the lines are relatively deep (90 < EW < 140 mÅ), therefore Fe abundance calculated from them depend strongly on v_{turb}; and the other three are relatively weak

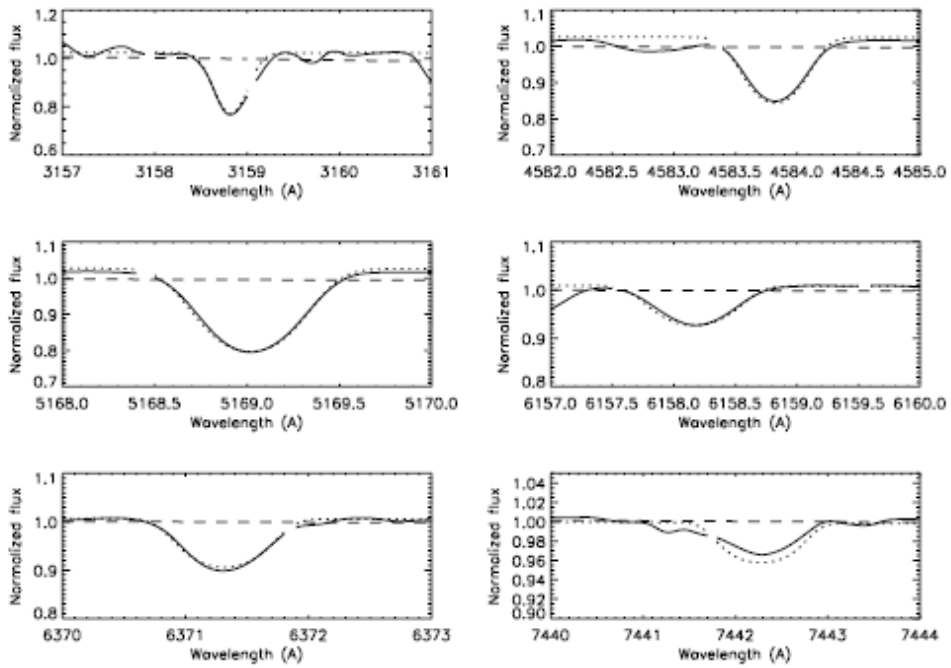

FIGURE 6.3— The same comparison as in Fig. 6.2, but now using the synthetic flux (divided by the same normalization constant) of the best fit to the observed one using rapidly rotating models (dotted lines) with [M/H] = −0.7: $T_{\rm eff} = 9576$ K and $i = 6.589$ degrees. We have also used $v_{\rm equat} \cdot \sin i = 23$ km s^{-1} (Gray 1980), $v_{\rm turb} = 2.0$ km s^{-1} (Castelli & Kurucz 1994) and a Gaussian profile with FWHM = 0.2 Å, according to the spectral resolution of the observed spectrum.

TABLE 6.2— Lines used to calculate the metallicity and microturbulence velocity of Vega.

Ion	Wavelength (Å)	EW_{obs} (mÅ)
Fe II	4178.87	59 ± 5
Fe II	4515.33	50 ± 6
Fe II	4583.83	93 ± 8
Fe II	4923.92	118.5 ± 8
Fe II	5169.03	140 ± 8
Fe II	5276.00	64 ± 8

(50 < EW < 70 mÅ), and then their Fe abundance is less dependent on $v_{\rm turb}$, while they are not as weak as to have very high uncertainties due to S/N. The value of [M/H] for each value of $v_{\rm turb}$ for the observed EWs is shown in Fig. 6.4. It can be summarized as: $v_{\rm turb} = 2.11 \pm 0.13$ km s^{-1} and [M/H] = −0.96 ± 0.03. Fixing $v_{\rm turb}$, we then computed the mean value of $v_{\rm equat} \cdot \sin i$ for the 6 Fe lines, obtaining $v_{\rm equat} \cdot \sin i = 21.65$ km s^{-1}, with a standard deviation of ±0.32 km s^{-1}. The comparison of the relative observed and computed fluxes with the model parameters found is shown in Fig. 6.5.

6.4 Calculation of abundances and new values of i and $T_{\rm polar}$

Using the line parameters found in §6.3, we have calculated the inclination of the rotation axis with respect to the line of sight, the polar temperature and Ca, O, Si and N abundances of Vega from the lines in Table 6.1. This time, the grid of fluxes was obtained using i from 5 to 6 degrees and $T_{\rm polar}$ from 9700 to 9900 K. The abundances of the grid are: log $\epsilon_{\rm Ca}$ from 5.56 to 5.96, log $\epsilon_{\rm O}$ from 8.58 to 8.98, log $\epsilon_{\rm Si}$ from 6.88 to 7.28, and log $\epsilon_{\rm N}$ from 7.89 to 8.29. The values of $T_{\rm polar}$ and i were chosen like these because preliminary tests show a linear tendency in the $T_{\rm polar}$,i field for the best fit of computed to observed spectra, while the abundances are those obtained from classical models plus and minus 0.2 dex. By minimizing again the χ^2 value of the fit between the computed and the observed spectrum, we obtained: $i = 5.33$ degrees and $T_{\rm polar} = 9802$ K, with log $\epsilon_{\rm Ca} = 5.86$, log $\epsilon_{\rm O} = 8.66$, log $\epsilon_{\rm Si} = 7.01$ and log $\epsilon_{\rm N} = 7.82$, with $\chi^2 = 0.040$. These values imply $v_{\rm equat} = 233$ km s^{-1}, $T_{\rm equat} = 8238$ K, $w = 0.84$, log $g_{\rm polar} = 4.08$ and log $g_{\rm equat} = 3.77$.

Since the computed continuum flux using the parameters above is different to the observed one, especially around the N I λ7442.30 Å line, we rederived the abundances using the previous set of parameteres to compute the normalized flux around each line to compare it with the observed flux. We have obtained log $\epsilon_{\rm N} = 7.96$, log $\epsilon_{\rm Ca} = 5.77$, log $\epsilon_{\rm O} = 8.70$ and log $\epsilon_{\rm Si} = 7.08$. Using these

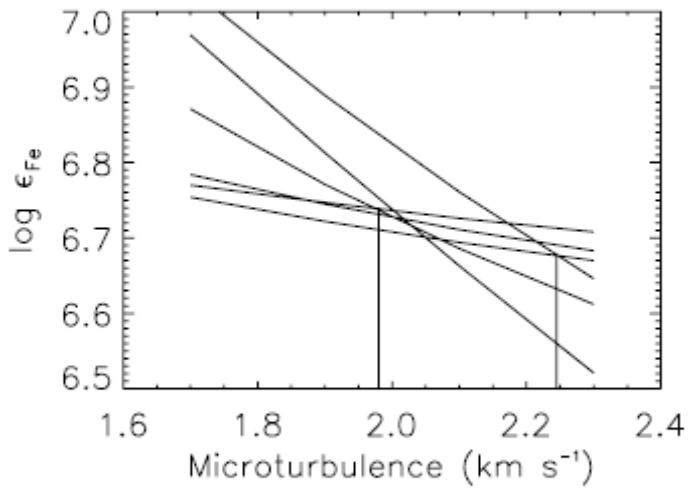

FIGURE 6.4— Fe abundance versus microturbulence velocity for 6 spectral lines (see Table 6.2). The overlapping region is defined by the following values: $v_{\rm turb} = 2.11 \pm 0.13$ km s^{-1} and log $\epsilon_{\rm Fe} = 6.71$, corresponding to [M/H] $= -0.96 \pm 0.03$.

abundances, we have derived again the parameters, obtaining the values shown in Table 6.3, where they are compared with those from Gulliver et al. (1994). The new total χ^2 is 0.061. These values imply $w = 0.84$ and log $g_{\rm equat} = 3.77$. The shape of a star with these rotational parameters is shown in Fig. 6.6. A comparison between the computed spectrum using the last mentioned parameters and the observed spectrum is shown in Fig. 6.7. It is also remarkable the fact that the χ^2 of the fit does not almost get worse when $T_{\rm polar}$ and i are changed in a specific way. For instance, when fixing a polar temperature 50 K lower or higher, the best fit of the synthetic to the observed flux is obtained with the following inclinations:

- for $T_{\rm polar} = 9757$ K: $i = 5.54$ degrees, with $\chi^2 = 0.066$
- for $T_{\rm polar} = 9857$ K: $i = 5.16$ degrees, with $\chi^2 = 0.065$

Thus, the best fit has $\chi^2 < 0.067$ when increasing or decreasing $T_{\rm polar}$ in 50 K when at the same time i is changed in a specific way. The three values of $T_{\rm polar}$ and i are shown in Fig. 6.8.

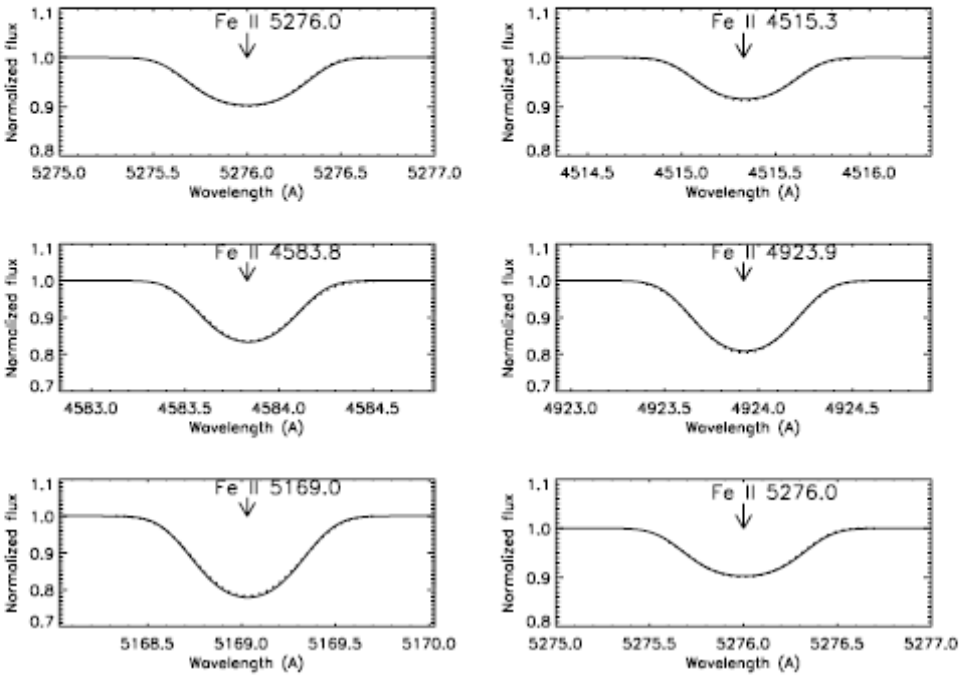

FIGURE 6.5— Comparison of the observed flux (dotted lines) around 6 Fe spectral lines (see Table 6.2) with respect to the synthetic ones (solid lines) using the following line parameters: $v_{\rm turb} = 2.11 \pm 0.13$ km s^{-1}, $v_{\rm equat} \cdot \sin i = 21.65$ km s^{-1} and [M/H] $= -0.96 \pm 0.03$.

TABLE 6.3— Comparison of parameters obtained using rapidly-rotating models.

	Gulliver et al. (1994, continuum)	Gulliver et al. (1994, lines)	this thesis
$v_{\rm equat} \cdot \sin i$ (km s^{-1})	21.8 ± 0.2	21.8 ± 0.2	21.65 ± 0.32[1]
$v_{\rm equat}$ (km s^{-1})	210	245	233
i (degrees)	6.0 ± 0.7	5.1 ± 0.3	5.33
$T_{\rm polar}$ (K)	9595 ± 20	9695 ± 25	9807
$T_{\rm equat}$ (K)	9325	9300	8240
$\log g_{\rm polar}$	3.80 ± 0.03	3.75 ± 0.02	4.08

[1]: only taking into account the typical deviation of the measurements.

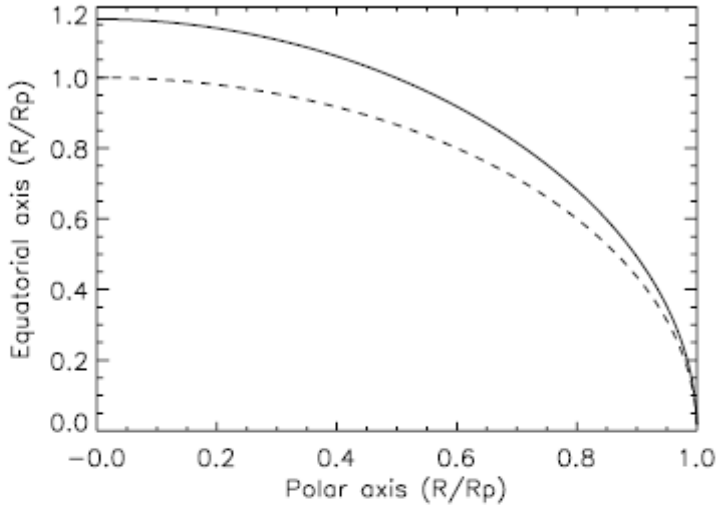

FIGURE 6.6— Comparison of the shape of a non-rotating star (dashed line) and the shape of Vega according to the rapidly-rotating model that best matches the observed flux ($w = 0.84$, solid line).

6.5 Comparison of the result with that from classical models

A wide variety of measurements have been carried out for Vega in the last few years. The effective temperature in the most recent works is usually between 9400 and 9700 K, while the angular diameter varies from $\sim$ 3.22 to 3.28 mas (see Table 4.1). The temperatures that we obtain for the best fit (T_{polar} = 9807 K, T_{equat} = 8240 K) will be compared with those from the literature later in this chapter.

In chapter 4, we calculated several chemical abundances using non-rotating models. Firstly, we employed the UV continuum, where some elements (C and Si) are the most important contributors to the continuum opacity for Vega, so we searched for the model atmosphere whose continuum UV flux best matched the observed flux. We also computed some chemical abundances using spectral lines in the visible range. We used the model parameters from our best fit using non-rotating model atmospheres, the parameters by Qiu et al. (2001) and those by Przybilla (2002), to calculate chemical abundances, which are compared with those obtained using the best fit with rapid rotation in Table 6.4. The abundances relative to iron using stellar models without and with rapid rotation are shown in Table 6.5. They have been compared like this because we use different stellar models in each case, so a relative value of abundances is

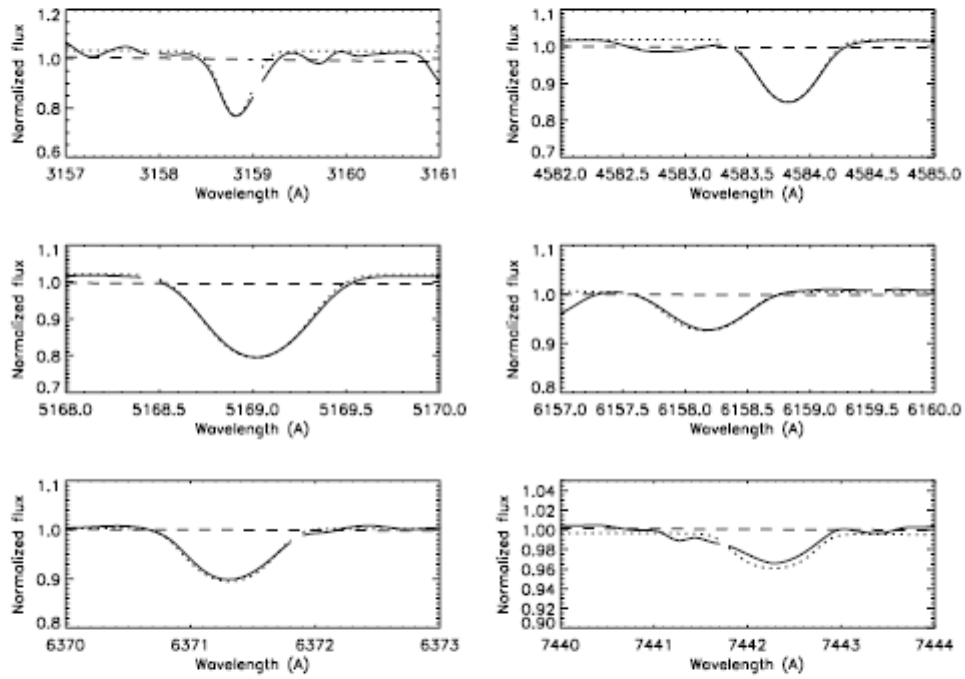

FIGURE 6.7— Comparison of the normalized high-resolution observed flux (solid lines) around 6 spectral lines (Ca II λ3158.87, Fe II λ4583.83, Fe II λ5169.03, O I λ6158.19, Si II λ6371.37 and N I λ7442.30 Å), the low-resolution observed flux normalized at the center of each line (dashed lines) and the synthetic flux (divided by the same normalization constant) for the best fit to the observed one using the abundances from Table 6.1 and parameters obtained in §6.4 (dotted lines): $v_{\rm equat} \cdot \sin i = 21.65$ km s^{-1}, $i = 5.33$ degrees, [M/H] $= -0.96$ and $T_{\rm polar} = 9807$ K.

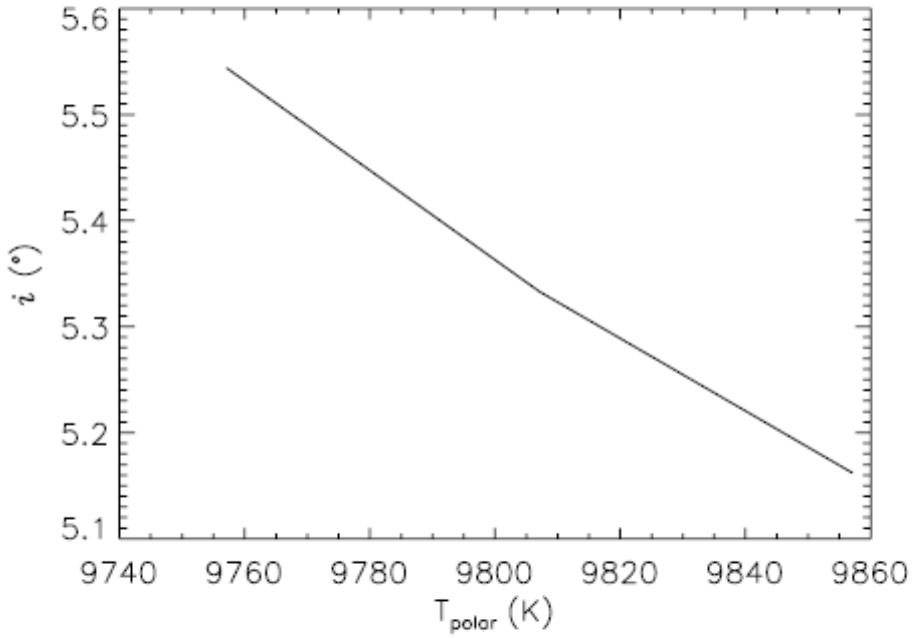

FIGURE 6.8— Lines connecting i and T_{polar} of the best fit between computed fluxes and the observed flux from §6.4 and the parameters of the best fit changing T_{polar} in 50 K, using the 6 spectral lines mentioned in Table 6.1. These points are: $i = 5.54$ degrees for $T_{polar} = 9757$ K, $i = 5.33$ degrees for $T_{polar} = 9807$ K and $i = 5.16$ degrees for $T_{polar} = 9857$ K.

more consistent for comparisons.

From this comparison with the relative abundances using rapid rotation, we obtain the following results:

- N and O relative abundances are almost the same using rapidly rotating models than using non-rotating ones,
- there is a difference of 0.2-0.3 dex in Si and Ca relative abundances between rapidly rotating and non-rotating models. Both relative abundances are higher with rapidly rotating models,

where the deepest lines are those of C, Si and Fe, so their abundances are the most accurate.

Let us now calculate EW for the same spectral lines and the chemical abundances just derived, but using non-rotating models. The effective temperatures used are those of the best fit with this kind of models (see chapter 4) and a mean effective temperature of the rapid-rotating models, weighting it with the flux and the area projected to the line of sight. This is:

$$< \mathrm{T_{eff}} >= \frac{\int \mathrm{T_{eff}}(\theta)\frac{\mathrm{dL}}{\mathrm{d}\theta}\mathrm{dS}}{\int \frac{\mathrm{dL}}{\mathrm{d}\theta}\mathrm{dS}} = \frac{\int_0^{\pi/2} \mathrm{T_{eff}}(\theta)\frac{\mathrm{dL}}{\mathrm{d}\theta}\sin\theta\cos\theta\ \mathrm{d}\theta}{\int_0^{\pi/2} \frac{\mathrm{dL}}{\mathrm{d}\theta}\sin\theta\cos\theta\ \mathrm{d}\theta}. \tag{6.25}$$

With the stellar parameters used when calculating abundances, we obtain $< \mathrm{T_{eff}} >= 9210$ K. This value is clearly lower than the $\mathrm{T_{eff}}$'s from the literature when using non-rotating atmospheric models. In Table 6.6, EW's for the spectral lines using slow-rotating stellar models with this $\mathrm{T_{eff}}$ and that from chapter 4 using the abundances obtained using rapidly rotating models is shown. The computed EW's are within the error bars of the observed EW's or close to them for most lines (for the Ca line, we used the EW obtained when duplicating the left side of the line) when using the recently derived $\mathrm{T_{eff}}$. However, when using the $\mathrm{T_{eff}}$ obtained with non-rotating models, the computed EW's are outside or on the border of the error bars of the observed EW's. For this reason, $< \mathrm{T_{eff}} >$ can be considered a reasonable approximation of the $\mathrm{T_{eff}}$ of a non-rotating model necessary to reproduce the observed spectral lines using the abundances obtained with rapidly rotating models.

TABLE 6.4— Comparison of chemical abundances obtained using non-rotating models (from spectral lines in the visible and from the UV continuum) and from spectral lines in the visible using rapidly rotating models. Stellar parameters from chapter 4 are always used.

Ion	log ϵ_X with no rotation	log ϵ_X with rapid rotation
C I		
mean[1]	8.39±0.07	
UV continuum[2]	$8.55\ ^{+0.34}_{-0.48}$	
N I		
mean[1]	8.09±0.04	7.96±0.06
O I		
mean[1]	8.83±0.09	8.70±0.04
Mg I		
mean[1]	7.17±0.15	
Mg II		
mean[1]	6.91±0.06	
Al II		
mean[1]	5.77 (1 line)	
Si II		
mean[1]	7.08±0.14	7.08±0.03
UV continuum[2]	$6.65\ ^{+0.57}_{-2.10}$	
Ca I		
mean[1]	5.76 (1 line)	5.77±0.1[3]
Cr I		
mean[1]	5.40±0.02	
Fe I		
mean[1]	7.06±0.09	
Fe II		
mean[1]	6.92±0.15	6.71±0.04

[1]Calculated in chapter 4

[2]Using the continuum opacity

[3]Using a Ca II line

TABLE 6.5— Chemical abundances relative to iron in logarithmic scale obtained using the parameters of the best fit in chapter 4 and models without rotation and with rapid rotation.

Ion	No rotation	Rapid rotation
N I	1.17	1.25
O I	1.91	1.99
Si II	0.06	0.37
Ca II	−1.16	−0.94
Fe II	0	0

TABLE 6.6— Comparison of the observed EW and EW's using non-rotating stellar models for the lines used to calculate the abundance of Vega using the abundance obtained from models with rapid rotation, including [M/H] = −0.96.

Ion	Wavelength (Å)	EW_{obs} (mÅ)	EW_{9210K} (mÅ)	EW_{9620K} (mÅ)
Ca II	3158.87	110[1] ± 15	98	85
Fe II	4583.83	93 ± 8	88	80
Fe II	5169.03	140 ± 8	126	118
O I	6158.2	58 ± 6	52	51
Si II	6371.37	80 ± 6	72	69
N I	7442.30	31 ± 4	29	27

[1]This is the value when duplicating the left half side of the line, because there is a close line: Cr II λ3159.095 Å, with a EW of 5-10 mÅ

7

Conclusions and future work

7.1 Conclusions

The main aim of this thesis has been the quantitative study of near ultraviolet, visible and near infrared spectra of Vega and Procyon. We summarize in this chapter the main conclusions obtained.

We have compiled observed spectra of Vega and Procyon from existing archives and complemented them with new observations. For Vega, we have considered different calibrations of the low-dispersion UV spectra obtained from the IUE mission. The comparison of the observed flux (taking also into account the visible and near-IR regions) with our calculations considering in detail metal opacities favors the Hubble Space Telescope (HST) flux scale over the INES scale, since the χ^2 statistics of the best fit is clearly lower in the near-UV when using the HST scale. As there are no high-dispersion UV spectra in the HST flux scale, we have used the other calibration (INES), but corrected in absolute flux to the HST flux scale. We have used the spectrum by Hayes (1985), with a low flux uncertainty, as low-dispersion visible spectrum, and two spectra acquired from the McDonald Observatory (Mount Locke, Texas) as high-dispersion visible spectrum.

For Procyon, we have obtained new spectra with STIS on board the HST. These spectra have a higher resolving power and similar spectrophotometric accuracy than the UV spectrophotometric data available for the Sun. We have compared different visible spectra of Procyon with the spectrum of STIS to choose between them, concluding that Burnashev's and Glushneva's fluxes are the most similar in the overlapping region, so the mean of both has been used as medium-dispersion visible spectrum. A high-dispersion spectrum taken from McDonald Observatory has been used to derive abundances from spectral lines.

For the IR, the Moscow Spectrophotometric Catalog has been adopted, showing a flux similar to the visible spectrum used in the overlapping region.

We have identified the main contributors to the continuum opacity in Vega by comparing the synthetic flux using the most abundant ions with the flux only using H, obtaining: H, H^-, C I and Si II. These ions (except H and H^-) only contribute significant opacity in the UV for wavelengths lower than ~1500 Å. Taking this into account, we have derived the effective temperature and the angular diameter of Vega (adopting the preferred surface gravity and metallicity) by comparing fluxes obtained using different model atmospheres with the observed visible, near-IR and near-UV spectrum. The values obtained are similar to those in the literature.

With the effective temperature and angular diameter derived for Vega, we have investigated the chemical abundances of Si and C by comparing synthetic fluxes with that observed in the UV in regions where the continuum opacity produced by these elements is important. Then, these and other chemical abundances have been derived from spectral lines in the visible range, obtaining a similar value for C. However, the Si abundance obtained is quite different to that obtained from spectral lines due to the large uncertainty of this abundance when derived from the continuum, but it is within the error bars.

A similar study of Procyon A has been carried out. As this star has a lower effective temperature, the effect of metal opacity on the emitted flux is more relevant. We have found that there is a larger number of species that contribute significant UV continuum opacity: H, H^-, C I, Mg I, Al I, Si I, Ca I and Fe I. Opacity from these ions must be taken into account for wavelengths below ~3000 Å (Fe and H elements also contribute over this wavelength), almost reaching the visible range.

We have used the near-IR and the visible region to derive the effective temperature and the angular diameter using the same method as for Vega. We have derived chemical abundances for several elements in Procyon A. Iron and magnesium abundances have been obtained from the UV flux in the region where their continuum opacity is important. These abundances have also been derived from spectral lines in the visible, obtaining compatible results. We have also found the abundance of other elements from spectral lines in the visible, and our results are compatible with those from other authors.

The compatibility of the abundances obtained from the UV continuum and from spectral lines in the visible for the main contributors to the continuum opacity is one important result of the thesis. We have developed an independent method to derive abundances in late-type stars apart from the study of spectral lines.

Finally, we have carried out a study of Vega's spectrum using rapidly ro-

tating stellar models and have compared the flux computed using them with the observed flux. Several spectral lines of different elements covering a wide wavelength range and with different equivalent widths were used. Fitting fluxes computed with different atmospheric parameters to the observed flux has allowed us to estimate the polar temperature and the inclination of the rotational axis.

We have then used 6 iron lines with quite different equivalent widths (and therefore different sensitivity to the microturbulent velocity) to derive the microturbulent velocity, the projected rotational velocity and the metallicity. We have obtained $v_{\rm equat} \cdot \sin\, i = 21.65$ km s^{-1}, $v_{\rm turb} = 2.11 \pm 0.13$ km s^{-1} and [M/H] $= -0.96 \pm 0.03$. The first two values are in very good agreement with previous works, while the metallicity is ~ 0.2 dex lower than that obtained using non-rotating models.

Using these values for the fast-rotation models, we have re-derived the abundances, the polar temperature and the inclination of the rotational axis. We have obtained: $i = 5.33$ degrees and $T_{\rm polar} = 9802$ K, $\log \epsilon_{\rm N} = 7.96$, $\log \epsilon_{\rm Ca} = 5.77$, $\log \epsilon_{\rm O} = 8.70$ and $\log \epsilon_{\rm Si} = 7.08$.

We have compared the chemical abundances relative to iron with those from non-rotating models. The chemical abundances are in good agreement for N and O, but they are 0.2-0.3 dex higher for Si and Ca when using rapidly-rotating models. The low value of the inclination (5.33 degrees) is consistent with other works. The polar temperature (9802 K) is somewhat higher than the usual values of the effective temperature from the literature (9400-9700 K). However, the equatorial temperature (8240 K) is very low compared to it, and the mean photospheric temperature over the observed surface (9210 K) is lower than in other works, which explains partially the different abundances and the low metallicity obtained using our rapidly-rotating models.

7.2 Future work

I sum up in this section our intention for the future about the work to carry out related to this thesis. Firstly, it is necessary to improve our fits of synthetic spectra to the observed spectrum of Procyon, since it is unsatisfactory in some spectral regions. In order to achieve this, a further study of Procyon is a must. A comparison of the observed flux with that obtained by means of 3D stellar atmosphere simulations of Procyon introducing our preferred parameters would give us an idea about the importance of this effect.

It is also important to extend this study to later-type stars, because the contribution of metal opacity to their flux is larger and therefore these stars are harder to model. Our experience with the study of Vega and Procyon will

help us carry out a similar work with this type of stars.

In this work, a preliminary study of the effect on the flux of the departure from LTE has been carried out for Vega and Procyon. However, it has been scarce and limited to the calculation of level populations, but fixing the atmospheric structure. A further study of these and other late-type stars taking into account the change in the atmospheric structure produced by the departure from LTE will allow us to specify more accurately stellar parameters and will help us understand deeply stars, both their structure and their evolution, by comparing the result with evolutionary models.

8

Appendix: near-UV atlas of Procyon

The atlas of the near-UV spectrum of Procyon is presented here. It was taken with the STIS spectrograph on board HST by a proposal of our group (# 9368) included in cycle 11. Gratings G230MB (with six tilts providing coverage between 2200 and 3050 Å, approximately) and G430M (with four tilts covering the spectrum from about 3022 to slightly longer than 4000 Å), one taken during each of the 2 orbits, on September 9, 2002, were used to carry out medium-resolution spectra of Procyon calibrated in flux. The central wavelengths are shown in Table 8.1. Two expositions were made for each tilt. The S/N (at least 200, as measured at the short plateau at $\sim$ 2386.5 Å) is very useful in identifying errors in the adopted atomic parameters of strong lines, and obtaining the total opacity at particular wavelengths.

The atlas covers the wavelength region from $\sim$ 2200 to $\sim$ 4080 Å, and is shown in 50 Å-wide pieces for $\lambda < 3050$ Å (where the mean wavelength difference between neighboring pixels is $\sim$ 0.15 Å) and in 100 Å-wide pieces for $\lambda > 3050$ Å (where the mean wavelength difference between neighboring pixels is $\sim$ 0.28 Å, so the spectral resolution is worse), except in the first and the last figures. The observed flux is given in erg s^{-1} cm^{-2} $Å^{-1}$. Some of the deepest lines (EW > 10 Å) are labelled in the figures, including the wavelength and the ion that produces the opacity. The deepest lines between 2600 and 2650 Å are not labelled for clarity, because there are too many deep lines: Fe II λ 2607.1, 2611.9, 2613.8, 2617.6, 2625.7, 2628.3, 2631.0 and 2631.3 Å.

The accuracies of the CCD spectroscopic data are the following. In each exposure, relative wavelengths have an uncertainty of 0.1-0.3 times the wavelength difference between neighboring pixels, due to limiting factors such as the stability of the optical distortion and the accuracy of the dispersion solu-

TABLE 8.1— Central wavelength (λ_c), wavelength separation between neighboring pixels ($\Delta\lambda$), inicial wavelength (λ_i) and final wavelength (λ_f) of the tilts for every grating.

Grating	λ_c (Å)	$\Delta\lambda$ (Å)	λ_i (Å)	λ_f (Å)
G230MB	2276	0.15	2198	2352
	2416	0.15	2339	2493
	2557	0.15	2479	2633
	2697	0.15	2620	2773
	2836	0.15	2759	2912
	2976	0.15	2899	3052
G430M	3165	0.28	3022	3306
	3423	0.28	3280	3564
	3680	0.28	3537	3820
	3936	0.28	3794	4078

tions. The absolute wavelength accuracy (applied for different exposures) is 0.2-0.5 pixels, limited by thermal stability, derivation of the wave calibration zero point and the accuracy of the dispersion solutions. The accuracy of the absolute flux is ~5 % and that of the relative flux is ~2 %, due to factors such as instrument stability, evolution of charge transfer efficiency and photometric calibration.

The reduction of the spectra was carried out as follows. One of the spectra with the lowest wavelength was fixed and used to calibrate the other spectra in wavelength. The difference in radial velocity between both expositions of each tilt was computed using the *fxcor* routine of IRAF, and then one exposition of each tilt was shifted and then interpolated to the wavelengths of the other exposition using the *spline* routine of IDL, averaging both fluxes for each tilt. As each two neighboring tilts have an overlapping region in wavelength, we have computed the difference in radial velocity between each two neighboring tilts, starting from the fixed tilt with the lowest wavelength, and then we have shifted and interpolated the fluxes of the tilt with longer wavelength to the wavelengths of the tilt with lower wavelength, using the radial velocity difference. Following this procedure, we have created an atlas of Procyon's spectrum, with a changing wavelength step, but with the same radial velocity for all the spectrum. From the comparison of the atlas with respect to the computed spectrum in Fig. 5.3, the derived radial velocity of the atlas spectrum is $\sim +52$ km s^{-1}.

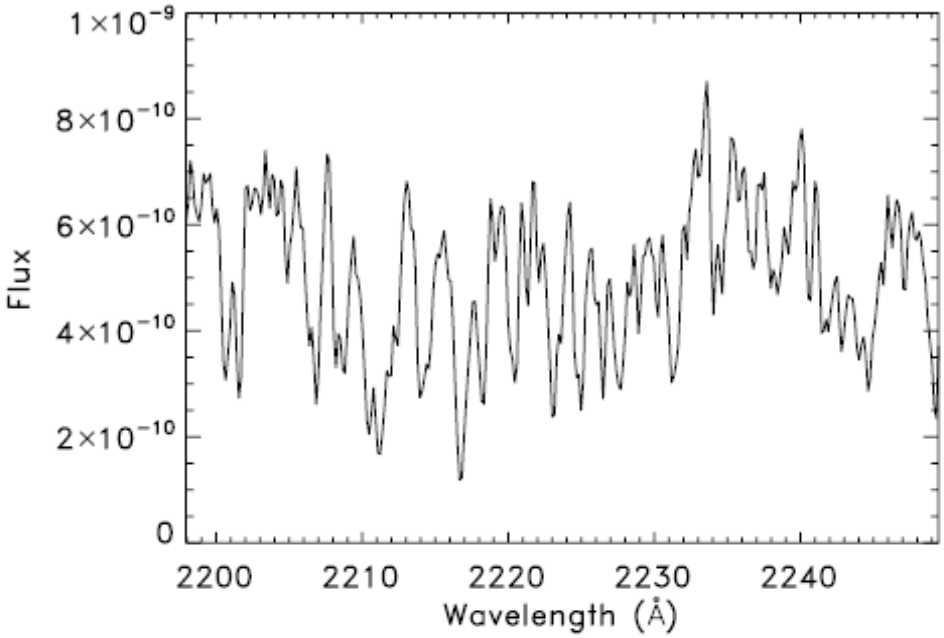

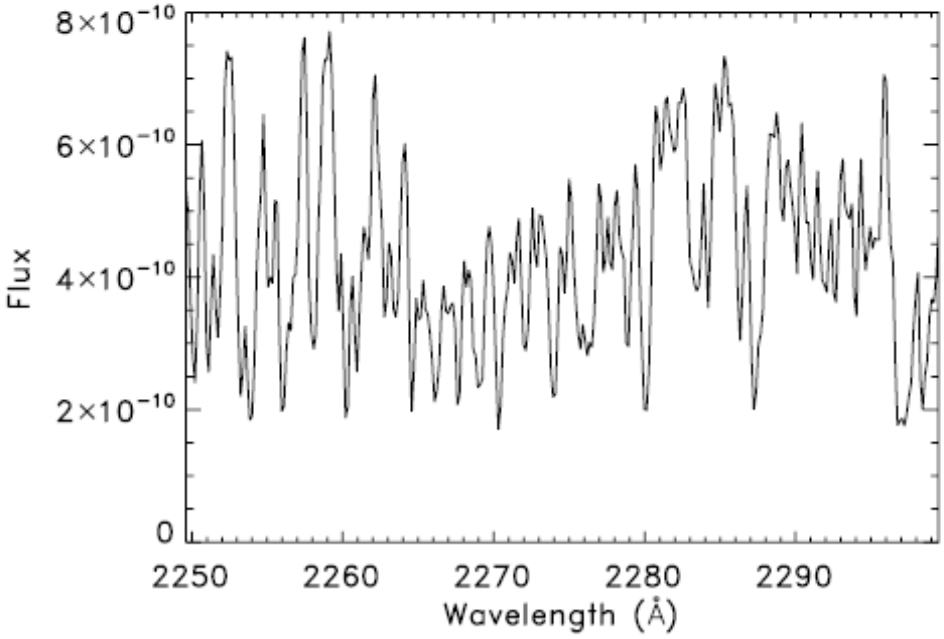

FIGURE 8.1— Atlas of Procyon: from 2198 to 2300 Å.

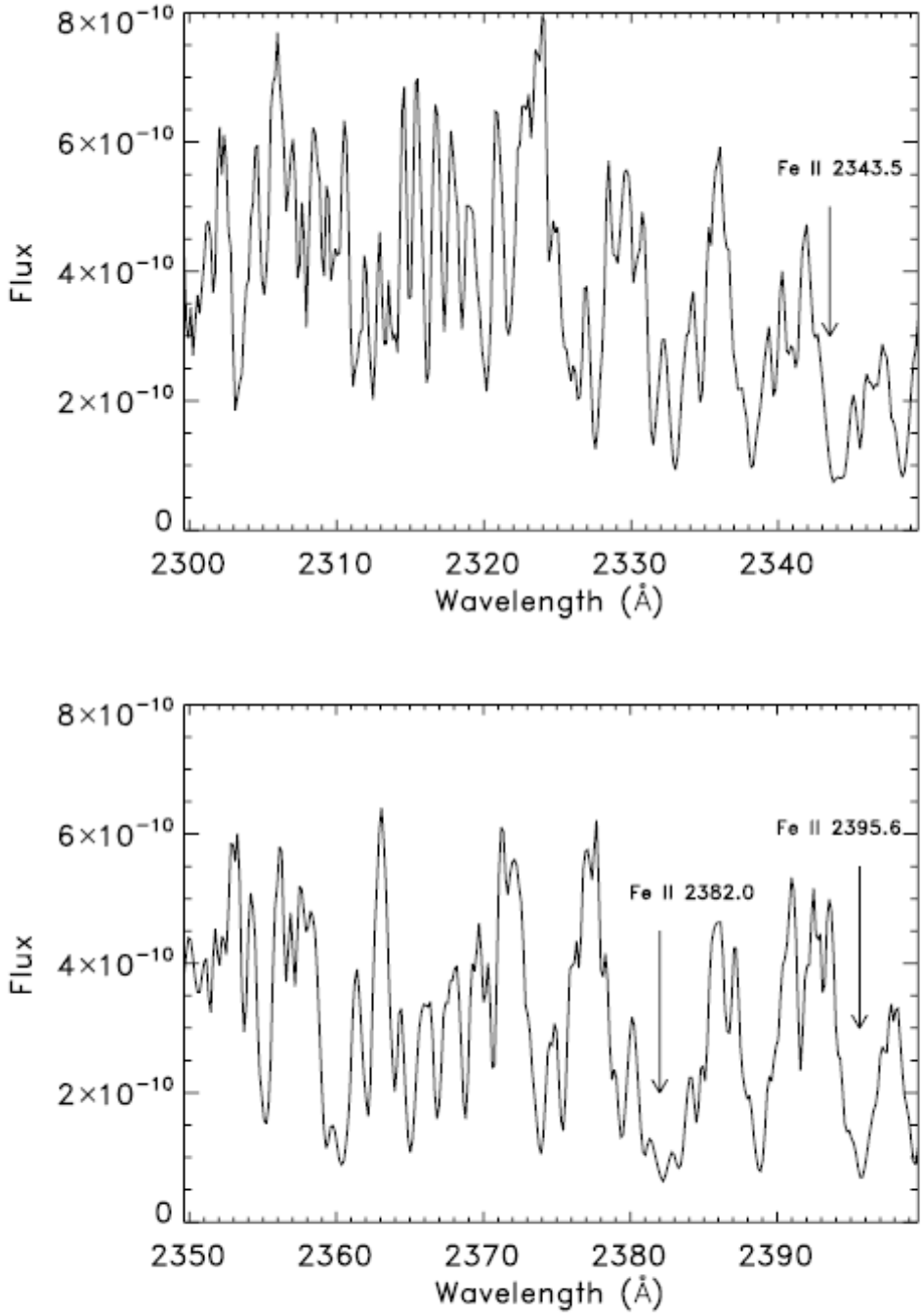

FIGURE 8.2— Atlas of Procyon: from 2300 to 2400 Å.

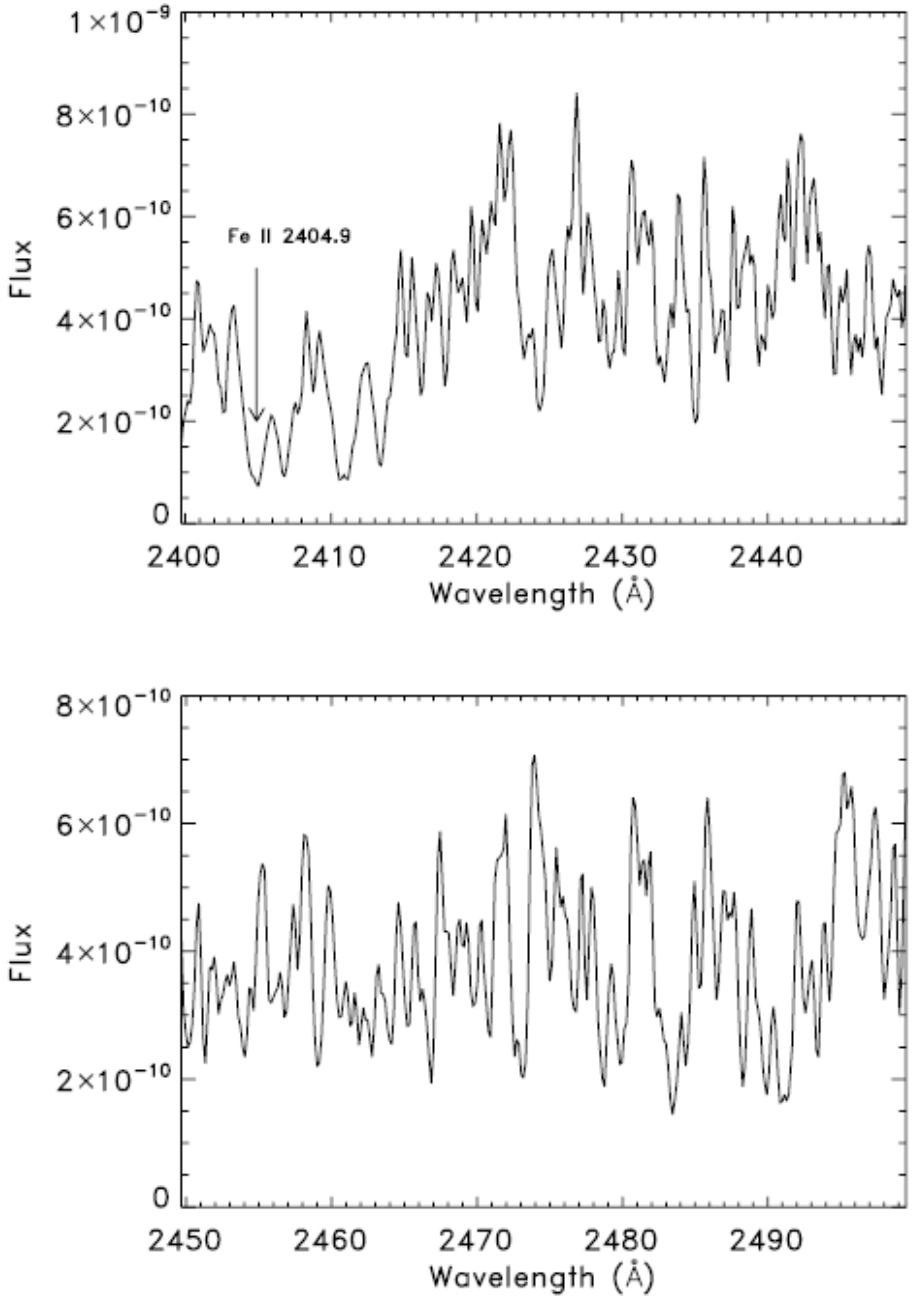

FIGURE 8.3— Atlas of Procyon: from 2400 to 2500 Å.

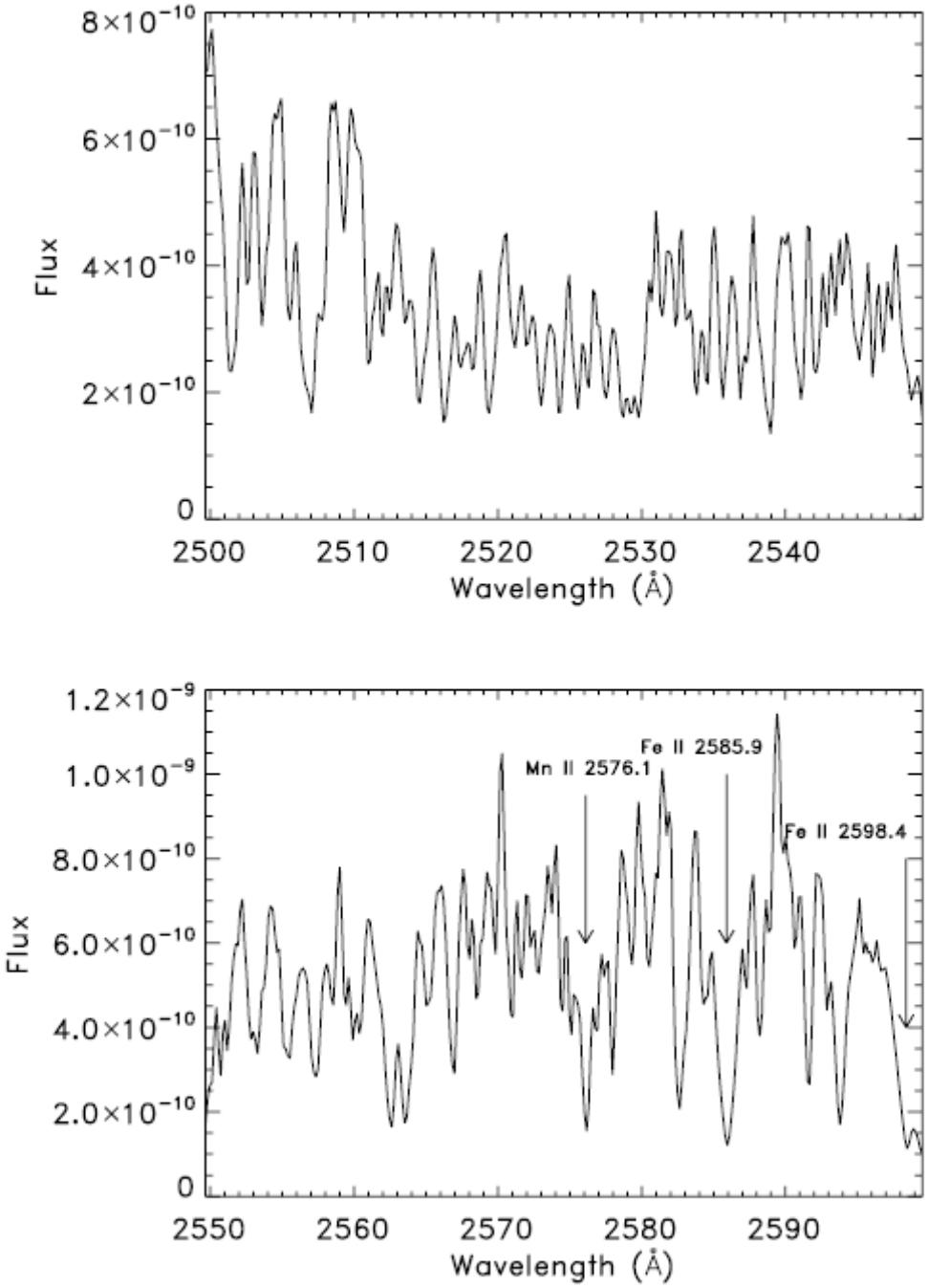

FIGURE 8.4— Atlas of Procyon: from 2500 to 2600 Å.

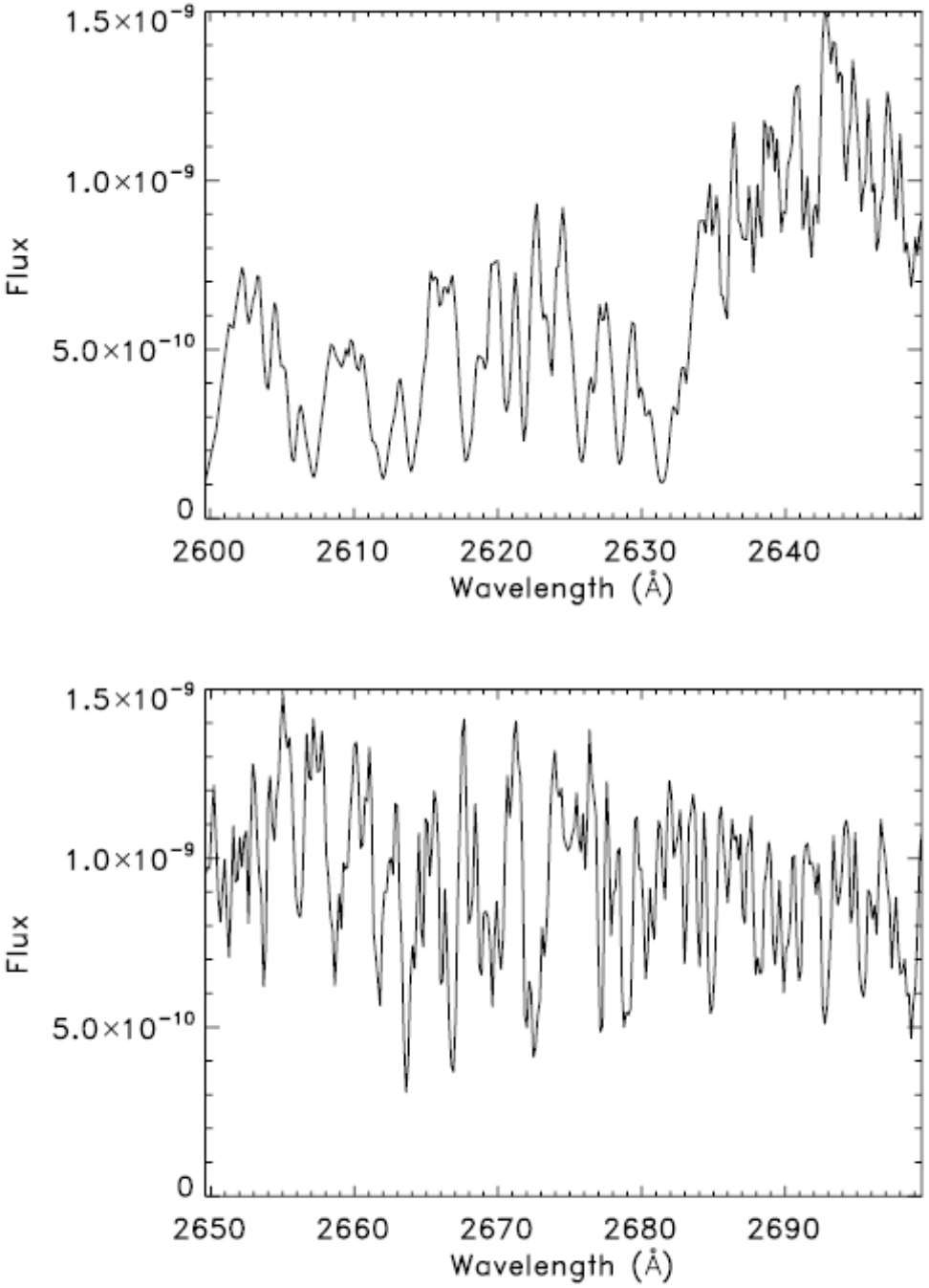

FIGURE 8.5— Atlas of Procyon: from 2600 to 2700 Å.

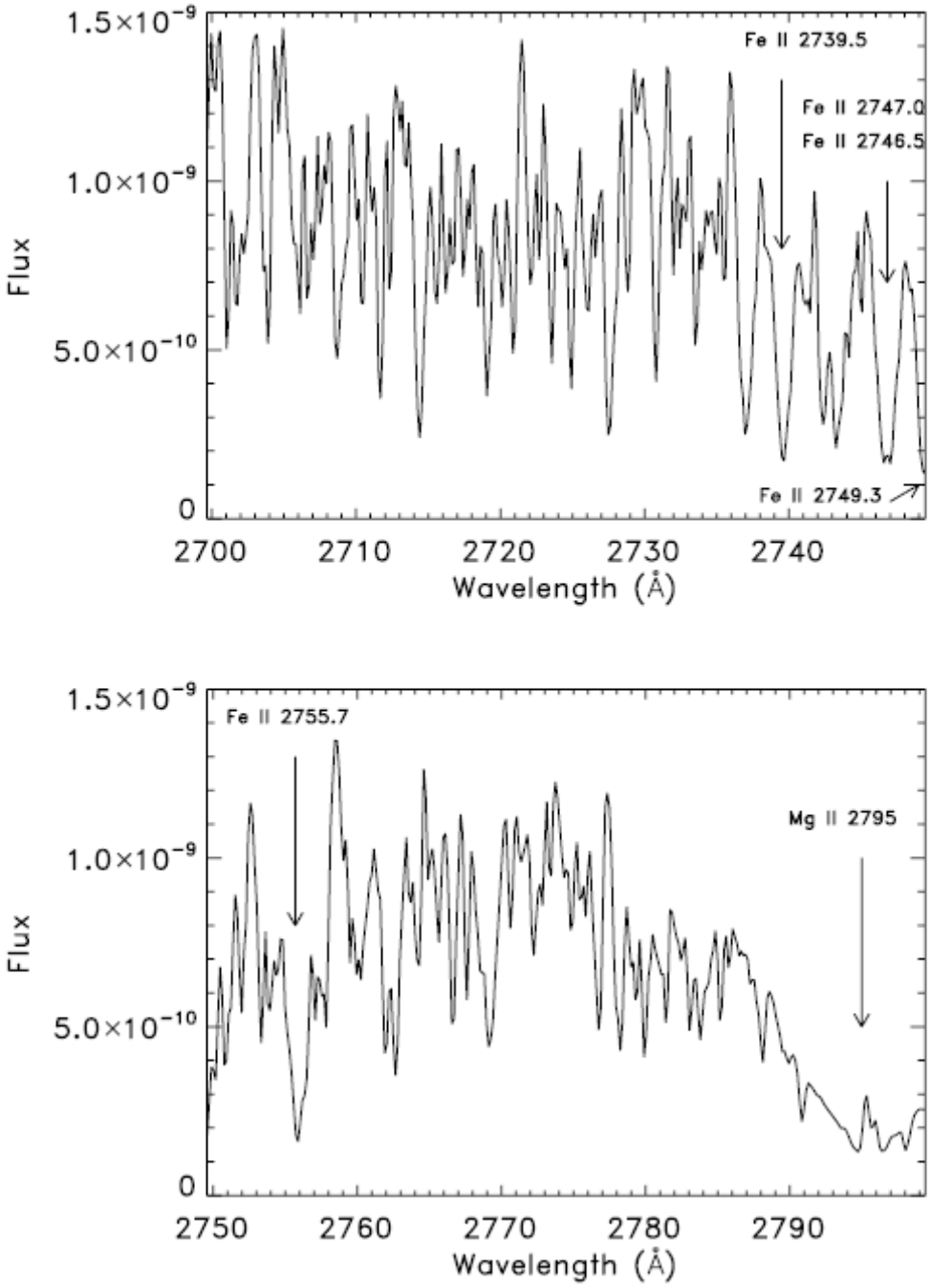

FIGURE 8.6— Atlas of Procyon: from 2700 to 2800 Å.

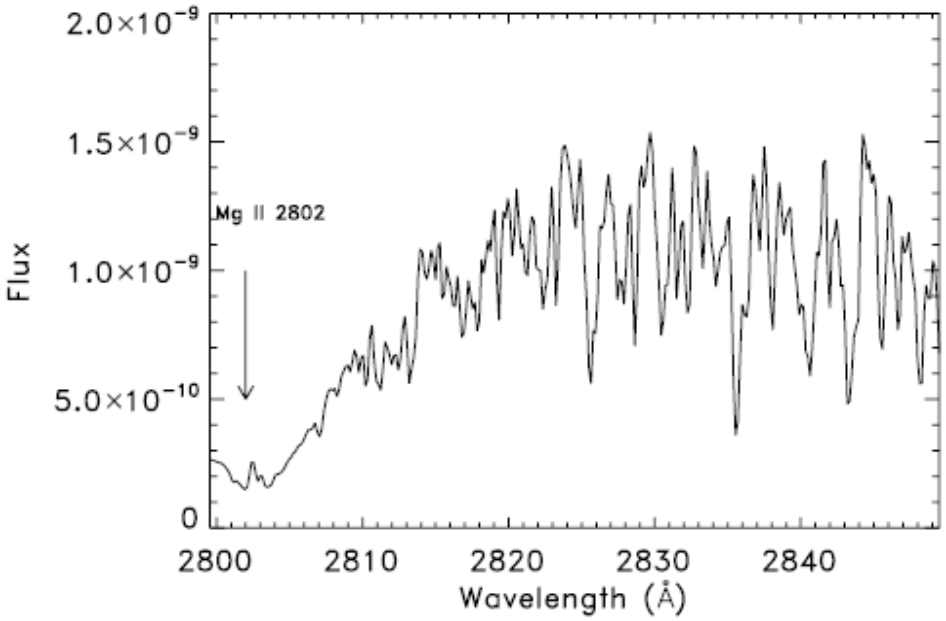

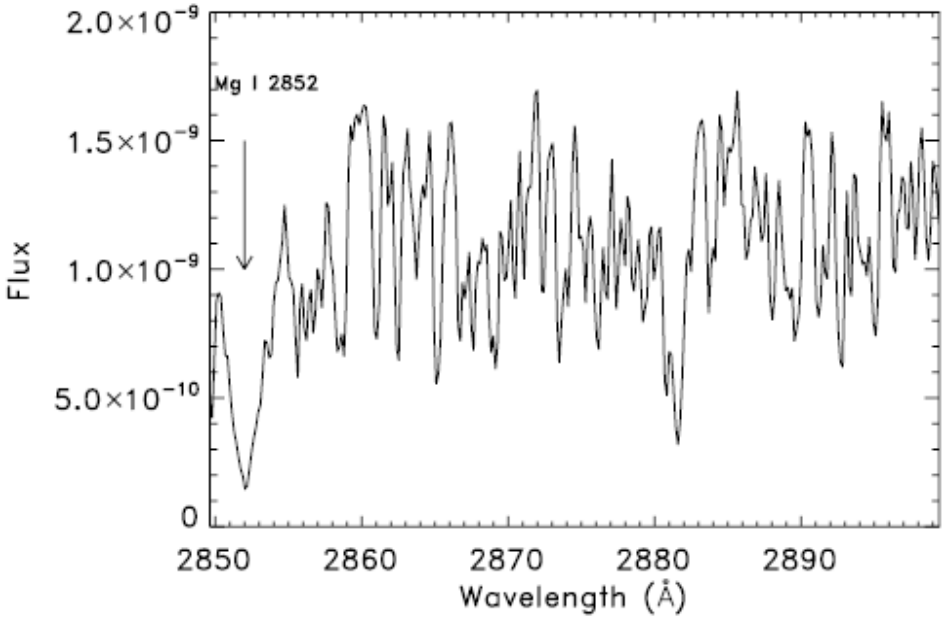

FIGURE 8.7— Atlas of Procyon: from 2800 to 2900 Å.

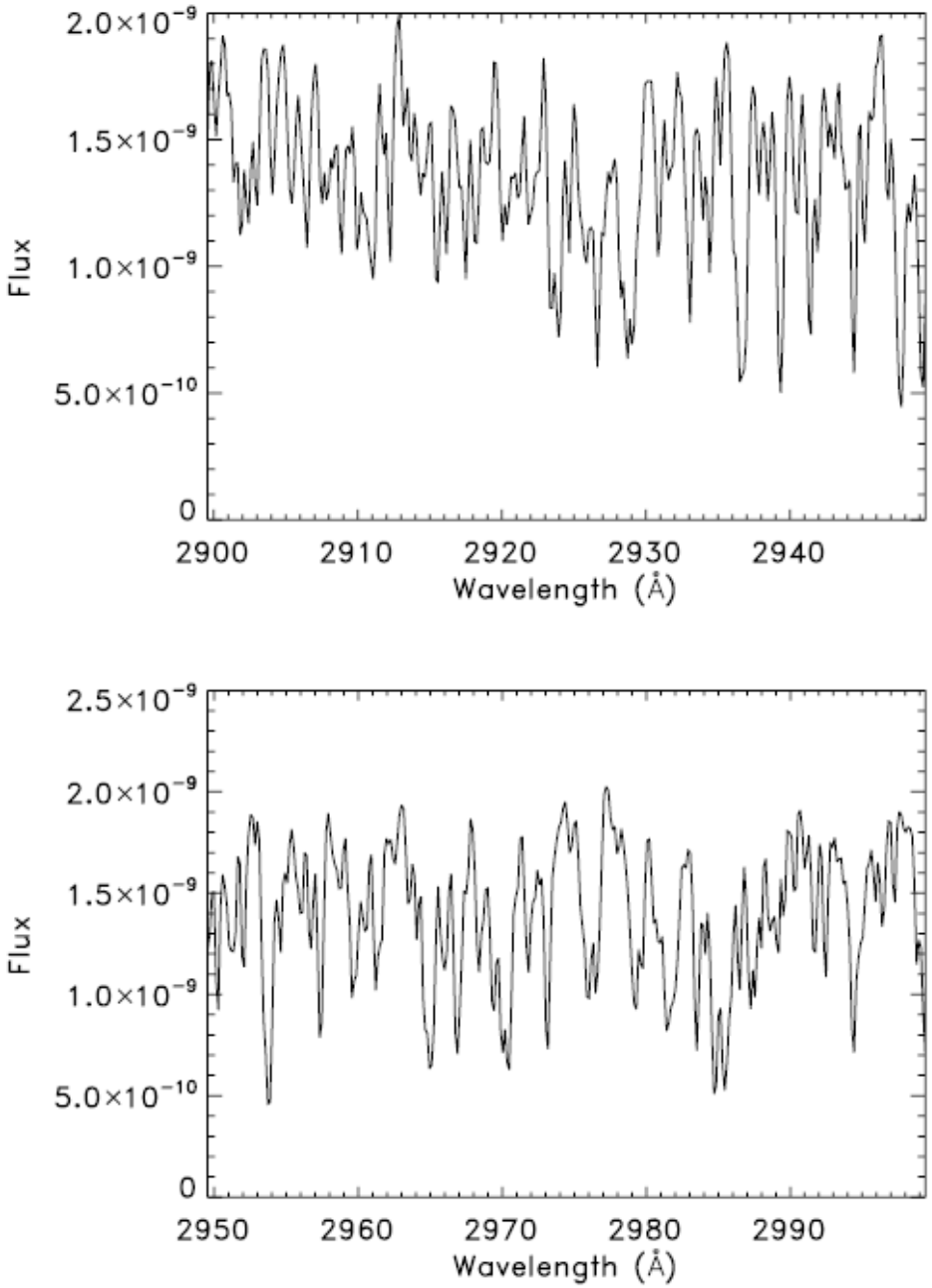

FIGURE 8.8— Atlas of Procyon: from 2900 to 3000 Å.

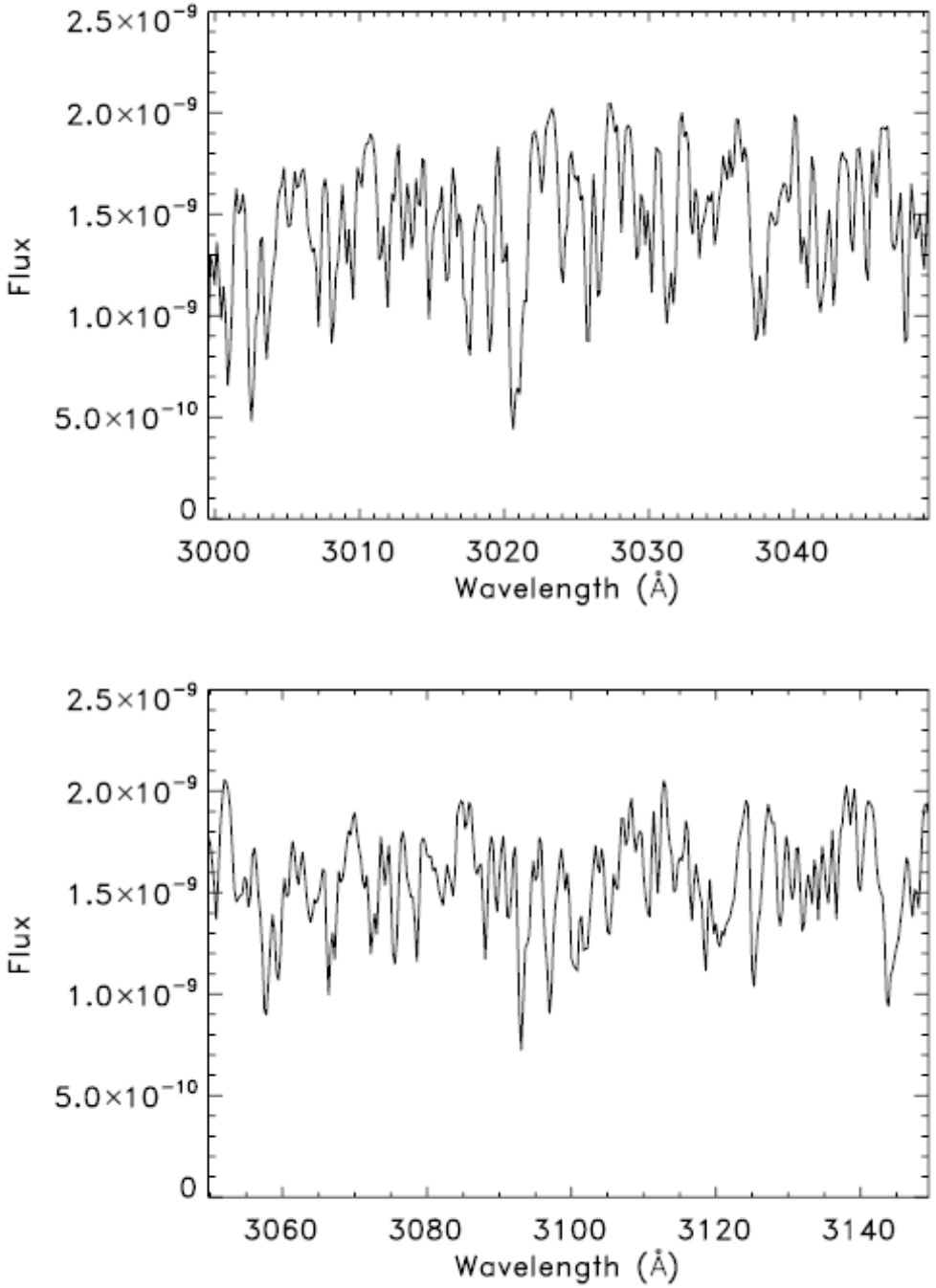

FIGURE 8.9— Atlas of Procyon: from 3000 to 3150 Å.

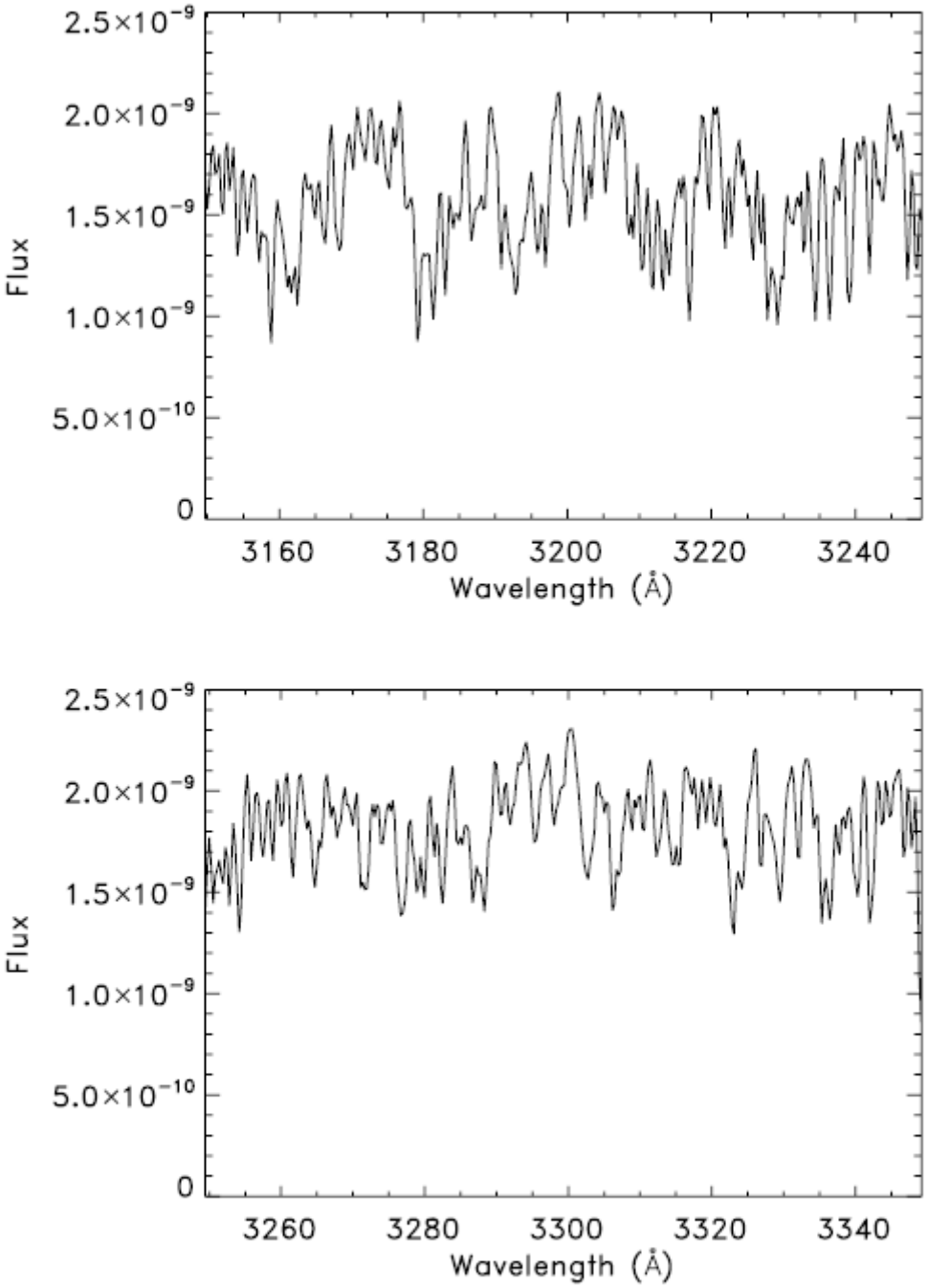

FIGURE 8.10— Atlas of Procyon: from 3150 to 3350 Å.

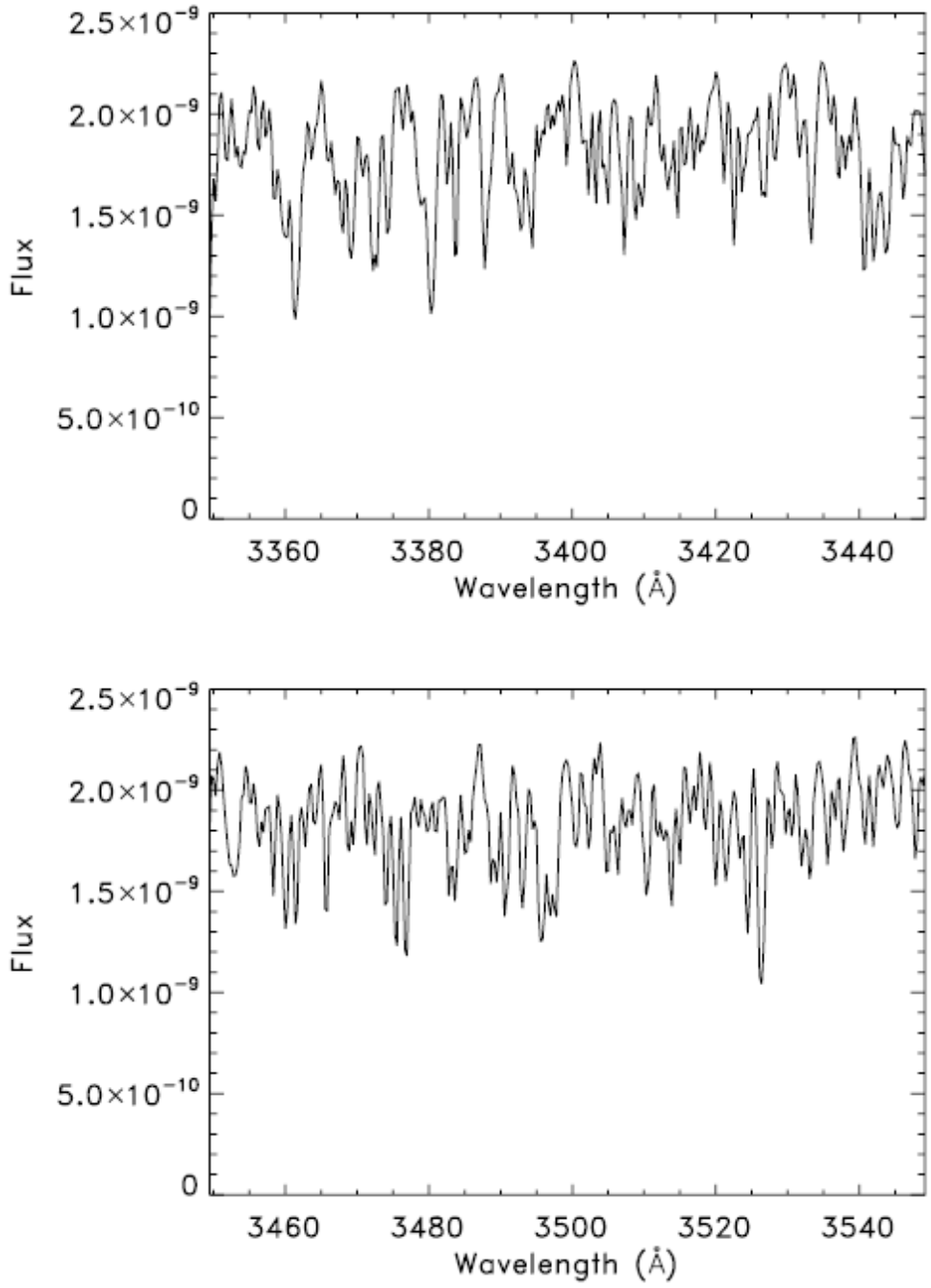

FIGURE 8.11— Atlas of Procyon: from 3350 to 3550 Å.

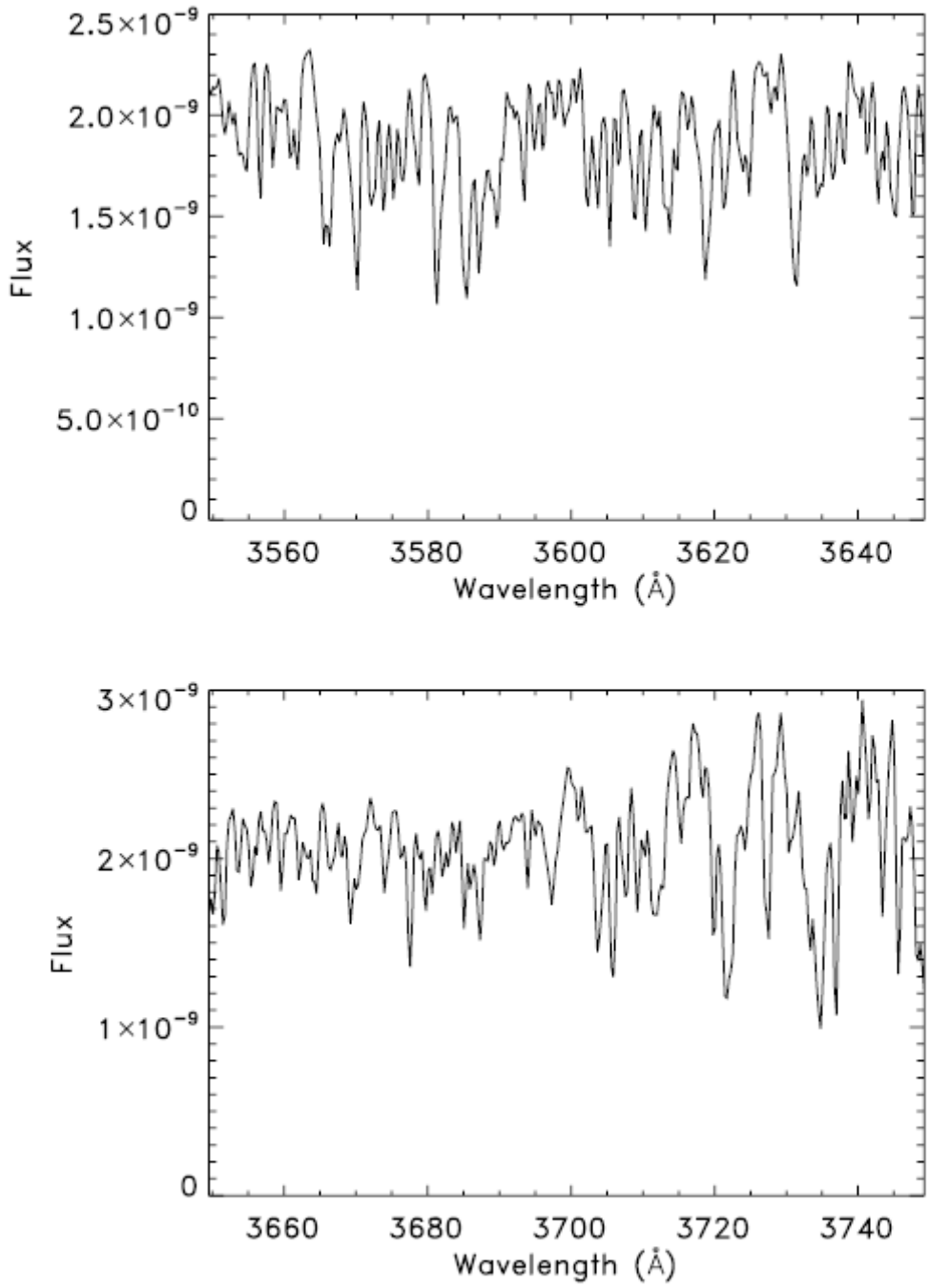

FIGURE 8.12— Atlas of Procyon: from 3550 to 3750 Å.

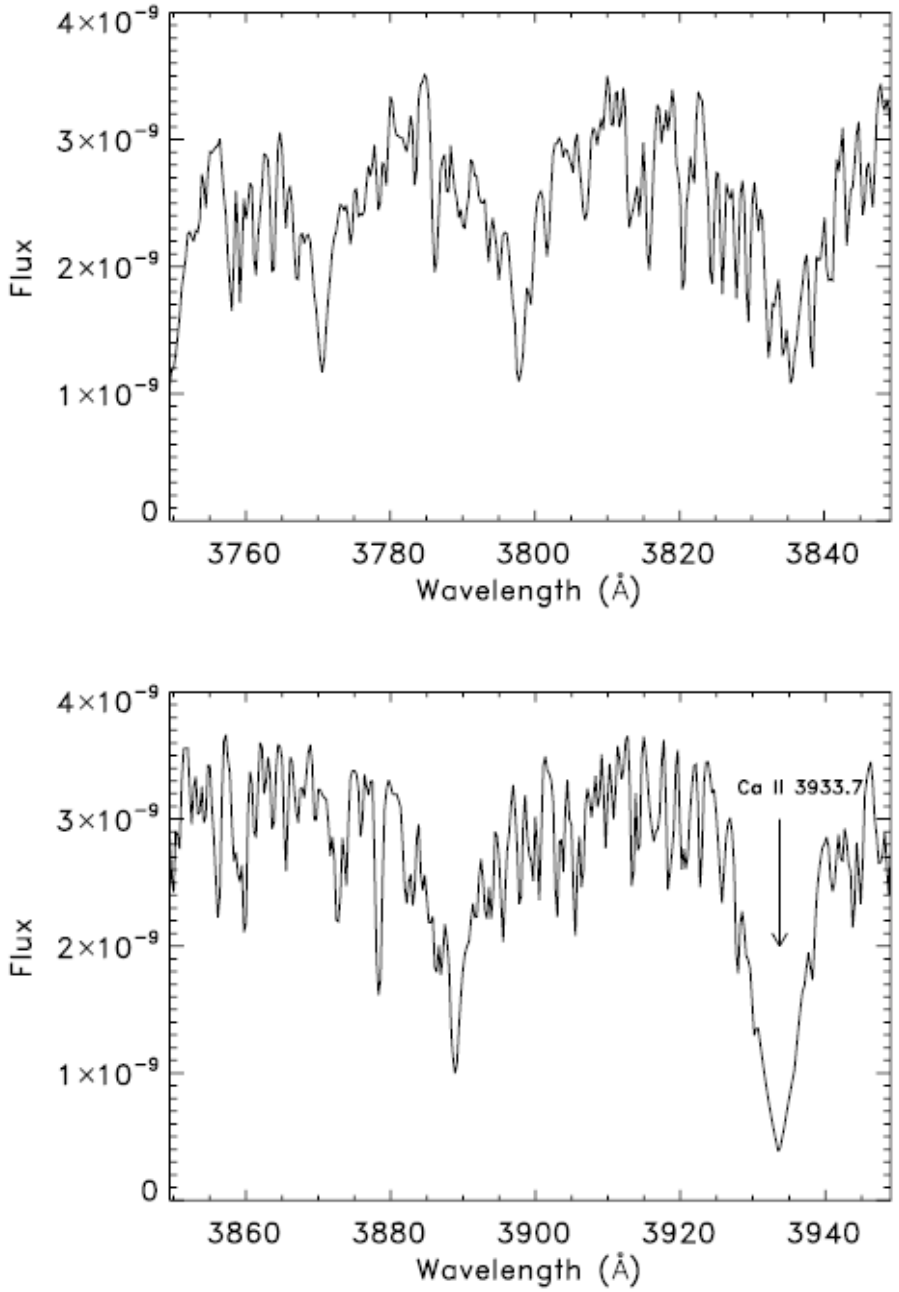

FIGURE 8.13— Atlas of Procyon: from 3750 to 3950 Å.

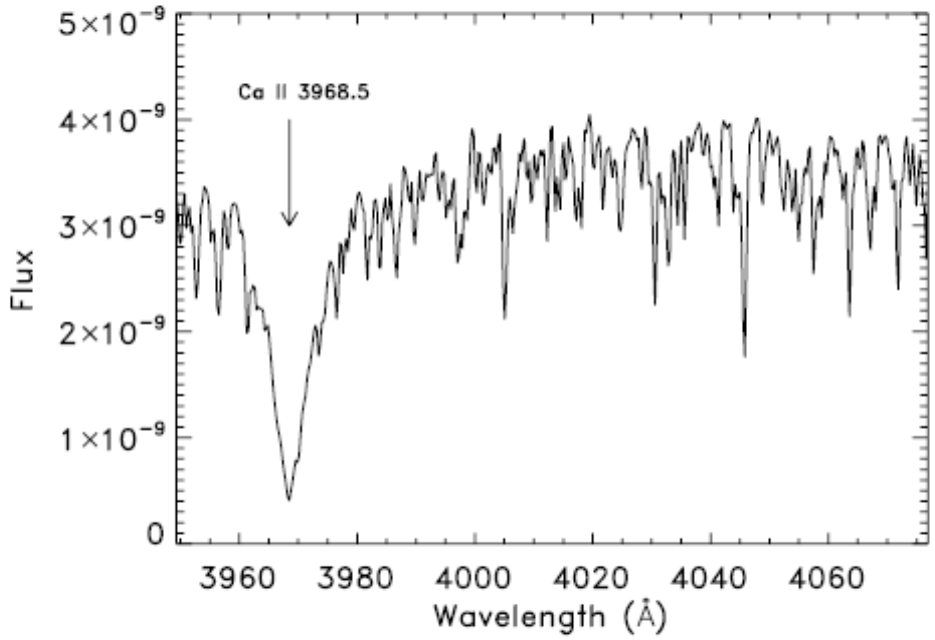

FIGURE 8.14— Atlas of Procyon: from 3950 to 4075 Å.

Bibliography

Alekseeva, G. A., Arkharov, A. A., Galkin, V. D. et al. 1996, Baltic Astronomy, 5, 603

Allende Prieto, C. & Lambert, D. L. 1999, A&A, 352, 555

Allende Prieto, C. & Lambert, D. L. 2000, AJ, 119, 2445

Allende Prieto, C., Asplund, M., García López, R. J. & Lambert, D. L. 2002, ApJ, 567, 544

Allende Prieto, C., Lambert, D. L., Hubeny, I. & Lanz, T. 2003, ApJS, 147, 363

Allende Prieto, C., Barklem, P. S., Lambert, D. L. & Cunha, K. 2004, A&A, 420, 183

Alonso, A., Arribas, S. & Martínez-Roger, C. 1994, A&A, 282, 684

Alonso, A., Arribas, S. & Martínez-Roger, C. 1996, A&ASS, 117, 227

Anders, E. & Grevesse, N. 1989, Geochimica et Cosmochimica Acta, 53, 197

Asplund, M., Nordlund, Å., Trampedach, R., Allende Prieto, C. & Stein, R. F. 2000, A&A, 359, 729

Auer, L. H. & Mihalas, D. 1973, ApJ, 184, 151

Barklem, P. S., Piskunov, N. & O'Mara, B. J. 2000, A&A, 363, 1091

Bautista, M. A., Romano, P. & Pradhan, A. K. 1998, ApJS, 118, 259

Bell, R. A., Eriksson, K., Gustafsson, B. & Nordlund, Å. 1976, A&AS, 23, 37

Bell, R. A., Paltoglou, G. & Tripicco, M. J. 1994, MNRAS, 268, 771

Bell, R. A., Balachandran, S. C. & Bautista, M. 2001, ApJL, 546, L65

Bertelli, G., Bressan, A., Chiosi, C., Fagotto, F. & Nasi, E. 1994, A&AS, 106, 275

Bertone, E., Buzzoni, A., Chávez, M. & Rodríguez-Merino, L. H. 2004, AJ, 128, 829

Bohlin, R. C. 1990, Harris, A. W., Holm, A. V. & Gry, C. 1990, ApJS, 73, 413

Bohlin, R. C. 1996, AJ, 111, 1743

Bohlin, R. C., Dickinson, M. E. & Calzetti, D. 2001, AJ, 122, 2118

Bohlin, R. C. & Gilliland, R. L. 2004, astro-ph, 3712

Burnashev, V. I. 1985, Abastumanskaya Astrofiz. Obs. Bull., 59, 83

Castelli, F., Gratton, R. G., & Kurucz, R. L. 1997, A&A, 318, 841

Castelli, F. & Kurucz, R. L., 1994, A&A, 281, 817

Castelli, F. & Kurucz, R. L. 2003, in Modelling of Stellar Atmospheres, IAU Symp., 210, ed. N. E. Piskunov, et al., in press

Ciardi, D. R., van Belle, G. T., Akeson, R. L., Thompson, R. R., Lada, E. A. & Howell, S. B. 2001, ApJ, 559, 1147

Code, A. D., Davis, J., Bless, R. C. & Hanbury Brown, R. 1976, ApJ, 203, 417

Collins, G. W. II 1963, ApJ, 138, 1134

Collins, G. W. II 1965, ApJ, 142, 265

Collins, G. W. II & Sonneborn, G. H. 1977, ApJS, 34, 41

Cowan, J. J. et al. 2002, ApJ, 572, 861

Cunto, W., Mendoza, C., Ochsenbein, F. & Zeippen, C. J. 1993, A&A, 275, L5

Davis, J., Tango, W. J. & Booth, A. J. 2000, MNRAS, 318, 387

Edvardsson, B., Andersen, J., Gustafsson, B., Lambert, D. L., Nissen, P. E. & Tomkin, J. 1993, A&A, 275, 101

Eggenberger, P., Carrier, F. & Bouchy, F. 2005, New Astronomy, v. 10, issue 3, 195

Fitzpatrick, E. L. & Massa, D. 1999, ApJ, 525, 1011

Fraunhofer, J. 1817, Denkschriften der Münch, Akademie der Wissenschaften, 5, 193

Fraunhofer, J. 1821, Denkschriften der Münch, Akademie der Wissenschaften, 8, 1

Fraunhofer, J. 1823, Gilberts Ann., 74, 337

Fuhrmann, K., Pfeiffer, M., Frank, C., Reetz, J. & Gehren, T. 1997, A&A, 323, 909

García-Gil, A., García López, R. J., Allende Prieto, C. & Hubeny, I. 2005, ApJ, 623, 460

García López, R. J., Lambert, D. L., Edvardsson, B., Gustafsson, B., Kiselman, D. & Rebolo, R. 1998, ApJ, 500, 241

Garhart, M. P., Smith, M. A., Levay, K. L., Thompson, R. W. 1997, *International Ultraviolet Explorer New Spectral Image Processing Information Manual, Version 2.0*

Girard, T. M., et al. 2000, AJ, 119, 2428

Glushneva, I. N. et al. 1982, 'Spectrophotometry of Bright Stars', 'Nauka', 255 pages

Glushneva, I. N., Doroshenko, V. T., Fetisova, T. S. et al. 1984, Trudy Gosud. Astron. Inst. Shternberga, 54, 3

Glushneva, I. N., Doroshenko, V. T., Fetisova, T. S. et al. 1991, Trudy Gosud. Astron. Inst. Shternberga, 62, 119

González-Riestra, R., Cassatella, A. & Wamsteker, W. 2001, A&A, 373, 730

Gray, D. F. 1980, PASP, 92, 154

Gray, R. O. 1988, J. Roy. Astron. Soc. Can., Vol. 82, No.6, 336

Gray, D. F. 1992, *The observation and analysis of stellar photospheres*, Cambridge Astrophysics Series, 20

Gray, R. O., Napier, M. G. & Winkler, L. I. 2001, AJ, 121, 2148

Grevesse, N. & Sauval, A. J. 1998, Space Science Review, 85, 161

Griffin, R. E. & Griffin, R. 1979, 'A Photometric Atlas of the Spectrum of Procyon (3140-7470 Å)', publishers, Cambridge, U.K.

Gulliver, A. F., Adelman, S. J., Cowley, C. R. & Fletcher, J. M. 1991, ApJ, 380, 223

Gulliver, A. F., Hill, G. & Adelman, S. J. 1994, ApJ, 429, L81

Gustafsson, B., Bell., R. A., Eriksson, K. & Nordlund, Å. 1975, A&A, 42, 407

Gustafsson, B., Edvardsson, B., Eriksson, K., Mizuno-Wiedner, M., Jørgensen, U. G. & Plez, B. 2003, Stellar Atmosphere Modeling, ASP Conference Proceedings, Vol. 288. Abstracts from a conference held 8-12 April 2002 in Tuebingen, Germany. Editors: Ivan Hubeny, Dimitri

Mihalas, and Klaus Werner. San Francisco: Astronomical Society of the Pacific, p.331

Hanbury Brown, R., Davis, J., Allen, L. R., & Rome, J. M. 1967, MNRAS, 137, 393

Hauschildt, P. H., Allard, F. & Baron, E. 1999, ApJ, 512, 377

Hayes, D. S. 1985, Proc. of IAU Symposium No. 111, 225

Holweger, H. 1970, A&A, 4, 11

Hubeny, I. 1981, A&A, 98, 96

Hubeny, I. & Lanz, T. 2000, *SYNSPEC A User's Guide, v. 43*

Hubeny, I. & Lanz, T. 2003, *TLUSTY A User's Guide, v. 200*

Ilijić, S., Rosandić, M., Dominis, D., Planinić, M. & Pavlovski, K. 1998, Contributions of the Astron. Observatory Skalnate Pleso, 27, 467

Jedamzik, K. Fuller, G. M., Matheus, G. J. & Kajino, T. 1994, ApJ, 422, 423

Kajino, T. & Boyd, R. N. 1990, ApJ, 359, 267

Kato, K. & Sadakane, K. 1982, A&A, 113, 135

Kato, K., Watanabe, Y. & Sadakane, K. 1996, PASJ, 48, 601

Kervella, P., Thévenin, F., Morel, P. et al. 2004, A&A, 413, 251

Kharitonov, A. V., Tereshchenko, V. M. & Knyazeva, L. N. 1978, 'Stellar Spectrophotometric Catalog', Alma-Ata, 'Nauka', 198 pages

Kupka, F., Piskunov, N., Ryabchikova, T. A., Stempels, H. C. & Weiss, W. W. 1999, AASS, 138, 119

Kurucz, R. L. 1979, ApJSS, 40, 1

Kurucz, R. L. 1992, Rev. Mexicana Astron. Astrofis., 23, 181

Kurucz, R. L. 1993, ASP Conf. Ser. 44, Peculiar versus Normal Phenomena in A-Type and Related Stars, ed. M. M. Dworetsky, F. Castelli & R. Faraggiana (San Francisco: ASP), 87 (see also CD-ROM distribution)

Kurucz, R. L. & Avrett, E. H. 1981, Smithsonian Astrophys. Obs. Spec. Rep., No. 391

Lagarias, J. C., Reeds, J. A., Wright, M. H. & Wright, P. E. 1998, SIAM J. Optim., 9, 112

Lane, M. C., & Lester, J. B. 1987, ApJS, 65, 137

Lucy, L. B. 1967, Zeitschrift für Astrophysik, 65, 89

Malaney, R. A. & Fowler, W. A. 1989, ApJ, 345, L5

Massa, D. & Fitzpatrick, E. L. 2000, ApJS, 126, 517 (M&F)

McKinnon, K. I. M. 1998, SIAM J. Optim., 9, 148

Mihalas, D. 1972, ApJ, 177, 115

Moon, T. T. & Dworetsky, M. M. 1985, MNRAS, 217, 305

Mozurkewich, D. et al. 1991, AJ, 101, 2207

Mozurkewich, D., Armstrong, J. T., Hindsley, R. B., Quirrenbach, A., Hummel, C. A., Hutter, D. J., Johnston, K. J., Hajian, A. R., Elias, Nicholas M., II, Buscher, D. F., Simon, R. S. 2003, AJ, 126, 2502

Nahar, S. N. 1999, ApJS, 120, 131

Nahar, S. N. & Pradhan, A. K. 1997, ApJS, 111, 339

Nelder, & Mead 1965, Computer Journal, 7, 308

Nitschelm, C. 1988, A&AS, 74, 67

Pérez Hernández, F., Claret, A., Hernández, M. M. & Michel, E. 1999, A&A, 346, 586

Peterson, R. C., Dorman, B. & Rood, R. T. 2001, ApJ, 559, 372

Petrie, R. M. 1964, Pub. Dom. Astrophys. Obs., 12, 317

Plez, B., Brett, J. M. & Nordlund, Å. 1992, 256, 551

Price, C. J., Coope, I. D. & Byatt, D. 2002, Journal of Optimization Theory and Applications, 113, 5

Price, S. D., Paxson, C., Engelke, C. & Murdock, T. L. 2004, AJ, 128, 889

Provencal, J. L., et al. 1997, ApJ, 480, 777

Provencal, J. L., Shipman, H. L., Detlev Koester, Wesemael, F. & Bergeron, P. 2002, ApJ, 568, 324

Przybilla, N. 2002, PhD Thesis, Ludwig-Maximilians-Universität München

Qiu, H. M., Zhao, G., Chen, Y. Q. & Li, Z. W. 2001, ApJ, 548, 953

Ramaty, R., Kozlovsky, B. & Lingenfelter, R. E. 1996, ApJ, 456, 525

Ramaty, R., Kozlovsky, B., Lingenfelter, R. E. & Reeves, H. 1997, ApJ, 488, 730

Reeves, H., Richer, J., Terasawa, N. & Sato, K. 1990, ApJ, 355, 18

Steffen, M. 1985, A&AS, 59, 403

Stürenburg, S. & Holweger, H. 1990, A&A, 237, 125

Su, K. Y. L., Rieke, G. H., Misselt, K. A., et al. 2005, astro-ph/0504086, accepted for publication in ApJ

Tassoul, J.-L. 1978, *Theory of rotating Stars*, Princeton Series in Astrophysics, Princeton University Press

Terasawa, N. & Sato, K. 1990, ApJ, 362, L47

Terez, G. A., and Terez, E. I. 1979, Astronomicheskii Zuhrnal, 56, 800, in Russian

Tull, R. G., MacQueen, P. J., Sneden, C., & Lambert, D. L. 1995, PASP, 107, 251

van Regemorter, H. 1962, ApJ, 136, 906

Vasil'Yev, I. A., Merezhin, V. P., Nalimov, V. N. & Novosyolov, V. A. 1989, Information Bulletin on Variable Stars, 3308, 1

Vernazza, J. E., Avrett, E. H. & Loeser, R. 1976, ApJS, 30, 1

von Zeipel, H. 1924, MNRAS, 84, 665

Walgate, R. 1983, Nature, 304, 681

Walker, T. P., Steigman, G., Schramm, D. N., Olive, K. A. & Kang, H.-S. 1991, ApJ, 376, 51

Wedemeyer, S. 2001, A&A, 373, 998

Wilner, D. J., Holman, M. J., Kuchner, M. J. & Ho, P. T. P. 2002, ApJL, 569, L115

Wollaston, W. H. 1802, Phil. Trans. R. Soc., 92, 365